NTNU
Norwegian University of
Science and Technology

Investigation of thrust loss due to steering while trawling

Dag Kristian Åsbø

Marine Technology
Submission date: June 2017
Supervisor: Sverre Steen, IMT
Co-supervisor: Øyvind Dalheim, IMT

Norwegian University of Science and Technology
Department of Marine Technology

NTNU Trondheim
Norwegian University of Science and Technology
Department of Marine Technology

MASTER THESIS IN MARINE TECHNOLOGY

SPRING 2017

FOR

Dag Kristian Åsbø

Investigation of thrust loss due to steering while trawling

From practical experience, it is found that a large part of the propeller thrust is lost due to excessive use of rudder to maintain direction of the trawler while trawling. The use of rudder is necessary to keep wanted heading and track, which is offset due to environmental forces (wind, waves, current). Like for a tug, the forces in the tow lines are important for the control of the trawler while trawling. Although the magnitude of the forces are mainly given, the point of application on the ship might be changed to improve the control of the ship. The trawler "Prestfjord" has recently had an extensive measurement package installed – unique to such a ship. These measurement results will be made available to the candidate as an important resource in the project. The overall objective for the combined project and master thesis is to identify ways to improve the efficiency of the operation, for instance by controlling the application point of the trawl wires to help steer the ship during trawling. To investigate this and other possible ways, it is necessary to be able to simulate the performance of the ship with various trawl configurations. Furthermore, the full scale measurements should be viewed as an important resource.

The objective of the master thesis is to determine how much power can be reduced by shifting the application points of the trawl wires to help steer the ship during trawling.

In the thesis the candidate shall present his personal contribution to the resolution of problem within the scope of the thesis work.

Theories and conclusions shall be based on mathematical derivations and/or logic reasoning identifying the various steps in the deduction.

The thesis work shall be based on the current state of knowledge in the field of study. The current state of knowledge shall be established through a thorough literature study, the results of this study shall be written into the thesis. The candidate should utilize the existing possibilities for obtaining relevant literature.

The thesis shall be organized in a rational manner to give a clear exposition of results, assessments, and conclusions. The text should be brief and to the point, with a clear language. Telegraphic language should be avoided.

The thesis shall contain the following elements: A text defining the scope, preface, list of contents, summary, main body of thesis, conclusions with recommendations for further work, list of symbols and acronyms, reference and (optional) appendices. All figures, tables and equations shall be numerated.

NTNU Trondheim
Norwegian University of Science and Technology
Department of Marine Technology

The supervisor may require that the candidate, in an early stage of the work, present a written plan for the completion of the work. The plan shall include a budget for the use of laboratory or other resources that will be charged to the department. Overruns shall be reported to the supervisor.

The original contribution of the candidate and material taken from other sources shall be clearly defined. Work from other sources shall be properly referenced using an acknowledged referencing system.

The thesis shall be submitted electronically (pdf) in DAIM:

- Signed by the candidate
- The text defining the scope (this text) (signed by the supervisor) included
- Computer code, input files, videos and other electronic appendages can be uploaded in a zip-file in DAIM. Any electronic appendages shall be listed in the main thesis.

The candidate will receive a printed copy of the thesis.

Supervisor : Professor Sverre Steen
Start : 12.01.2017
Deadline : 11.06.2017

Trondheim, 12.01.2017

Sverre Steen
Supervisor

Preface

This thesis is the final work, fulfilling a master's degree in marine hydrodynamics at the Norwegian University of Science and Technology, department of Marine Technology.

The topic assessed in this thesis is movable trawl blocks: How is the power delivered to the propeller affected if the yaw moment is altered by transversely moving the blocks the trawl warps run through?

Many thanks to my supervisor, Professor Sverre Steen, for taking the time to give guidance despite a full schedule as Head of Department, and always having either a direct answer or a title where it can be found. My co-supervisor, PhD Candidate Øyvind Øksnes Dalheim, has shown interest and enthusiasm during meetings, and especially deserves recognition for his support when handling the data set. The collaboration with Rolls-Royce Marine has been without any problems. Leif Aarseth has been Rolls-Royce's main representative for this thesis, and has given supervision and rapid responses over mail, exceeding what is commonly expected from company contacts.

Dag Kristian Åsbø
Trondheim, 25th June 2017

Summary

This thesis investigates the potential for a reduction in required propeller power by optimizing the transverse position of attachment points for trawl warps, simulating a system of movable trawl blocks. Full scale measurements from the 65 meter long stern trawler F/T Prestfjord is used as a basis.

A surge, sway and yaw manoeuvring model based on Lagrangian mechanics is used together with control forces from trawl, rudder and propeller is put into a bounded optimization algorithm to find the transverse position of trawl blocks requiring the lowest thrust. The bounds are the original placement of the port-side and starboard blocks, i.e 5.08 meters.

The result is a small reduction in power. For the operational profile from the data-set, the mean reduction in power is 0.64%. During trawling, the mean reduction in power is 1.13% when pulling a double trawl, and 1.11% when a single trawl is pulled.

This is smaller than earlier reports have found, and it is not certain that such a system will be beneficial in an economical perspective when investment and maintenance cost is included. Differences to earlier reports seem to be based on rudder size and efficiency. The power reduction is greatest in relation to manoeuvring, while it is more stable when trawling on a straight course with a drift angle.

Sammendrag

Denne rapporten omhandler reduksjon i nødvendig effekt levert til propellen ved optimal tverrskips plassering av tilkoblingspunkter(trålblokker) for trålvarp(vaiere). Fullskala målinger fra tokter med den 65 meter lange tråleren F/T Prestfjord er brukt som grunnlag.

Manøvreringsligninger for jag, svai og gir, basert på Langrangemekanikk er brukt i kombinasjon med modellerte kontrollkrefter fra tråd, ror og propell, er brukt i en optimeringsalgoritme for å finne plasseringen tverrskips for trålblokkene som krever lavest skyvekraft fra propellen. Algoritmen er avgrenset med den originale plasseringen av blokkene på babord og styrbord side, dvs. 5.08 meter.

Resultatet er en liten reduksjon i nødvendig propelleffekt. For operasjonsprofilen tilhørende datasettet er den gjennomsnittlige reduksjonen på 0.64%. Under tråling er gjennomsnittlig reduksjon 1.13% ved bruk av dobbel tråd, og 1.11% ved bruk av enkel tråd.

Dette er en lavere reduksjon enn tidligere rapporter tilsier, og det er usikkert om det vil være en økonomisk gevinst ved bruk av et slikt system, dersom investeringskostnad og vedlikehold blir tatt i betraktning. Forskjellen fra tidligere rapporter er tilsynelatende grunnet forskjeller i rorets areal og effektivitet. Reduksjonen i propelleffekt er størst under kursendringer, men mest stabil ved konstant kurs med avdriftsvinkel.

Contents

List of Figures

List of Tables

Nomenclature

(x_g, y_g, z_g)	Vector of distances relating CO to COG.
α	Angle of attack. The angle between the flow and a foil.
α_s	Angle of trawl warps in the body fixed xy-plane, relative to the x-axis
β	Drift angle, the angle between course and heading. Positive when flow comes from starboard(course larger than heading).
β_r	Relative drift angle, the angle between flow axis and heading. β corrected for currents. Positive when flow comes from starboard.
β_{rud}	Angle between flow over the rudder and the x-axis in the body reference frame
η	Generalized position vector
$\mathbf{v_r}$	Generalized velocity vector relative to current.
$\boldsymbol{C_A}$	Matrix of centripetal terms due to hydrodynamical parameters proportional to acceleration (Added mass centripetal). Proportional to velocities
$\boldsymbol{D}$	Damping matrix. Hydrodynamic terms proportional to velocities
$\boldsymbol{M_A}$	Matrix of hydrodynamical parameters proportional to acceleration (Added mass)
$\boldsymbol{M_{RB}}$	Rigid body inertial matrix (mass and moment of inertia). Proportional to acceleration
δ	Rudder angle in body reference system
$\hat{\mu}$	μ - expected value, $\hat{\mu}$ - estimated expected value
Λ	Aspect ratio, $\frac{b}{c}$ or $\frac{2b}{c}$ for foils with only one free end due to mirroring.
ν	Kinematic viscosity. For seawater: $1.0 \cdot 10^{-6}$ to $1.2 \cdot 10^{-6}$
ω	Angular frequency
τ_i	Force vectors, i: hs-hydrostatic, hyd-hydrodynamic, RB-rigid body.

θ	Angle between the xy-plane and the trawl warps
$\{b\}, \{n\}, \{f\}$	Sub- and super-scripts for body-, NED-, and flow-reference frames
b	Foil span. Length of foil orthogonal to flow.
c	Chord length, or mean chord length. Length of foil parallel to flow.
C_f	Frictional drag coefficient, for a smooth plate.
C_R	Roughness addition to frictional drag coefficient.
D	Drag force
F_i^C	Cross flow force (i=2) and moment (i=6)
F_N	Froude number, ratio between inertia and gravity forces. $F_N = \frac{U}{\sqrt{gL}}$
F_{N_h}	Depth Froude number $U(gh)^{-1}$, where h is depth
h	Depth
HS	Hull straightening
k	Form factor. $(1+k)$ gives additional drag due to accelerated flow due to thickness.
K_Q	Non-dimensional torque
K_T	Non-dimensional thrust, subscripts: d-duct, p-propeller, none or t - total
L	Lift force
L_{OA}	Length overall, the total length of a ship.
P	Propeller pitch
Q	Torque
r	Radius of propeller slipstream.
R_n	Reynolds number. $\frac{u_r \cdot L}{\nu}$
T	Thrust, Kinetic energy in Lagrangian mechanics
t	Thrust deduction
t'	Dimensionless time related to flow separation

U	Total velocity
V_{corr}	Velocity over rudder corrected for turbulent mixing
w	Wake - Change of inflow velocity due to the presence of a hull
X_i, Y_i, N_i	SNAME notation of forces. See Tables 3.1 and 4.1

Acronyms

BAR blade area ratio. 36

CI Confidence Interval . 74, 76–78

CO Centre of origin. 17

COG Centre of gravity. 17, 54

CPP controllable pitch propeller. 33

DOF Degree Of Freedom. 91

GRS80 Geodetic Reference System 1980. 46

MCR Max Continuous Rating. 13

NED North-East-Down. 12, 17, 50

R propeller radius. 36

R_N Reynold's number. 36, 52

RPM revolutions per minute. 36, 66, 67

SG Specific gravity. 48

UTM Universal Transverse Mercator. 45, 46

Chapter 1

Introduction

1.1 Motivation

During trawling operations, most of the propeller thrust is used to pull the trawl. The tension in the wires are known, as well as the attachment points, so the moments can be calculated. By moving the blocks the wires run through, referred to as trawl blocks throughout the thesis, the moment in yaw can be changed, therefore steering the vessel. Steering the ship by moving the application points of trawl forces will reduce the necessary rudder angle, and therefore the rudder drag. Due to the large amount of thrust necessary to pull the trawl, the velocities across the rudder become large, meaning rudder drag is increased. During trawling, experience has shown that large rudder angles are necessary to maintain heading and track in a seaway, resulting in large drag forces on the rudder (Enerhaug 2009). Reducing the rudder angles will therefore reduce the necessary thrust. From Figure 1.1 it is visible that the trawl can create a large yaw-moment, and that moving them can reduce the yaw-contribution from the trawl significantly when a trawler has a drift angle due to environmental effects.

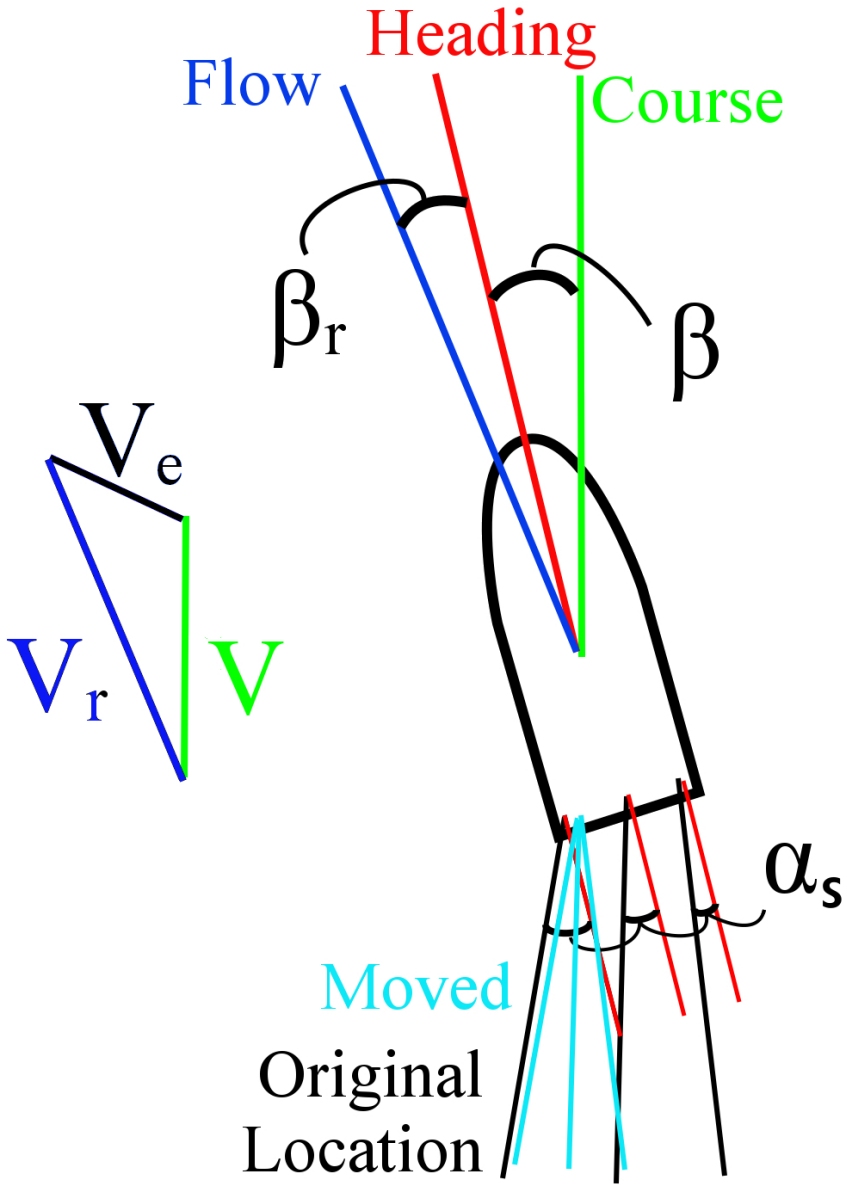

Figure 1.1. Illustration of currents and horisontal trawl angles: Some of the important definitions are illustrated here. Course, parallel to velocity over ground (green). Flow axis, parallel to incoming flow, including currents(blue). Heading, the compass direction the ship points towards, the reference system used in calculations. β_r is the relative drift angle, accounting for currents, negative in the figure. β is the drift angle, positive in the figure. α_s is a vector containing the angles between the trawl warps and the heading (black). The blocks are moved as one point, keeping α_s constant (cyan).

1.2 A brief introduction to trawling

Trawling is done by pulling a cone-shaped net, that guides fish into a permeable bag. The bag is also made of a net, thus making it permeable. Trawling is usually separated in two categories; pelagic, and bottom trawl. Trawling is generally considered pelagic as long as nothing touches the seabed. Other methods than trawling is usually used when fishing the pelagic species in the Norwegian fishery fleet. The bottom trawls have a wider and lower net, to guide fish into the bag, and a "roof" to prevent fish from escaping over the trawl. Trawl doors, also called otter boards, are foils that keep the net open in the horizontal direction. The trawl doors, are heavy, and moves along the sea bed. Vertical opening of the net is done with weights and buoyancy elements. The trawl doors are connected to the ship with wires, known as warps, and to the net with another set of wires called sweeplines. When bottom trawling, it is possible to use a double trawl, not to be misinterpreted as pair-trawling(one trawl, two vessels). Double-trawling means that two nets are placed between the trawl doors instead of one, and a third wire runs between the ship and the connection between the nets (Oljedirektoratet 2010). The case vessel uses a three-wire set up for double trawl, as illustrated in Figure 1.2. The mid-wire is attached to a weight to keep it, and the net, at the seabed. The weight is slightly behind the trawl doors, so the mid-wire will have approximately the same length as the side-wires. The sweeplines have two main goals; connection between the trawl and trawl doors/the weight, and to guide fish into the trawl. Robust and heavy wires are used for this purpose, to handle large loads due to a larger angle, and for staying at the bottom, scaring the fish towards the trawl (Karlsen 1997). To reduce the amount of bycatch, different sorting mechanisms are used to release most of the unwanted fish, for environmental and economic reasons. When fishing white-fish, the sorting is mainly done with mesh-size of the net, to reduce the catch of smaller fish. To remove other species that are unwanted, but too large for the mesh, such as flatfish, a tilted sorting grid pushes unwanted fish up towards a hole. A trawl haul is separated into different operations (Karlsen 1997):

- Positioning and locating fish: Looking for fish is not a large part of operations during bottom trawling, as echolocation is unable to accurately find bottom fish.
- Deployment of trawl-net/cod-end, sweeplines and trawl doors.
- Launching: The trawl set-up is pulled a short distance behind the ship until it is certain that the net has opened, and the trawl doors pull apart before the

trawl is launched. This is to avoid warps or trawl doors getting intertwined.

- Towing: The most time consuming part of the haul, with typical duration of three to five hours. This thesis focuses on the towing operation. The ship velocity during towing is mostly decided by the type of trawl and the species the trawl operation aims for. The velocity is therefore larger when catching fish that swim fast. Type of trawl mainly influences the velocity through the net's mesh size.
- Hoisting: Typically, the winches are ran at full power when hoisting. Some vessels keep the heading when hoisting, while some steer to account for the weather.
- Recovering the trawl: The trawl doors are first secured. Sweepline winches then tighten so the trawl is resting on them, making it possible to disconnect the warps(the towing wires). When the sweeplines are taken all the way in, Gilson winches are connected, pulling the cod-end into the trawl deck, where it is emptied into the fish receiving bin.

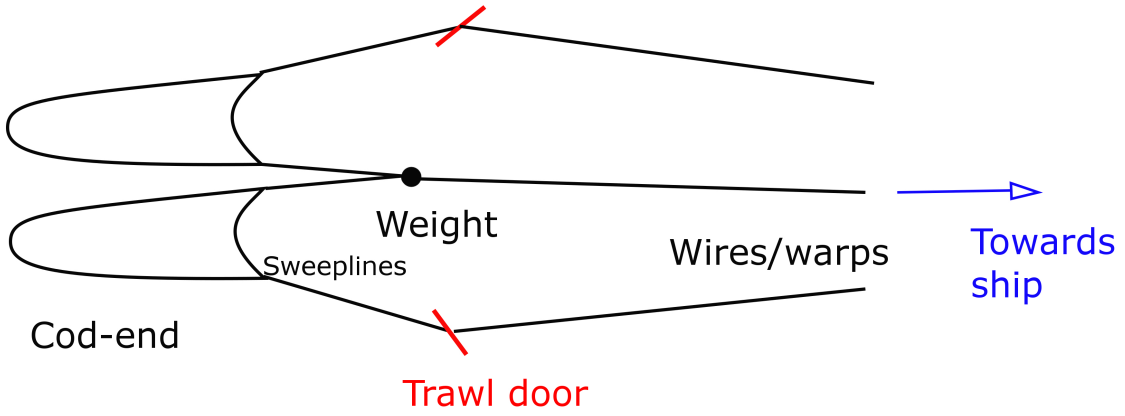

Figure 1.2. Illustration of double trawl set up: The cod-end is not properly modelled here. The different parts listed is described in the text. A single trawl has a similar set up, found by removing the middle part: The trawl door wire set-up on each side of one cod-end. Based on descriptions in Karlsen (1997)

.

1.2.1 Manoeuvring with trawl

Sharp manoeuvres while trawling is done according to a specific procedure, as turning normally could lead to problems, for example tipping the trawl doors. To turn around 180°, the manoeuvre starts with a turn towards one side, then travelling

a distance on that course, before completing the turn. This gives the trawl track a circular shape, manageable to follow. The difference in ship and trawl track, is that the trawl takes an inner turn. This leads to larger manoeuvres of the ship, to get the trawl in the correct track, e.g when avoiding obstacles (Karlsen 1997).

1.2.2 Trawling in bad weather

For the smaller vessels, large waves or messy seas usually means smaller reward. Slamming scares the fish away from the path of the vessel, therefore also the trawl. Involuntary speed loss, and speed variations due to weather also leads to less catch, mostly because it leads to uneven movements of the trawl, and oscillations in warp tension. Larger vessels, including Prestfjord, have a system for reducing such oscillations, which Karlsen calls Trawl-guard or Syncro. Prestfjord has Rolls-Royce's Synchro RTX installed.

1.3 Case vessel: F/T Prestfjord

The case vessel for this thesis is a 65 meter long (L_{OA}) stern-trawler named Prestfjord, with the possibility of double-trawling. Prestfjord was delivered in 2012, with a design that focuses on energy efficiency, such as a hybrid machinery system, and a new hull design. It operates at sea, fishing white-fish during the data used; however, it is also designed to operate pelagic and shrimp trawls. Rolls-Royce Marine have installed a large measurement package on Prestfjord, as a part of the SINTEF's Improved Vessel Design and Operation (IMPROVEDO) project (Sintef 2012). The vessel has a flapped rudder and a controllable pitch propeller with an accelerating duct. The aft-body of Prestfjord, with the trawl blocks pointed out, is presented in Figure 1.3. Some relevant principal values are presented in Table 1.1.

Table 1.1. Principal values of F/T Prestfjord

Description	Abbreviation / Type	Value	Unit
Length overall	L_{OA}	65	m
Breadth moulded	B	15	m
Main Engine	B32:40L9PCD	4500	kW
Year		2012	
Propeller diameter	D	3.8	m
Propeller Duct	N19A		
Freezing hold		1236	m^3
Remote control	Helicon-X		

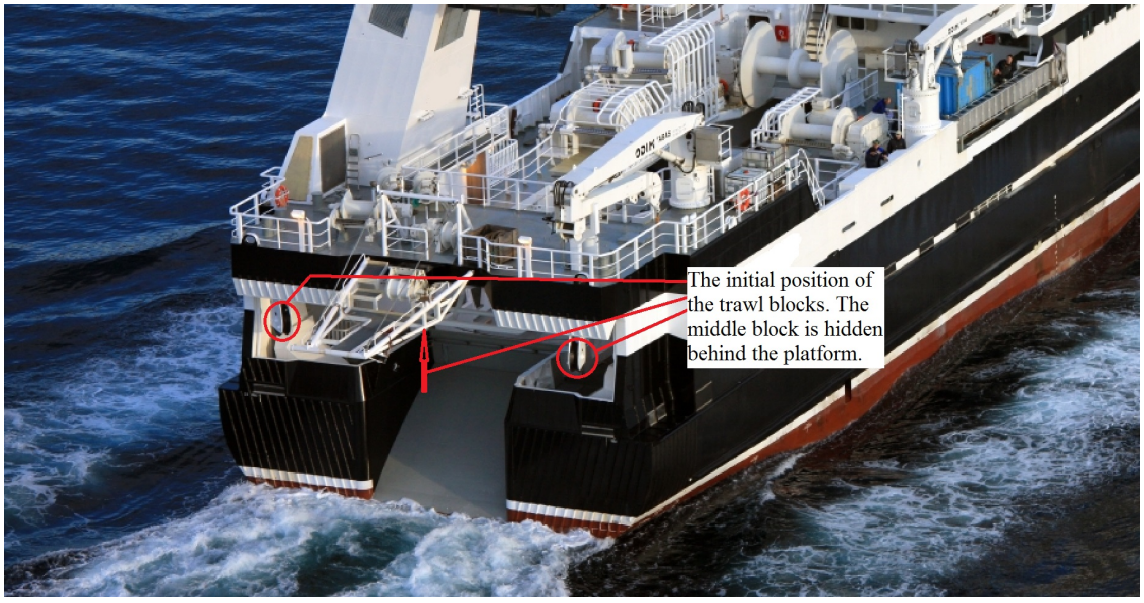

Figure 1.3. Position of blocks: The blocks that could be used for steering is pointed out in this Figure. The image is modified. The original image was provided by Rolls-Royce.

1.4 Background

The concept of movable trawl blocks is not new, as several trawlers already have a system in place. The concept has been used on coastal shrimp trawlers, and stern trawlers in the North sea, with the purpose of increasing manoeuvrability of the vessels (Bjørkum 1989). A side effect of the instalments have been reduced fuel consumption. Bjørkum & Farstad (1991) has written a detailed report on estimated

fuel saving and the economical impact movable trawl blocks would have on trawlers of different sizes. The category of largest vessels is cod trawlers with on-board production, larger than 250 gross register tonnes (GRT). Bjørkum & Farstad's conclusion is that even with significantly higher investment-cost than predicted, movable trawl blocks would result in economical savings for this category, which Prestfjord also belongs. Bjørkum & Farstad (1991) is based on the previous report (Bjørkum 1989), and the savings for vessels of this category is assumed to be 20% during trawling. In Bjørkum (1989), fuel saving due to movable trawl blocks are found using a trawler with movable blocks installed, by comparing similar conditions with the blocks stationary or moving. This gives a very direct and reliable approach when estimating the amount of fuel saved. Unfortunately, the results are for a very specific vessel, operating in an area with strong currents. The vessel in Bjørkum (1989) is an old, refurbished coastal shrimp-trawler, operating at very low speeds, between half a knot and two knots. Shrimp-trawlers operate at the lowest velocity of the different trawlers, while large white-fish trawlers have the highest velocity (Oljedirektoratet 2010). Bjørkum (1989) does not give a decisive conclusion, as preparations became more expensive than expected, giving a shorter test-period. Bjørkum expresses doubts about the interpretation of results. It is stated that a larger test base would be necessary for a universal conclusion, and the results are only valid for the tested vessel during the conditions experienced during the tests.

1.5 Contributions from this thesis

As there currently is no universally applicable results regarding the potential for saving fuel with movable trawl blocks, this thesis aims to investigate the potential for saving fuel on a large stern trawler fishing white-fish at sea. The basis of guidelines regarding movable trawl blocks will therefore be wider. There is also a difference in modernity between the vessel used in this thesis and Bjørkum (1989). As trawling operations are done at higher speeds compared to the shrimp-trawler used by Bjørkum, drift angles should be smaller for the same currents, as currents are weaker relative to the ship velocity. The currents encountered at sea, is also expected to be weaker, while wave effects are expected to be larger, when comparing with the data from Bjørkum (1989). It is focused on relative propeller power instead of relative fuel consumption, as it is more translatable to other vessels.

1.6 Structure of the thesis

Discussion on partial results are done continuously in this thesis.

- **Chapter 1:** In the introduction, the topic is explained, with an introduction to trawling. The case vessel is presented, along with important characteristics. Background information on the topic is studied and the difference between this thesis and the background is discussed.
- **Chapter 2:** The data-set used in this thesis is presented. A description of methods used when processing this data then follows. Information about the operational profile of the vessel, including velocities and a comparison of power and velocity when manoeuvring or trawling at a drift angle.
- **Chapter 3:** The theoretical background for the manoeuvring model is presented here. Most of this chapter consists of sections from the project thesis.
- **Chapter 4:** Methods used to develop the model are presented here, along with discussions of their accuracy. The first section explains how the manoeuvring coefficients were found, and used. Modelling of the propeller, rudder, and trawl forces are presented in the following three sections. Finally, the forces are gathered into the set of equilibrium equations used in this thesis.
- **Chapter 5:** A small study of the possibility of reducing power is presented here, followed by a discussion of the model's accuracy by using an example trawl operation.
- **Chapter 6:** The method used to optimize the transverse position of trawl blocks is presented here. Methods used to process the result of the optimization are also described.
- **Chapter 7:** The results are presented relative to turning rate, drift angle, and averaged values. An example is used to show how drift angle, rudder angle, thrust, transverse position of blocks, and reduction in power is changes from the optimization.
- **Chapter 8:** The discussion is based on the end results presented in Chapter 7. Results and discussions from previous chapters are included if they significantly change the accuracy of the end result.
- **Chapter 9:** Conclusions and examples of possible categories for further work.

Chapter 2

Processing of data

2.1 Information about the data

A large set of measurements is used, containing more than 250 trawling operations, and 1238 hours of total duration. Data used in this thesis was gathered between 30th of May and 20th of July 2015, when operating at different locations in the Barents Sea in an area enclosing Bjørnøya. The measurements are part of the data gathered from the measurement package installed on Prestfjord in relation to IMPROVEDO. Resolution and frequency of measurements differs between the channels, and is delivered as a set logged every second. Data that never changes two consecutive seconds is assumed to be previous neighbour interpolated, as the measurements are taken real-time.

2.1.1 Overview of the most important data

In Table 2.1, the measurement channels that have been the most important for this thesis is listed, with the resolution and logging period.

Table 2.1. Channels used. Units were supplied by Leif Aarseth

	Unit	Resolution	Logging period
Speed over ground	$[knots]$	0.1	1
Latitude	$[dd.mm]$	0.1	2
Longitude	$[dd.mm]$	0.1	2
Rudder angle	$[degrees]$	0.5	1
Heading	$[degrees]$	0.1	1
Course	$[degrees]$	0.017	1
Propeller pitch	[%]	0.002	1
Propeller torque	$[kNm]$	1	1
Propeller RPM	[%]	0.035	1
Tension PS wire	$[tons]$	$1 \cdot 10^{-4}$	1
Tension mid wire	$[tons]$	$1 \cdot 10^{-4}$	1
Tension SB wire	$[tons]$	$1 \cdot 10^{-4}$	1
Length PS wire	$[m]$	0.1	1
Length mid wire	$[m]$	0.1	1
Length SB wire	$[m]$	0.1	1
Time	$[s]$	1	1

2.2 Quality of the data

Some measurement channels are empty. The channels that are in use gives reasonable values for all points, so the measured data is assumed to be accurate. There are some points regarding the rudder and the wire tension that could contain errors. The rudder angle sometimes jump gradually to roughly $\pm 30°$, where it stays, and sometimes jumps to a reasonable value. The value it jumps to is not the same every time, and it could be the correct rudder angle, not a value

set for erroneous points. Two things points to these values being erroneous; the manoeuvring equations fall far from equilibrium, and the rotation rate of the rudder becomes unreasonably fast. This happens occasionally during very sharp turns. A possible, but unlikely, explanation is that the rudder angle measured is the desired rudder angle, not the rudder angle feedback. The wire tension will in some regions start oscillating between a value roughly $30 - 60\%$ larger than a regular value and slightly below the regular value. This happens both at sharp turns and on a straight course, as well as during a region of hoisting. This could be due to elastic effects, for example due to a trawl door getting stuck. It is uncertain how the Synchro RTX deals with this type of response; however, an important purpose is to automatically release more wire if the tension becomes too large, and 160% of the average could be within safe limits regarding loads of short duration.
There is a speed-log channel that was not used because of many faults in the data, as expected from such sensors. It is checked that the data is properly zeroed, and every channel used is zero when reasonable. Calibration is not checked, other than observing that equilibrium equations are close to zero. It is assumed to not be amongst the larger error sources in the calculations.
Overall, the measured data is of good quality, and it is expected that the logging resolution makes sensor inaccuracies negligible.

2.3 Data preparation

Resolution of data makes them hard to incorporate accurately in a manoeuvring model, especially for the accelerations. To remove noise, and the largest part of effects regarding resolution, most of the data was filtered. For filtering, a low-pass Butterworth filter is used. To avoid affecting the phase of the signal, the function *filtfilt* is used (MATLAB 2015). Different filter orders and cut-off frequencies are used, to best keep the wanted signal without including too much noise.

Instead of using the measured speed over ground, the speed was found using the GPS-signal, and then applying a low-pass filter to remove noise. The filter coefficients were adjusted to make the signal follow the measured speed. A phase difference between the two was found and corrected. The GPS-signal was not used to find course, as it was found better to use the logged signal.

Heading and course were used to find the drift angle, β, and the relative drift angle,

β_r, used to decompose velocity and acceleration into surge and sway. Heading was used to calculate yaw-rate and acceleration. Rapid changes in heading, made it difficult to filter drift angle, yaw-rate and yaw-acceleration properly, as noise frequencies and signal frequencies coincide. Too much filtering would make the signal distorted, with lower amplitudes and wider peaks. Some noise in these signals are therefore left unfiltered. The same problem was encountered when filtering the rudder angle, which was filtered to remove round-off errors. The exact angle of the rudder is impossible to find, and the goal of the filtering was to remove oscillations between two points. The round-off related oscillations were not completely removed. As the derivative of the rudder angle will not be used, this is a minor inconvenience, not resulting in significant errors.

2.3.1 Currents

Due to the low velocity during trawling, currents become an important part of the manoeuvring equations. To account for currents, the sway velocity is found by decomposing the velocity using the drift angle. The entire time-series of sway velocity is then transformed into the North-East-Down (NED)-reference system. The North and East component of the sway velocity is then filtered with a low-pass filter, with a cut-off frequency of $1 \cdot 10^{-4}$, corresponding to a period of roughly three of the manoeuvres of longest duration. The longest duration of manoeuvres can be considered as half a period, so a period twice of this duration is necessary for the cut-off. The filter has a band around the cut-off frequency where the amplitude response is neither one nor sufficiently close to zero. The cut-off is set lower to make sure that most of the sway velocity due to manoeuvring is removed. Relative velocity, $\boldsymbol{v_r}$, and relative drift angle, β_r, is then calculated. For irrotational currents, both rigid body forces and hydrodynamic forces can be found using the acceleration and velocity relative to flow, according to *Property 8.1* in Fossen (2011). As the accelerations due to currents are small, and assumed negligible, accelerations stay the same as without currents. The drift angle relative to course, β, is therefore used for decomposing the acceleration. The velocity is decomposed using the drift angle relative to flow, β_r. The drift angles are illustrated in Figure 1.1.

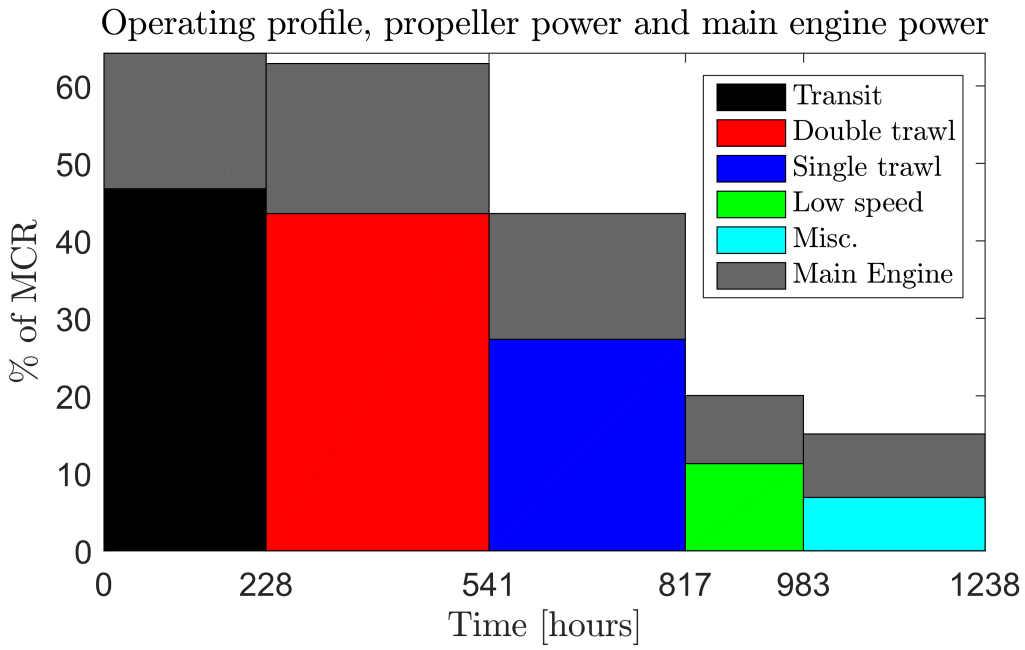

Figure 2.1. Operational Profile: Tick marks for time is placed at the intersections between profiles. Transit is rapid movement without trawls deployed. Low speed is a profile where the ship has a velocity greater than 2 knots, while not being fast enough for transit (10 knots), and is without trawl. The miscellaneous profile consists of all other points.

2.4 Operational Profile

The operational profile of Prestfjord, for the data used, is shown in Figure 2.1. Along the x-axis, time in hours is marked at the changes in mode. At the y-axis, Max Continuous Rating (MCR) is used to show the engine load. In gray, the channel logging the main engine load is used to describe the total power consumption of the vessel during the different modes. The coloured bars show the power in the propeller shaft, showing how much of the engine power is used for propulsion. There is a rather large amount of power delivered to other facilities than the propeller shaft. This is expected, as Prestfjord has an on-board production facility for the fish, and the shaft-generator is rated to more than half of the engines rating (mostly due to the hybrid drive). There are also other plausible reasons for the large difference in power. There could be a difference in what is considered to be 100% load, even though MCR is most common; the channel for engine load is taken directly in percent, while the propeller shaft is calculated as the ratio to the rated power of the engine. Another reason is mechanical losses between the engine and the point of measurement on the shaft, e.g. in the reduction gear.

The trawl operations could be split into more operations, as explained in Section 1.2. Not all of the trawl operations are in the trawling parts of the operational profile, and it mostly consists of *launching* and *towing*. The miscellaneous part consists of different parts such as being in port, use of bow-thruster, and some parts of the trawling, such as hoisting. It is clear that the ship spends most of the time trawling.

2.4.1 Velocity during trawl

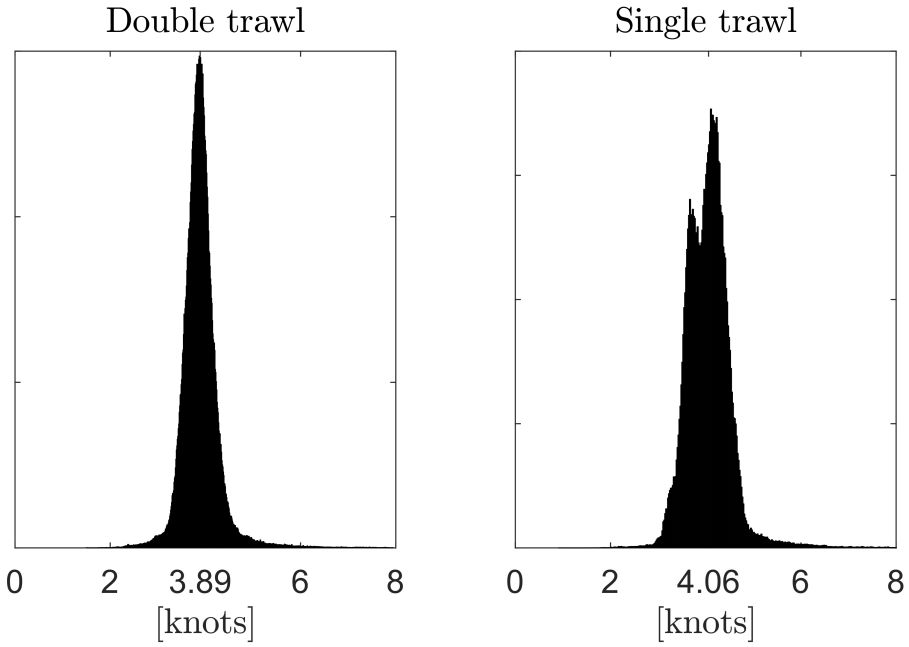

Figure 2.2. Histogram of velocities during trawl: The different velocities during the trawl operations are presented here. Mean velocity of the respective trawl mode is set as one of the tick labels on the x-axis. Prevalence of each velocity is on the y-axis.

An important factor during trawling is the velocity. The velocity varies significantly between different vessels and between the species the trawl haul aims for, as explained in Section 1.2. In Figure 2.2 the different velocities, and their prevalence in the time series is presented. A larger variation in velocity is seen when trawling with a single trawl, than with a double trawl. With a single trawl two peaks are present instead of one, and the average velocity is slightly higher. It is observed in the data that there is more manoeuvring during single-trawling, and a single-trawl is used at both deep water and shallow water. Double-trawl is not used when the water is shallow. The larger applicability of a single-trawl is therefore regarded as the reason for the wider range of velocities.

2.4.2 Velocity and power in relation to turning or drifting

To capture this correlation, the channels are filtered with a bandpass filter with cut-off frequencies of $2.5 \cdot 10^{-4}$ and $1 \cdot 10^{-2}$, for this purpose only. The first cut-off frequency removes slow changes, more probably occurring due to for example change in desired velocity or bottom friction of the trawl. The second frequency removes noise. Cross correlation shows the *linear* dependencies between signals (MATLAB 2015), meaning non-linear parts of the correlation is not found. Non-linear correlation is definitely important here; however, the linear part alone should be enough to give an impression of how responses are connected.

Table 2.2. Cross correlation of power and velocity to drift angle and turning rate: The cross correlations are without phase shift.

	Drift angle		**Turning rate**	
Cross correlation between	Double trawl	Single trawl	Double trawl	Single trawl
Shaftline power	0.39	0.23	0.20	0.21
Velocity	0.19	0.09	0.12	0.13

Table 2.2 gives some relevant information in how different possibilities for speed-loss are handled. In general, the power is either increased to keep velocity constant, or the power is kept constant, resulting in lower speed. When calculating the cross-correlation, the turning rate and the drift angle is in absolute values. As all correlations are positive, it implies that the velocity increases with turning rate and drift angle. Velocity is expected to increase in relation to turning rate according to Karlsen (1997), as the trawl takes a shorter path, leading to decreased tension in the wires, and the tension is lowest when exiting a turn. This can be the reason for the increased velocity when enduring a drift angle, as the drift angle is not necessarily due to environmental forces; it could be after a turn, when the drift angle corrects for the course-normal trawl forces. The correlation is stronger for the propeller power than the velocity, meaning Prestfjord prefers increasing the power to losing velocity. This refers to the velocity of the trawl, as both power and ship velocity is increased.

Chapter 3

Manoeuvring theory

3.1 Newton-Euler versus Lagrangian Formulation

Section 3.1 is taken from Åsbø (2016). Some modifications are made to adapt it to the current task.

The different ways to set up nonlinear equations of motion is discussed in Fossen (1994). Using Newton's Second Law, Euler proposed axioms to conserve angular and linear momentum. This approach of formulating the equations is commonly known as vectorial mechanics, and is often used in manoeuvring models. The Lagrangian formulation express energy preservation instead, using well established models for hydrodynamic effects. The Lagrangian approach leads to a set of differential equations equal to the number of DOF. This means the regular surge-pitch-yaw model of Euler angles must be used, as Euler-parameters contain one extra parameter. As the Euler-parameter approach is more efficient, and avoids singularities at yaw angles larger than $\pm 180°$, it would be more robust and efficient. Selecting the Euler-angles approach is therefore less robust, despite being most used. This problem is related to singularities, and can be easily avoided with wrapping the angles to stay within range.

The Lagrangian approach uses generalized coordinates. Generalizing the body-fixed coordinate system gives little sense as $\int \mathbf{v} dt$ has no relevant physical interpretation. Methods are developed, making body-fixed coordinates applicable for a Lagrangian approach. Kirchhoff's equation is a common method, but it does not include gravitational forces. If the gravitational forces are important, the quasi-Lagrange equations of motion can be used. In application to a 3DOF manoeuvring model, gravity is not considered important, so the Kirchhoff equations should be sufficient for making generalized coordinates based of the body-fixed coordinate system. The Kirchoff equations can be found in Fossen (2011):

$$T = \frac{1}{2}\mathbf{v^T M v} \tag{3.1.1}$$

$$\tau_\mathbf{1} = \frac{d}{dt}\left(\frac{\partial T}{\partial \mathbf{v_1}}\right) + \mathbf{S}(\mathbf{v_2})\frac{\partial \mathbf{T}}{\partial \mathbf{v_1}} \tag{3.1.2}$$

$$\tau_\mathbf{2} = \frac{d}{dt}\left(\frac{\partial T}{\partial \mathbf{v_2}}\right) + \mathbf{S}(\mathbf{v_2})\frac{\partial \mathbf{T}}{\partial \mathbf{v_2}} + \mathbf{S}(\mathbf{v_1})\frac{\partial \mathbf{T}}{\partial \mathbf{v_1}} \tag{3.1.3}$$

$$\mathbf{S}(\lambda) = \begin{bmatrix} 0 & -\lambda_3 & \lambda_2 \\ \lambda_3 & 0 & -\lambda_1 \\ -\lambda_2 & \lambda_1 & 0 \end{bmatrix} \tag{3.1.4}$$

$$\mathbf{v_1} = [u, v, w]^T$$

$$\mathbf{v_2} = [p, q, r]^T$$

$$\tau_\mathbf{1} = [X, Y, Z]^T$$

$$\tau_\mathbf{2} = [K, M, N]^T$$

3.2 Reference frames

The equations of motion can be solved in any reference frame. Reference frames are either inertial or not inertial, meaning they either conserve kinetic energy directly, or the equations need to be modified to do so. The truly inertial reference frame is the Earth-Centred-Inertial frame, with origin at the centre of the Earth, not rotating with the Earth, therefore also including Coriolis acceleration. The NED reference system, denoted $\{n\}$, is here used as the inertial system, a common and sufficiently inertial system for most ship operations because the Coriolis accelerations are small compared to other accelerations.

The ship's reference system is called the body fixed reference system, denoted $\{b\}$. It is not inertial. The origin of the body-fixed reference system, is preferably the Centre of gravity (COG). Very often, the COG is varying. An arbitrary Centre of origin (CO) can be used as origin instead, usually placed midship on the waterline (Fossen 2011), with the distance between CO and COG as an input for the model. The manoeuvring model used is derived from Kirchhoff's equations (Ross 2008), so centripetal terms correct the inertial terms in the body fixed reference frame, as it is not an inertial reference frame, so the kinetic energy is conserved.

Transformation to other coordinate systems is still necessary here, despite the conservation of kinetic energy of the ship. The trawl forces will not move with the ship when reducing drift angle. They are assumed constant in the inertial reference

frame. Environmental forces are also set to stay constant in the inertial reference frame.
Another relevant reference frame is the flow reference frame, with the x-axis parallel to the flow axis, used to transform the rudder forces, and currents.
Transformation between the reference frames including heave, roll and pitch can be found in Ross (2008) and Fossen (2011). Transformation between the different reference frames, when only surge-sway-yaw is considered is done the following way:

$$\mathbf{v^{to}} = \mathbf{R^{to}_{from}} \mathbf{v^{from}} \tag{3.2.1}$$

$$\mathbf{R^n_b} = \begin{bmatrix} cos(\psi) & -sin(\psi) & 0 \\ sin(\psi) & cos(\psi) & 0 \\ 0 & 0 & 1 \end{bmatrix} \tag{3.2.2}$$

$$\mathbf{R^b_n} = \begin{bmatrix} cos(\psi) & sin(\psi) & 0 \\ -sin(\psi) & cos(\psi) & 0 \\ 0 & 0 & 1 \end{bmatrix} \tag{3.2.3}$$

$$\mathbf{R^f_b} = \begin{bmatrix} cos(\beta) & sin(\beta) & 0 \\ -sin(\beta) & cos(\beta) & 0 \\ 0 & 0 & 1 \end{bmatrix} \tag{3.2.4}$$

$$\mathbf{R^b_f} = \begin{bmatrix} cos(\beta) & -sin(\beta) & 0 \\ sin(\beta) & cos(\beta) & 0 \\ 0 & 0 & 1 \end{bmatrix} \tag{3.2.5}$$

b	Body reference system
n	North-East-Down reference system
f	Flow reference system

3.3 Manoeuvring models

Section 3.3 is taken from Åsbø (2016). Some modifications are made to adapt it to the current task.

Some standard manoeuvring models are described in Fossen (2011).

Knowledge about the forces acting on a ship during manoeuvring is essential to set up the parameters in the model. Not including environmental forces and control forces, three groups of forces act on a ship. These are the rigid body kinetics, hydrodynamic kinematics, and hydrostatic and gravitational forces. Hydrostatic forces and gravity is not discussed in this thesis, as they are only relevant for heave, pitch and roll. In a vectorial setting, the equations of motion for marine craft can be presented as (Fossen 2011):

$$\tau_{\mathbf{RB}} = \tau_{\mathbf{hyd}} + \tau_{\mathbf{hs}} + \tau_{\mathbf{wind}} + \tau_{\mathbf{wave}} + \tau_{\mathbf{control}} \tag{3.3.1}$$

$$\tau_{\mathbf{hs}} = -\mathbf{g}(\eta) - \mathbf{g_0} \tag{3.3.2}$$

$$\tau_{\mathbf{hyd}} = -\mathbf{M_A}\dot{\mathbf{v}}_\mathbf{r} - \mathbf{C}(\mathbf{v_r})_\mathbf{A}\mathbf{v_r} - \mathbf{D}(\mathbf{v_r})\mathbf{v_r} \tag{3.3.3}$$

$$\begin{aligned}\tau_{\mathbf{control}} + \tau_{\mathbf{wind}} + \tau_{\mathbf{wave}} &= \mathbf{M_{RB}}\dot{\mathbf{v}} + \mathbf{C}(\mathbf{v})_\mathbf{RB}\mathbf{v} \\ &\quad + \mathbf{M_A}\dot{\mathbf{v}}_\mathbf{r} + \mathbf{C}(\mathbf{v_r})_\mathbf{A}\mathbf{v_r} + \mathbf{D}(\mathbf{v_r})\mathbf{v_r} + \mathbf{g}(\eta) + \mathbf{g_0}\end{aligned} \tag{3.3.4}$$

$$\eta = [x, y, z, \phi, \theta, \psi]$$

$$\mathbf{v} = [u, v, w, p, q, r]$$

$$\mathbf{v_r} = \mathbf{v} - \mathbf{v_{current}}$$

A linear coupled 6 degree of freedom (DOF) model will have 36 elements in the matrices for mass, damping and restoring forces, in addition to external forces such as control surfaces, waves, and propulsion. The elements in the mass and centripetal matrices also contain two parameters each, the kinematic, or hydrodynamic parameters, and the kinetic, rigid body parameters. This leads to a very large number of parameters. Many are zero by symmetry, such as coupled sway and surge, while the restoring coefficients in surge, sway and yaw are zero, as long as there is no mooring system in place. For a ship in trawl, there will be a small restoring coefficient for the ship in these degrees of freedom. If the model is non-linear as well, such as proposed by Abkowitz (1964), where a Taylor series expansion is used to the third power for damping, while added mass is assumed linear. Only the odd terms (proportional to $\dot{\eta}$ or $\dot{\eta}^3$) is included. The even terms would be unphysical, as a constant force and a force with constant direction. The

non-linearity can also be approximated with the second-order part of the Taylor series, by use of absolute values, i.e. proportional to $\dot{\eta}|\dot{\eta}|$. The non-linearity in the damping terms are motivated by the square law damping in fluid dynamics Fossen (2011).
Instead of the full 6DOF model, a 3DOF model can be applied for the horizontal movement of a ship. These models are most relevant here, as the full-scale data does not include motions in roll, heave or pitch. SNAME notation is used throughout this report, and is listed in Table 3.1 (Fossen 2011).

Table 3.1. SNAME notation.

DOF		**SNAME, forces and moments**	**Translational and angular velocities**	**Positions and Euler angles**
1	Surge (Translation along x)	X	u	x
2	Sway (Translation along y)	Y	v	y
3	Heave (Translation along z)	Z	w	z
4	Roll (Rotation around x)	K	p	ϕ
5	Pitch (Rotation around y)	M	q	θ
6	Yaw (Rotation around z)	N	r	ψ

The degrees of freedom relevant for the data is surge sway and yaw, or 1, 2 and 6 as listed in Table 3.1

3.4 Added Mass

Section 3.4 is taken from Åsbø (2016). Some modifications are made to adapt it to the current task.

Added mass is hydrodynamic pressure forces that are proportional to acceleration, coming from the kinetic energy that arises in the water around the ship. This is very often grouped with the mass of the ship, while in reality it is related to the acceleration and velocity of the movement relative to the current. It is related to the velocity because of centripetal forces, generally not negligible. The validity of this is related to the validity of assuming that current is negligible. As the ship is equipped with a speed logger, and the velocity during trawling is low, the possibility of including currents should be investigated.

The added mass terms are frequency dependent and velocity dependent. For infinite frequency or zero-speed, the added mass matrix is symmetric (Ross 2008). A zero-frequency approximation is used in this thesis, as it is most sensible for surge, sway and yaw.

$$\mathbf{M_A} = -\begin{bmatrix} X_{\dot{u}} & X_{\dot{v}} & X_{\dot{w}} & X_{\dot{p}} & X_{\dot{q}} & X_{\dot{r}} \\ Y_{\dot{u}} & Y_{\dot{v}} & Y_{\dot{w}} & Y_{\dot{p}} & Y_{\dot{q}} & Y_{\dot{r}} \\ K_{\dot{u}} & K_{\dot{v}} & K_{\dot{w}} & K_{\dot{p}} & K_{\dot{q}} & K_{\dot{r}} \\ M_{\dot{u}} & M_{\dot{v}} & M_{\dot{w}} & M_{\dot{p}} & M_{\dot{q}} & M_{\dot{r}} \\ N_{\dot{u}} & N_{\dot{v}} & N_{\dot{w}} & N_{\dot{p}} & N_{\dot{q}} & N_{\dot{r}} \end{bmatrix} \approx -\begin{bmatrix} X_{\dot{u}} & 0 & 0 \\ 0 & Y_{\dot{v}} & Y_{\dot{r}} \\ 0 & N_{\dot{v}} & N_{\dot{r}} \end{bmatrix} \tag{3.4.1}$$

In Equation 3.4.1, heave, pitch and roll velocities are 0, and surge is assumed separable from sway and yaw. Applying Kirchhoff's equations, 3.1.1-3.1.3, the forces can be derived. This is shown for $Y_{\dot{r}}$:

$$T = \frac{1}{2} v \cdot Y_{\dot{r}} r \tag{3.4.2}$$

$$\frac{\partial T}{\mathbf{v_1}} = \begin{bmatrix} 0 & \frac{1}{2}Y_{\dot{r}} r & 0 \end{bmatrix}^T \tag{3.4.3}$$

$$\frac{\partial T}{\mathbf{v_2}} = \begin{bmatrix} 0 & 0 & \frac{1}{2}Y_{\dot{r}} v \end{bmatrix}^T \tag{3.4.4}$$

$$\tau_{\mathbf{1}}(\mathbf{Y_{\dot{r}}}) = \begin{bmatrix} 0 \\ \frac{1}{2}Y_{\dot{r}}\dot{r} \\ 0 \end{bmatrix} + \begin{bmatrix} 0 & -r & 0 \\ r & 0 & 0 \\ 0 & 0 & 0 \end{bmatrix} \cdot \begin{bmatrix} 0 \\ \frac{1}{2}Y_{\dot{r}} r \\ 0 \end{bmatrix} = \begin{bmatrix} -\frac{1}{2}Y_{\dot{r}} r^2 \\ \frac{1}{2}Y_{\dot{r}}\dot{r} \\ 0 \end{bmatrix} \tag{3.4.5}$$

In equation 3.4.5, it ends up with a force in x-direction proportional to the square of the yaw velocity. This is a centripetal acceleration term, while the element in y-direction is an inertia term. Two matrices then appears for the equations; the added mass inertia, and the added mass centripetal forces. The added mass matrix is as in equation 3.4.1, and the centripetal forces becomes:

$$\mathbf{C_A}(\mathbf{v_r}) = \begin{bmatrix} 0 & 0 & Y_{\dot{v}}v_r + \frac{1}{2}(N_{\dot{v}} + Y_{\dot{r}})r \\ 0 & 0 & -X_{\dot{u}}u_r \\ -Y_{\dot{v}}v_r - \frac{1}{2}(N_{\dot{v}} + Y_{\dot{r}})r & X_{\dot{u}}u_r & 0 \end{bmatrix} \tag{3.4.6}$$

3.5 Rigid Body Kinetics

Section 3.5 is taken from Åsbø (2016). Some modifications are made to adapt it to the current task.
The mass matrix is

$$\mathbf{M_{RB}} = \begin{bmatrix} m & 0 & -m \cdot y_g \\ 0 & m & m \cdot x_g \\ -m \cdot y_g & m \cdot x_g & I_z \end{bmatrix} = \begin{bmatrix} m & 0 & 0 \\ 0 & m & m \cdot x_g \\ 0 & m \cdot x_g & I_z \end{bmatrix} \tag{3.5.1}$$

In Equation 3.5.1, symmetry of the xz-plane is assumed, leading to $y_g = 0$. The mass matrix is assumed to be time-invariant. This is not really true for a trawler, as it is not carrying a fixed load from one port to another. This is done due to the fact that no information is given about change in draught or the weight of fish caught, so a variable mass would increase the number of parameters to identify.

It is useful to make the centripetal matrix velocity independent, so that velocities relative to current can be used. This is shown in Fossen (2011). By looking at Kirchoff's equations for 6DOF, and filling into a 2x2 matrix with elements of 3x3

matrices, it becomes:

$$\mathbf{C}(\mathbf{v})\mathbf{v} = \begin{bmatrix} \mathbf{0} & -\mathbf{S}(\frac{\partial \mathbf{T}}{\partial \mathbf{v_1}}) \\ -\mathbf{S}(\frac{\partial \mathbf{T}}{\partial \mathbf{v_1}}) & -\mathbf{S}(\frac{\partial \mathbf{T}}{\partial \mathbf{v_2}}) \end{bmatrix} \begin{bmatrix} \mathbf{v_1} \\ \mathbf{v_2} \end{bmatrix} \tag{3.5.2}$$

$$\begin{aligned} \mathbf{C_{RB}}(\mathbf{v}) &= \begin{bmatrix} \mathbf{0} & -m\mathbf{S}(\mathbf{v_1}) - \mathbf{mS}(\mathbf{v_2})\mathbf{S}(\mathbf{r_g^b}) \\ -m\mathbf{S}(\mathbf{v_1}) + \mathbf{mS}(\mathbf{v_2})\mathbf{S}(\mathbf{r_g^b}) & -\mathbf{S}(\mathbf{I_b}\mathbf{v_2}) \end{bmatrix} \\ &= \begin{bmatrix} m\mathbf{S}(\mathbf{v_2}) & -m\mathbf{S}(\mathbf{v_2})\mathbf{S}(\mathbf{r_g^b}) \\ m\mathbf{S}(\mathbf{v_2})\mathbf{S}(\mathbf{r_g^b}) & -\mathbf{S}(\mathbf{I_b}\mathbf{v_2}) \end{bmatrix} \end{aligned} \tag{3.5.3}$$

In equation 3.5.3, the cross-product property of a skew-symmetric matrix is used, meaning $\mathbf{S}(\mathbf{v_1})\mathbf{v_2} = -\mathbf{S}(\mathbf{v_2})\mathbf{v_1}$. If the current velocity is then irrotational and constant, it will not affect the solution to use $\mathbf{M}\dot{\mathbf{v}} + \mathbf{C_{RB}}(\mathbf{v})\mathbf{v} = \mathbf{M}\dot{\mathbf{v_r}} + \mathbf{C_{RB}}(\mathbf{v_r})\mathbf{v_r}$.

$$\mathbf{C_{RB}} = \begin{bmatrix} 0 & -m \cdot r & -m \cdot x_g \cdot r \\ m \cdot r & 0 & -m \cdot y_g \cdot r \\ m \cdot x_g \cdot r & m \cdot y_g \cdot r & 0 \end{bmatrix} \tag{3.5.4}$$

3.6 Ship resistance, drag in pure surge

3.6.1 Frictional resistance

Subsection 3.6.1 is taken from Åsbø (2016). Some modifications are made to adapt it to the current task.

$$X = -\frac{\rho}{2} \cdot S(1+k)C_f(u_r)|u_r|u_r = X_{|u|u}|u_r|u_r \tag{3.6.1}$$

$$C_f(u_r) = \frac{0.075}{log_{10}(R_n) - 2} + C_R \tag{3.6.2}$$

Equation 3.6.2 can be recognized as the friction formula of a flat plate, from ITTC 1957, with the roughness contribution. In Equation 3.6.1, k represents the form factor, a factor used to represent the increase in velocity, and therefore drag, due to thickness. For very small R_n this expression would blow up, and the ITTC'57 formula is only valid for fully turbulent flow. As long as $R_n > 10^6$, it is usually satisfactory to assume fully turbulent flow. This value is common to use for ships.

3.6.2 Low-Speed Drag

Subsection 3.6.2 is taken from Åsbø (2016). Some modifications are made to adapt it to the current task.

As trawling is happening at relatively low velocities in the vicinity of 4 knots, drag should be modelled with this in mind. At low-speed, the induced drag dominates, and decays as the velocity increases. The previously mentioned drag is of higher order, as profile drag is dominating during moderate velocities. In the proximity of 0-velocity, the derivative of drag with respect to velocity is then 0, so a linear term should be added. This linear term of induced drag should disappear as velocity is larger. An augmentation to the drag, satisfying this is given by Fossen (2011):

$$\mathbf{D_l} = \mathbf{D} \cdot \mathbf{v_r} \cdot \mathbf{exp}(-\alpha \mathbf{V_{rc}}) \tag{3.6.3}$$

$$\mathbf{D} = \begin{bmatrix} -X_u & 0 & 0 \\ 0 & -Y_v & -Y_r \\ 0 & -N_v & -N_r \end{bmatrix} \tag{3.6.4}$$

V_{rc} and $\mathbf{v_r}$ includes current velocities. α is a typical value to tune while perfecting the model. A convenient value to begin with is $\alpha = \frac{1}{2}$ (Ross 2008).

3.6.3 Other resistance components

Even though the frictional resistance usually is the definitively largest resistance component, there is other components that can be fairly large. Potential flow effects results in a ship's wake, a wave pattern transporting energy away, usually the second largest resistance component. This wave resistance is strongly dependent on F_N. The wake is produced along the whole ship, and results in two main wave patterns; diverging waves(a v-pattern behind the ship) and transverse waves (Steen 2014*b*). The strongest contributions to wake are produced where the hull-curvature is greatest; the bow and stern regions of the ship. Interference between these wave contributions leads to crests and troughs in the resistance as function of F_N.

For a ship with a submerged transom stern, transom stern resistance can be a large contribution to the total resistance. At low speed, this resistance is mostly due to recirculation of water, a chaotic backflow decreasing the pressure. At high speed, parts of the transom stern will be dry, leading to a loss of hydrostatic pressure in the aft, giving an even larger resistance.

Air resistance can be large for high-speed vessels, and for ships with large

superstructures. For conventional vessels it is usually taken as a values found for similar vessels (Steen 2014*b*). During trawl, air-resistance should therefore be small, even if including wind.

3.7 Drag forces, due to sway and yaw

There are different methods to include the forces that arise when the ship has a transverse velocity component. These forces are usually based on two principles: The ship as a low aspect ratio wing, linearly dependent on the transverse velocity, and cross-flow drag, proportional to the square of the transverse velocity.

3.7.1 Low Aspect-Ratio Lifting Surface

Section 3.7.1 is taken from Åsbø (2016). Some modifications are made to adapt it to the current task.

The ship can be regarded as a low-aspect-ratio foil, meaning that when heading and flow axis are different, there is an angle of attack creating lift and drag forces in the horizontal plane. The free surface condition gives an image body for the relevant Froude numbers, so the span of the foil is equal to twice the draught of the ship (Faltinsen 2005). In infinite fluid, with span s, chord length l, and a rectangular form, we get the following equations:

$$L = \rho U^2 \pi \frac{s^2}{2} \beta = \frac{\rho}{2} U^2 s l C_L(\beta) \tag{3.7.1}$$

$$M = -\rho U^2 0.125 \pi s^2 l \beta \tag{3.7.2}$$

$$C_L = 0.5 \Lambda \pi \beta \tag{3.7.3}$$

$$U = \sqrt{u^2 + (v + rx)^2} \tag{3.7.4}$$

This is a simplified version, that describes the principle in a good way by assuming stationary flow with zero yaw velocity. C_L is actually dependent on the Reynolds number, however this dependency is very small, as the relevant range of velocities is in the turbulent region (Ross 2008). As the lift force is orthogonal to the flow, this

is converted to the body-fixed frame using the transformation below:

$$\begin{bmatrix} X_{LD} \\ Y_{LD} \end{bmatrix} = \begin{bmatrix} -cos(\beta) & sin(\beta) \\ -sin(\beta) & -cos(\beta) \end{bmatrix} \begin{bmatrix} D \\ L \end{bmatrix} \tag{3.7.5}$$

$$N_{LD} = x_{cp} Y_{LD} \tag{3.7.6}$$

The subscript LD is to notify that it is from lift and drag, and cp is for centre of pressure.

3.7.2 Cross-Flow Drag

Subsection 3.7.2 is taken from Åsbø (2016). Some modifications are made to adapt it to the current task.

Cross-flow drag is the non-linear part that arises from an angle between heading and flow. In Faltinsen (1990), cross-flow assumes separation from the ship due to a velocity in the transverse direction. It assumes that longitudinal velocities does not influence the transverse forces. This is valid for angles of attack in the vicinity of 90°, while for angles of attack close to 0° they are estimated with estimating the ship and rudder as lifting surfaces as discussed in 3.7.1. This method could still be used to describe the non-linear parts of sway and yaw damping. The cross-flow principle is also commonly used in 3DOF first-principle models together with surge resistance, where surge is assumed uncoupled from sway and yaw (Fossen 2011).
The transverse force then becomes:

$$F_2^C = \frac{\rho}{2} \cdot \left[\int_L \cdot C_D^{2D}(x) \cdot T(x) \right] U_C^2 sin(\beta)|sin(\beta)|dx \tag{3.7.7}$$

$$\begin{aligned} F_6^C =& \frac{\rho}{2} \cdot \left[\int_L \cdot C_D^{2D}(x) \cdot T(x) \cdot x \right] U_C^2 sin(\beta)|sin(\beta)|dx \\ &+ \frac{1}{2} U_C^2 (A_{22} - A_{11}) sin(2\beta) \end{aligned} \tag{3.7.8}$$

$$U_C^2 sin(\beta)|sin(\beta)| = |v_r + xr|(v_r + xr) \tag{3.7.9}$$

$$A_{11} = -X_{\dot{u}}$$

$$A_{22} = -Y_{\dot{v}}$$

In the equations above (Faltinsen 1990), U_C is originally the current velocity, $T(x)$ is local draught, and β is the angle between the heading and flow. The last term in the yaw equation represents the Munk-moment, included in the hydrodynamic Coriolis and centripetal forces matrix. To avoid double counting of the moment,

it is neglected from cross-flow. By curve fitting, the integrals are avoided, and the manoeuvring model for cross-flow is obtained (Fossen 2011):

$$Y = Y_{|v|v}|v_r|v_r + Y_{|v|r}|v_r|r + Y_{v|r|}v_r|r| + Y_{|r|r}|r|r \tag{3.7.10}$$

$$N = N_{|v|v}|v_r|v_r + N_{|v|r}|v_r|r + N_{v|r|}v_r|r| + N_{|r|r}|r|r \tag{3.7.11}$$

The equations 3.7.10 and 3.7.11 are approximated due to the curve-fitting, but the accuracy is usually very good. The exception is when v_r and xr have different signs (Ross 2008).

Chapter 4

Modelling the forces and parameters

4.1 The Manoeuvring Model

4.1.1 ShipX

It was first thought to do a parameter estimation. After contacting a representative from SINTEF, this was established as a too difficult task with a high probability of poor results. Hydrodynamic coefficients are therefore found using ShipX Hullvisc, a part of the SIMAN package, originally meant for calculations in an early design stage. The coefficients given are then put in the manoeuvring model presented in Ross (2008) and Fossen (2011). The manoeuvring model is not as large, as Hullvisc only presents a limited amount of parameters.
A file containing the geometry input for ShipX was supplied by Rolls-Royce Marine. Some inputs were still necessary, such as the starting position of the skeg. Draught at the perpendiculars were given in the dataset as constant values. This draughts did not coincide with the loading condition in the ShipX file, and a new loading condition was made, and used, by taking the average of the two values as mean draught, and setting the difference between the forward perpendicular and the mean as trim.
A coefficient that is probably wrong is the rigid body moment of inertia in yaw. ShipX does not have a proper basis for calculating this, as it does not know the mass distribution of the vessel. The total mass could also be subject to small errors, proportional to the error in water density. A water density of $1028 kg \cdot m^{-3}$ has been assumed, as water temperature in the operational area is expected to be low. The parameters in the manoeuvring equations are assumed frequency independent, even though they are strongly frequency dependent.

4.1.2 Frequency dependence

Added mass in sway, have an approximate range of $(0.13 \rightarrow 1.3) \cdot A_{22,0}$ seen in Figure 5.3 in Fossen (2011). Linear damping B_{22} is roughly five times as large as the zero frequency damping at its highest. The frequency dependencies are similar for surge and yaw. The main cause of the strong frequency dependence is radiation forces, i.e. waves generated by the ship. To include this frequency dependency, a seakeeping model must be used instead of a manoeuvring model. An approach that allows the continued use of the body fixed reference frame and a time-domain calculation is adding a vector of fluid memory effects, and using the seakeeping reference frame with transformation matrices between $\{b\}$ and $\{s\}$. Another approach is the classical approach of a frequency domain model. Both approaches are described in detail in Fossen (2011).

4.1.3 Depth

Fishing banks are relatively shallow. Depth effects could therefore be important. The parameters used in the manoeuvring equations are dependent on depth, in combination with velocity. Two numbers are generally used when discussing effects of depth; ratio between depth and ship length, h/L, and the depth Froude number $F_{N_h} = \frac{U}{\sqrt{gh}}$. Depth dependency is given in Hullvisc; however, it is given in relation to depth alone. Four knots where used as service speed, meaning the results could be used during trawling.

Dependencies between parameters and depth are not included in the calculations, as the depth dependency at four knots is given for depths smaller than 36.2 meters, where there is no dependency at 36.2m. The smallest depth experienced during trawling is 45 meters, equivalent to $F_{N_h} \approx 0.1$. Faltinsen (2005) states that depth effects are negligible when $F_{N_h} <\approx 0.6$.

4.1.4 The manoeuvring equations used

The model used is:

$$\begin{aligned}\tau_{\mathbf{control}} &= \mathbf{M_{RB}}\dot{\mathbf{v}} + \mathbf{C}(\mathbf{v})_{\mathbf{RB}}\mathbf{v} \\ &+ \mathbf{M_A}\dot{\mathbf{v}} + \mathbf{C}(\mathbf{v})_{\mathbf{A}}\mathbf{v} + \mathbf{D}(\mathbf{v})\mathbf{v} + \mathbf{crossflow}\end{aligned} \tag{4.1.1}$$

$$\mathbf{M_{RB}} = \begin{bmatrix} m & 0 & 0 \\ 0 & m & m \cdot x_g \\ 0 & m \cdot x_g & I_z \end{bmatrix} \tag{4.1.2}$$

$$\mathbf{C_{RB}}(\mathbf{v}) = \begin{bmatrix} 0 & -m \cdot r & -m \cdot x_g \cdot r \\ m \cdot r & 0 & 0 \\ m \cdot x_g \cdot r & 0 & 0 \end{bmatrix} \tag{4.1.3}$$

$$\mathbf{M_A} = \begin{bmatrix} -X_{\dot{u}} & 0 & 0 \\ 0 & -Y_{\dot{v}} & -Y_{\dot{r}} \\ 0 & -Y_{\dot{v}} & -N_{\dot{r}} \end{bmatrix} \tag{4.1.4}$$

$$\mathbf{C_A}(\mathbf{v}) = \begin{bmatrix} 0 & 0 & Y_{\dot{v}} \cdot v + Y_{\dot{r}} \cdot r \\ 0 & 0 & -X_{\dot{u}} \cdot u \\ -Y_{\dot{v}} \cdot v - Y_{\dot{r}} \cdot r & X_{\dot{u}} \cdot u & 0 \end{bmatrix} \tag{4.1.5}$$

$$\mathbf{D}(\mathbf{v}) = \begin{bmatrix} -D_{1,1}(u) & -X_{vv} \cdot v - X_{v^2\beta^2} \cdot \frac{v^3}{u^2} & -X_{rr} \cdot r - X_{rv} \cdot v \\ 0 & -Y_{uv} \cdot u & -Y_{ur} \cdot u \\ 0 & -N_{uv} \cdot u & -N_{ur} \cdot u \end{bmatrix} \tag{4.1.6}$$

$$D_{1,1} \cdot u = \sum_{k=1}^{5} X_{u^k} \cdot u^k \tag{4.1.7}$$

$X_{v^2\beta^2}$ is noted $X_{vvvvdivuu}$ in ShipX. The different parameters used in Equations 4.1.2 to 4.1.6 are described in Table 4.1. Hullvisc gives sectional cross flow drag. This makes it appropriate to apply 2D+t-theory to calculate the cross flow drag and moment on the ship, instead of a curve fitting to make non-linear parameters. The method is explained in Subsection 4.1.6.

Table 4.1. Manoeuvring coefficients

Parameter	Description
m	Ship mass
x_g	Distance between origin of body fixed coordinate system and the centre of gravity.
I_z	Yaw inertia
$\dot{\mathbf{v}}$	$[\dot{u} \quad \dot{v} \quad \dot{r}]^T$, is the acceleration vector, with surge, sway and yaw, respectively.
$\mathbf{v}$	$[u \quad v \quad r]^T$, is the velocity vector, with surge, sway and yaw, respectively.
$X_{\dot{u}}$	Added mass in surge.
$Y_{\dot{v}}$	Added mass in sway.
$Y_{\dot{r}}$	Coupled added mass in sway-yaw. This is equal to $N_{\dot{v}}$, and is therefore used in its place. Coupled added mass represents the force in one direction due to an acceleration in the other.
$N_{\dot{r}}$	Added mass in yaw.
X_{vv}	Force in surge due to sway velocity. A part of hull-lift forces.
X_{rv}	Force in surge due to sway and yaw velocity. A part of hull-lift forces.
X_{rr}	Force in surge due to yaw velocity. A part of hull-lift forces.
$X_{vv\beta\beta}$	Force in surge due to sway velocity. A part of hull-lift forces.

X_{u^k}	Part of the drag polynomial representing the surge resistance on a straight course without sway velocity. This is mainly due to friction, proportional to velocity squared, however, other effects such as wave-making.
Y_{uv}	Represents the circulatory hull-lift. It could also be written as $Y_{uu\beta}$, as $\beta = atan(v/u) \approx v/u$ for small angles.
Y_{ur}	Hull-lift force. Due to difference in sectional velocity as a function of yaw velocity, $v_n = v + r \cdot x_n$, total lift also changes with yaw velocity.
N_{uv}	The lift forces does not necessarily coincide with the origin, and is typically at a quarter chord length from the leading edge on a flat plate. Skeg, rudder and hull-shape changes the pressure distribution to move this behind the centre of gravity so it becomes a stabilising moment.
N_{ur}	The change of hull-lift moment due to difference in sectional velocity, $v_n = v + r \cdot x_n$.
$\tau_{control}$	Control vector, containing forces and moments from trawl, propeller and rudder.

4.1.5 The surge polynomial

The polynomial of surge resistance does not have an obviously largest second order parameter. Therefore it must an interpolation polynomial, not a result of a sum of equations representing the first principles. This does not mean the underlying data is not from first principles, only that the accuracy of the polynomial should decrease for velocities far from the service speed given as input. The first order term of the polynomial is fairly strong, giving reason to believe that low-speed drag is included during the calculations in ShipX. As ShipX is based on potential theory, usually giving good results for wave resistance, this is also assumed to be included.

4.1.6 Cross Flow Drag - 2D+time

Cross-flow drag assumes that the transverse velocity is much larger than the longitudinal velocity. This is of course not valid during most operations. Cross-flow drag is due to vortex shedding, which needs time to build up. The time variation of cross flow drag on cylinders has been investigated before, and is found in Faltinsen (2005). 2D+t is a strip-theory formulation of cross-flow drag, where the vortex shedding at a strip is assumed to have developed to the time $t = x/u$, where x is the strip's distance from the bow. As the development time of a vortex is also dependent on the transverse velocity and the radius of the cylinder, a non-dimensional time is used, $t' = \frac{v \cdot t}{R} - 0.351$. The reason for the time shift of $0.351[-]$, is that separation typically starts when the non-dimensional time is 0.351. When $t' < 0$, cross-flow drag is set to zero. Experimental data on the drag coefficients of circular cylinders have been fitted to a polynomial of t', in the fifth order. The validity of the polynomial is set to $t' = 26$, as it has reached a flat area, representing the steady state drag. Every polynomial coefficient is multiplied with the sectional cross-flow drag from ShipX, divided by the value of the polynomial for a circular cylinder at $t' = 26$. Sectional draught is used as radius in the calculations.

4.2 Propeller

Thrust provided by the propeller is rarely measured in full-scale, as it is a lot easier to measure the torque, revolutions, velocity, and pitch. Different propeller series are used to find thrust from the measured quantities represented as non-dimensional quantities, based on model tests. The Wageningen D-series has been selected for this purpose.

4.2.1 Information about the Wageningen C and D-series

The Wageningen C and D-series is a result from a joint industry project performed at The Maritime Research Institute Netherlands (MARIN). The C-series is for controllable pitch propellers (CPPs), and the D-series for ducted CPPs. The goal of the project was to better understand the off-design conditions of CPPs. The series are not publicly available, and the alternative is the older Wageningen Ka-series. The main difference is that the C and D-series are made for several design pitches, while the Ka-series assumes design pitch at the pitch input. Another large difference

is the coefficients used. Wageningen C and D-series uses coefficients better suited for off-design conditions than the regular K_T and K_Q.

$$K_T = \frac{T}{\rho \cdot n^2 \cdot D^4} = K_{TP} + K_{Td} \tag{4.2.1}$$

$$K_Q = \frac{Q}{\rho \cdot n^2 \cdot D^5} \tag{4.2.2}$$

$$J_A = \frac{V_A}{n \cdot D} = \frac{V(1-w)}{\cdot n \cdot D} \tag{4.2.3}$$

$$V_r = \sqrt{V_A^2 + (0.7\pi nD)^2} \tag{4.2.4}$$

$$C_T = \frac{T}{\left(\frac{1}{2} \cdot \rho \cdot V_r^2\right) \frac{\pi}{4} D^2} \tag{4.2.5}$$

$$C_Q = \frac{T}{\left(\frac{1}{2} \cdot \rho \cdot V_r^2\right) \frac{\pi}{4} D^3} \tag{4.2.6}$$

$$\beta = tan^{-1}\left(\frac{V_A}{0.7\pi nD}\right) \tag{4.2.7}$$

4.2.2 Method of calculation

Data from one quadrant for the D-series propeller most similar to Prestfjord's was provided by Rolls-Royce. The differences were insignificant. The data was in K_T, K_Q, J and pitch, not as in the full four quadrant series using $J \cdot cos(\beta)$, C_T and C_Q where β is the blade inflow angle, C_T is the thrust loading coefficient and C_Q is made non-dimensional similarly to C_T. Equations 4.2.1-4.2.7 shows how the different parameters are calculated. The set matched the points measured when making the series, and was not a series of coefficients for a polynomial or Fourier-expansion.

To make the series applicable to the measurements, different interpolation techniques were tried to make input/output functions for thrust and torque. Thrust and torque were given one model each, both having the advance number and the pitch as input. As there is two input parameters, the models are surface models, not curve models,

meaning some of MATLAB's built-in curve-fitting tools were not applicable, such as Fourier series and exponential series.

A polynomial fit was tried first, with MATLAB's highest order of 5 for each input. Coupled polynomial coefficients are also considered, to a total order of 5, e.g (3,2), (4,1), (3,1). The method was compared to different interpolation methods available. Thin-plate spline interpolation is good for smooth surfaces, and for extrapolation (MATLAB 2015). Extrapolation will not be necessary for this propeller series; however this property means it should be good at preserving the shape, a property desired due to the low resolution in pitch. Cubic spline interpolation, exclusive to surfaces, is a method that makes cubic polynomials between sets of three points. A biharmonic griddata method unique to MATLAB, mostly suited for scattered data, was also one of the methods tested here.

The quality of the resulting interpolations was easiest for the polynomial, as every parameter comes with a 95% confidence interval. Unfortunately, this method also provided one of the worse fits. In a visual interpretation, it is the only method that gives a visually clear deviation between the acquired surface, and the points from the series. When it comes to the R^2-values, the thin-plate spline interpolation is the only method, other than the polynomial fit, that is not exactly one. The other models managed to find a way to hit every point exactly with double precision, meaning that they follow thrust and torque as a function of advance number very well. When it comes to pitch, the points are too few to get an explicit solution. A perfect fit with the points does necessarily mean a physically reasonable solution, so the area between the points in the series must be validated in a different way. Mathematically, all points could be included in the model, if different polynomials are used for different points, or if the gradients are allowed to change sign as necessary for the fit. The last option would result in oscillation between the points, and therefore not be physical, despite the mathematical accuracy. The gradients should only change sign between points that are natural extremes. Selection of model was therefore done by a visual interpretation, where it was seen that the biharmonic method gives some peaks towards the corners, implying that the gradient changes sign too often to give a physical meaning.

The cubic spline and the thin-plate spline interpolation methods yield visually similar results, and looks physically reasonable between the points. As the

cubic spline model manages to follow every point, and gives a physically sound visualization of the surface, it is chosen to represent the series. The cubic spline interpolation is a piecewise polynomial, meaning different points use different polynomials. This is not desired; however, it is the best option due to limitations of tools, and it gives reasonable solutions.

4.2.3 Propeller scaling

Open water diagrams are often not scaled, because the common, and publicly available methods for scaling thrust and torque coefficients are unreliable. ITTC'78 (ITTC Revised 2011), based on Lerb's method, is standard way of scaling propulsive factors on open propellers. According to Bhattacharyya et al. (2015), using this method directly on ducted propellers fails to accord for scale effects on the duct thrust. From CFD results it is then concluded that ducted propellers require a different method. The model tests used by Bhattacharyya et al. (2015), was done at chord Reynold's numbers (R_Ns) in the range $7.5-8\cdot10^5$, at 70% propeller radius (R). Data regarding the Wageningen D-series is not easily accessible, so the chord R_Ns can only be assumed to be in the same range as for the C-4.40-series found in Dang et al. (2013), $2.2-5\cdot10^5$. The large spread in R_Ns for the Wageningen C-series is due to varying revolutions per minute (RPM), while for most of the series it is in the range $4-5\cdot10^5$. The alternatives for scaling the propeller series is then to use the method proposed by Bhattacharyya et al. (2015), or to not scale the propulsive coefficients. Bhattacharyya et al. states that the method shows promising results, but needs work before applying it to general cases. The duct-propeller model used has a blade area ratio (BAR) of 0.64, 4 blades, design pitch of 1.236, and a 19A duct. The propulsive coefficients does not have a large scale effect. A problem with the 19A-duct is flow separation that happens at light loads for model scale. Flow separation changes with R_N, and is hard to scale. The difference in R_N between the D-series and Bhattacharyya et al.'s test case could therefore be an issue. The propulsive coefficients are therefore not scaled for this thesis.

4.2.4 Wake and thrust deduction

The main reason for thrust-deduction is a pressure effect on the hull. Velocity of the water is higher close to the propeller, as it accelerates the water. With an accelerating duct, most of the water acceleration happens before the propeller, giving an even larger increase to velocity. The increased velocity means reduced pressure,

so that the pressure behind the ship is lower than in the bow, creating a pressure force pulling the ship backwards. Conservation of momentum makes this directly proportional to thrust, and is therefore simplified as a constant factor to multiply with thrust. As this is mainly a potential flow effect, it is commonly assumed to be free from scale effects (Steen 2014*c*). Model tests were done with a ducted propeller, and should provide good accuracy.

The propeller experiences a different velocity than the ship velocity due to the presence of a hull. Wake is made by wavemaking, potential effects (such as hull-shape), and friction. The frictional part of the wake is scale-dependent. Potential flow effects, are not, so they are collected in the term w_0, to not be included in the scaling. Waves are also potential flow effects, and therefore part of w_0. Wake has been scaled following Equation 4.2.8, by ITTC (Revised 2011):

$$w_s = w_0 + (w_m - w_0) \cdot \left(\frac{C_{Fs} + \Delta C_F}{C_{Fm}} \right)^m \tag{4.2.8}$$

$$m = 1$$

$$w_0 = 0.04 + t$$

Subscript s for ship and m for model

$t =$ thrust deduction

$C_F =$ Frictional resistance coefficient

$\Delta C_F =$ Roughness correction

This effect varies across the propeller, and is often assumed to be constant. Behind the propeller, a constant wake is more realistic, as the differences disappear due to violent mixing in the slipstream and across the propeller. The part of the rudder inside the slipstream therefore experiences a fairly constant velocity field, at least regarding the wake from the hull. The small section of the rudder that is outside the slipstream has been given the wake velocity the propeller blade tips experiences at the same radial position. For the propeller, a constant wake field is assumed, despite the fact that in reality, it is both radially varying, and harmonically oscillating.

4.2.5 Propeller Pitch

As the propeller pitch is given without unit, it must be found. This is done by finding the value corresponding to 100%, using the built-in MATLAB function *fminbnd* on

Equation 4.2.9, with boundaries 0.5 and 1.4, as used in the Wageningen-D series. The Helicon-X controller operates with different modes (Steen 2016). What is set to be 100% pitch depends on the mode, not the physical limitation of the propeller. The maximum pitch is therefore calculated separately for single-trawl, double-trawl, transit, and low-speed (See Section 2.4 for definition).

$$f(P_{max}) = median\left(\frac{\sqrt{\left(\boldsymbol{K}_{Q,wD}\left(\boldsymbol{J}, P_{max}\cdot\frac{\boldsymbol{P}[\%]}{100}\right) - \boldsymbol{K}_Q\right)^2}}{\boldsymbol{K}_Q}\right) \tag{4.2.9}$$

P_{max} = Maximum pitch

$\boldsymbol{K}_{Q,wD}$ = Torque coefficient from propeller series

$\boldsymbol{K}_Q$ = Torque coefficient calculated from data

Bold symbols are vectors, operations here are element-wise

4.3 Rudder

Most of the rudder span is inside the propeller disk. The small part of the rudder outside the disk, has the velocity of the wake field (Molland & Turnock 2007). The area of the far-field slipstream is found through axial momentum theory, showing that it is equal to the propeller area, varying with roughly 5%. This is sufficiently close to constant for an assuming the area of the far field slipstream is equal to the propeller disk area for potential theory without large errors. This is a common assumption (Steen 2014*c*). The area of the slipstream can't change a lot between operations, as flow across a foil (the duct), must leave a foil tangentially to the trailing edge. This is called the Kutta-condition. The small variations in area comes from a combination of a slightly blunt edge, giving a diffuse trailing edge, and simplifications in simple momentum theory. It is not surprising that the common duct number 19 follows the common assumption of a slipstream area equal to the propeller disk area. The ratio between area of the far-field slipstream and the propeller disk was calculated using Equations 4.3.1-4.3.1, derived from equations

on simple momentum theory found in Steen (2014*c*):

$$\tau = \frac{C_{Tp}}{C_T} \tag{4.3.1}$$

$$a = \sqrt{1 + C_{Tp}} - 1 \tag{4.3.2}$$

$$b = \left(1 + \frac{a}{2}\right) \cdot \frac{1}{\tau - 1} \tag{4.3.3}$$

$$\frac{A_0}{A_P} = \frac{1 + 0.5 \cdot a + b}{1 + a} \tag{4.3.4}$$

τ Duct loading coefficient (1 for open propeller)

C_{Ti} Thrust nondimensionalized using $\left(0.5\rho A_p V^2\right)^{-1}$
i: blank - total, p - propeller, d - duct

Three lift and drag curves are used to represent the rudder forces, one for each trawl mode and one of transit. The curves were created by Ray Thomas Grebstad at Rolls-Royce Marine, from propulsion points given by the author. Drag and lift from these curves are made non-dimensional as lift and drag coefficients, to make them applicable to different propulsion points. The lift coefficients are calculated using Helmbolds formula, (Equation 4.3.5), for low-aspect ratio foils. The formula assumes straight and flat foils (Steen 2014*c*).

$$C_L = \Lambda \cdot \frac{2\pi \cdot \alpha}{2 + \sqrt{\Lambda^2 + 4}} \tag{4.3.5}$$

$\Lambda =$ Aspect ratio

It is assumed that the flap affects the lift in the same way as increased angle of

attack. The total angle of attack is calculated using Equations 4.3.6 & 4.3.7:

$$\alpha = \alpha_{rud} + \eta\alpha_{flap} \tag{4.3.6}$$

$$\eta = 0.775\sqrt{\frac{c_{flap}}{2 \cdot c}} \tag{4.3.7}$$

$$c_{flap} = \text{Flap chord length}$$

$$c = \text{Total chord length}$$

4.3.1 Rudder zeroing & inflow angle

Zeroing

The true zero of the rudder angle is not certain, as the mean value of the true rudder angle could be different to zero. The time series is more than long enough to assume that removing the mean value would accurately set the zero value of any measurement expected to have a zero-mean value, such as a rudder. The measurements of the rudder angle could already be zeroed, as it is established in Section 2.2, meaning that the mean angle is due to asymmetries in the flow. The rudder has slightly more span above the propeller hub than below, giving a zero-lift angle different than zero. As the slipstream of a propeller is a very unpredictable flow pattern, which in general gives a non-zero angle of attack on the rudder. This angle of attack is different along the rudder span, because of the rotational flow in the slipstream. As a result, the rudder gives lift in one y-direction below the propeller hub, and the other direction above, at zero angle. Both sides of the hub will give a positive x-component in lift, often larger than the increased rudder drag from the slipstream induced angle of attack (Molland & Turnock 2007). For an ideal slipstream, and a rudder with equal area at both sides of the propeller hub, the y-component of lift is zero at zero rudder angle, as the top and bottom part cancels each other. As neither of these conditions are completely fulfilled, the rudder angle will be different to zero when not producing lift. The zero lift angle will be different for different propulsion points, zeroing of the rudder angle is therefore done separately for each mode. Preferably, large variations in thrust loading would be zeroed separately; however, these are the points where the lift is significantly different to zero, possibly with a non-zero mean.

Inflow angle on the rudder

The high thrust loading during trawling led to an initial assumption of $\alpha_{rud} \approx \delta$, meaning that the inflow to the rudder was assumed parallel to the ship. Large drift angles are also connected to trawl, and it was found that the assumption did not hold. Therefore, the sway velocity of the ship must be accounted for. This has been done the following way:

$$\alpha_{rud} = \delta - \bar{\delta}_{mode} - U \cdot \frac{HS \cdot sin(\beta_r)}{v_{rud}} \tag{4.3.8}$$

$$\bar{\delta}_{mode} = \text{Zeroing}$$

$$HS = \text{Straightening factor}$$

A value of 0.6 for hull straightening effects is suggested for additional foils in ShipX. The manual, Ringen (2017), does not discuss this value a lot, and it is meant for foils on the hull in general, such as roll damping foils, not the rudder. Including the value when a foil is added also gives a warning that this value is a coarse approximation. It is not clear how this factor is included, the most probable is $1-HS$. In Molland & Turnock (2007) studies are made on flow straightening effects. The effect is found to increase with increasing drift angle, thrust loading, and length of the hull. It should also be noted that the propeller duct gives an unknown flow straightening effect. Common values for HS should therefore not be valid, and it could be assumed that the flow straightening is stronger because of the duct. Literature discussing this effect when including a duct is not found. A few straightening factors were tried, and no flow straightening, $HS = 1$, was found to be best when considering residual yaw moment.

Reference system for rudder

Lift is orthogonal, while the drag is parallel to the flow. This means it is not completely accurate to assume that the lift acts purely in the sway direction. The largest error as a result from a change in inflow angle is not the direction of lift and drag, but the neutral angle of the rudder, and therefore the magnitude of lift and drag. For increased accuracy, the rudder was given its own flow reference system, decomposing the lift and drag forces into the body reference system using the zero-lift angle of the rudder.

4.3.2 Velocity over rudder

The propeller-rudder interaction can more accurately be defined by applying fluid-dynamics of jets. The shape of the velocity profile in the slipstream is hard to predict without using numerical tools. Velocities across the rudder are approximated as the mean velocity of the slipstream for the part affected by the propeller, and as the wake influenced velocity on the remaining part. Wake from the duct has not been considered. Some information about rudders in a propeller slipstream based on experimental data is found in Molland & Turnock (2007). The experimental data shows that the increased lift from propeller-induced velocities are less at high thrust loading, than what is found using momentum theory. This is evident when comparing Helmbold's lift coefficient for low aspect ratio wings to lift curves provided by Rolls-Royce, shown in Table 4.2.

The axial momentum theory assumes a uniform velocity field, while it is very different in reality. The propeller hub is an important influence, obstructing the flow, reducing the velocity in the centre. There is turbulent mixing between the slipstream and the water enclosing it. The turbulent mixing widens the slipstream, and changes the velocity profile, similar, yet different, to a uniform jet flow. In Brix (1993), an approximation to the radius and velocity is found. In Equation 4.3.9, the potential flow slipstream radius is assumed constant, equal to the propeller radius.

$$V_x = V_\infty \cdot \left(\frac{r_\infty}{r_x}\right)^2 = V_\infty \tag{4.3.9}$$

$$\Delta r = 0.15 \cdot x \cdot \frac{V_x - V_A}{V_x + V_A} \tag{4.3.10}$$

$$V_{corr} = (V_x - V_A)\left(\frac{r}{r + \Delta r}\right)^2 + V_A \tag{4.3.11}$$

∞	Values from the far-field in momentum theory
x	Distance from propeller
V_A	Advance velocity. Velocity corrected for wake

For the rudder forces to be accurately modelled, it is assumed that the magnitude of the lift coefficient compared to the theoretical value is not important, as long as it is sufficiently close. This is due to many unknown effects such as flap efficiency, rudder-hull aspect ratio effects (mirroring and gap), and the propeller induced

Table 4.2. Lift coefficient compared to theoretical values.

	Transit	Single trawl	Double trawl
Axial momentum theory	1.30	0.83	0.76
With turbulent mixing	1.04	1.04	1.06

velocities as mentioned earlier and in Molland & Turnock (2007). It is important that the ratio to the theoretical value is the same for different thrust loadings. The effect of turbulent mixing is therefore important to include, as seen in Table 4.2.

Sensitivity to number of strips

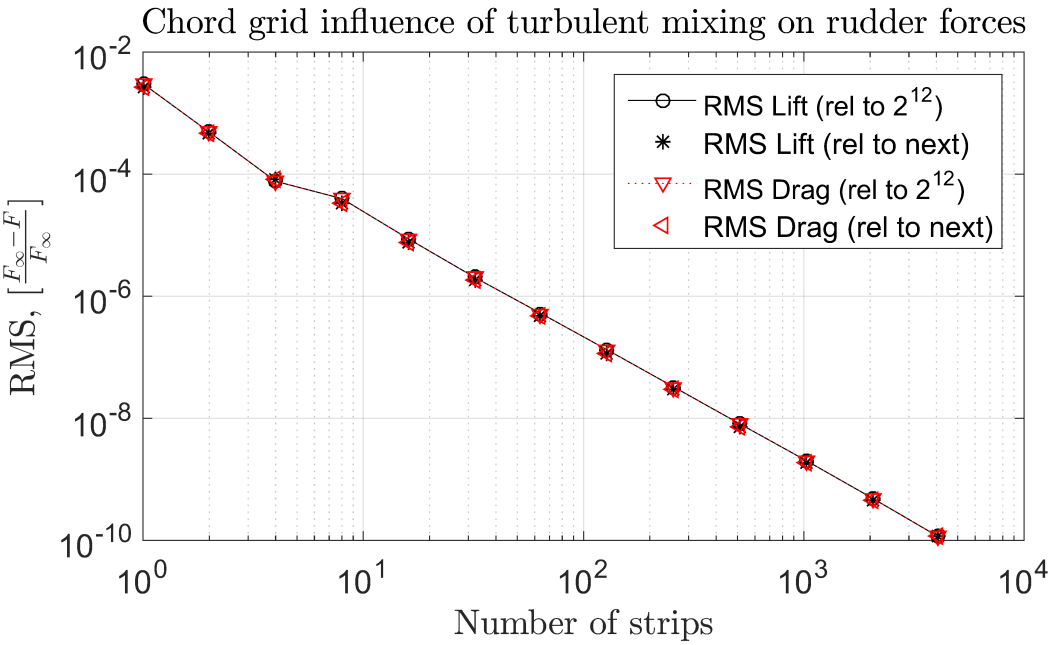

Figure 4.1. Influence of number of chord strips on lift and drag: Ratio of area of the two velocities, wake affected and slipstream affected, and the corresponding velocities are calculated for each strip, and the square of the velocities weighted by area is averaged.

In Figure 4.1 the error in lift force is shown to rapidly become negligible as the number of strips increase. Computationally expensive calculations with many strips are not necessary when finding the mean velocity across the rudder. Thirty strips are used, to make errors related to the grid size negligible.

4.3.3 Error sources

The errors related to the rudder is expected to be small, considering the fairly good fit between theory and the lift and drag curves. The rudder and propeller are treated separately, while they should be regarded as one unit. This leads to some error, that are minimized by basing the model on three curves, where propeller, rudder and ship are treated as one unit.

Time dependent lift

Time dependent lift is not taken into account when calculating the rudder forces. In potential theory, lift is made due to circulation in an otherwise uniform flow. This creates a higher total velocity on the low-pressure side, and a lower velocity on the high-pressure side of the foil, due to induced velocities from the vortex. This creates the pressure difference, resulting in lift. The vortex is bound, meaning the vortex does not stop at the tips of the foil. It continues orthogonal to the first vortex, creating *wash*. In other words, inducing velocities on the foil, reducing lift, due to a reduction in effective angle of attack. This tip vortex then continues to the point in the flow where the circulation was started. There it goes behind the foil, meeting the tip vortex from the other side, making the vortex bound. This last vortex is called a starting vortex, and it has the opposite sign of the vortex at the foil. In stationary flow, the starting vortex is neglected: Time has moved the foil so far ahead of it that it's effects are negligible, and the bound vortex is approximated with a horse-shoe (Steen 2014*c*).

A horse-shoe vortex is usually a good assumption, as the effect of circulation decays with distance squared. A change in circulation will also create a new bound vortex, equal to the change in magnitude, leading to a time dependent change in lift. Time dependent lift can be approximated using the Wagner-function or the Kuessner-function. A horse-shoe vortex is usually satisfactory when the starting vortex is ten chord lengths behind the foil (92% lift according to Kuessner, and 96% according to Wagner) (Steen 2014*c*). The Wagner-function is best for a sudden change in foil angle, while the Kuessner-function is better for changes in flow.

During manoeuvres it is seen that the rudder angle is increased for short periods of time, shape-similar to a sine-curve with a half-period of 20 seconds, constantly

changing the angle. Due to the large velocities across the rudder, the time-dependent lift only lasts between four and five seconds, and is therefore not important when a slowly changing rudder angle is assumed. The constantly changing rudder angles are unfortunate, as time dependencies will make the calculations exaggerate the lift forces during these periods.

For the steep part of such an oscillation in rudder angle, time dependent lift would be approximately 91% of the stationary-flow value. This is found by taking rudder angle at point $n-5$ and adding the change in rudder angle for each point up to n weighted by the Wagner function and comparing with the rudder angle at point n. The lift curve can be assumed linear with angle of attack at the points considered, relative difference in rudder angle can therefore be used in stead of lift. Values for the Wagner-function was read from Figure 8.2 in Steen (2014*c*).

4.4 Trawl

The tension in the wires are known. To apply this to the manoeuvring problem, the direction of these forces must be found. The first step is to project the forces onto the horizontal plane. To find the angle between the horizontal plane and the wires; water depth, and the shape of the wires, are needed. When the force in the horizontal plane is found, it must be decomposed into a longitudinal and a transverse component. To do this, the position of the trawl relative to the ship must be found.

4.4.1 Depth

A SHAPE file containing depth data of different resolution was downloaded from Geonorge (2011), and supplementary information about the projection was found at Kartverket (2016*a*) and Klokan Technologies (2012). The data is given as coordinates and depth of isobaths.

The map is subject to different inaccuracies and resolution, as it is collected from five different sources. It is therefore only meant for macro-scale computations and initial planning, not for navigation. The depth data is given as coordinates and depths of isobaths (lines through points of equal depth), in the Universal Transverse Mercator (UTM) coordinate system. UTM-coordinates are given as easting and northing,

relative to a reference point, in the same way a Cartesian coordinate system works. The world is divided into many zones of $6°E$ by $8°N$ (with exceptions). Zones have a number and a letter, e.g. $33N$, where the number is the latitude band, and the letter is the longitude band. The depth-curves are relative to UTM-zone 33N, and the reference system used is the Geodetic Reference System 1980 (GRS80). Reference systems are used to approximate the Earth's surface using an ellipsoid, generally represented as a major radius, and a flattening factor (Kartverket 2016*b*). This approximation results in a small error in the map projection.

The ships position is given in latitude and longitude. Latitude and longitude are geographic angles, giving an exact location on the surface of the earth, and is not subject to the errors of map projections (Kartverket 2016*c*). Projection errors of the ship are then hidden in the reference system used by the GPS. These errors are not important, as long as the isobaths and the ship is in the same system during calculations. The isobaths are interpolated from measurements with different grid sizes of 300m, 600m and 1000m. Down to 1000m depth, there is isobaths for every 50 meters of depth, and every 100 meters for deeper water. This is the best data available for the area, and it should suffice for finding depths to use in the catenary equations.

A scattered interpolant was used to create a function handle based on the ships UTM-coordinates. Matlab's mapping toolbox contains functions to accurately change between the latitude-longitude data for the ship, and the UTM-projection used in the map, as the reference ellipsoid is common, and one of the options in the toolbox. The isobaths relative to the coastline of Northern Norway with Svalbard is shown in Figure 4.2.

The largest error source is a result of the resolution, as the shape of the seabed between two isobaths is unknown. For example; small hills with elevation less than $50m$ has a possibility to not show. This error can be assumed to be less than $\pm 50m$. The grid resolution, when the data was collected, of up to 1000m could hide even larger variations in depth. The probability of such large errors is small, but could occur due to the length of the time series. It is also assumed that large gradients in depth is avoided during trawl, reducing the error.

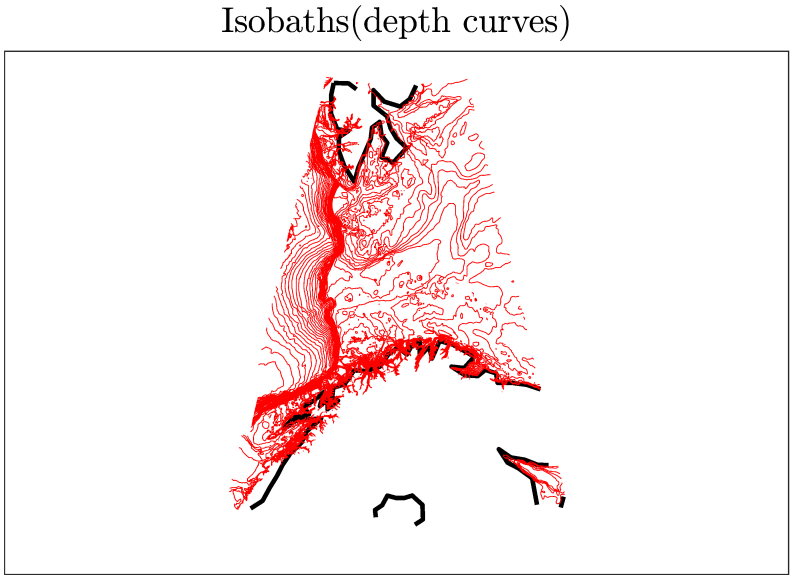

Figure 4.2. Depth curves: The loaded part of the depth contours/isobaths.

4.4.2 Angle between wires and the horizontal plane

Four methods have been tested. Two simple methods were compared first. The first is to use the Pythagorean theorem to assume a straight line between the ship and the trawl doors, neglecting change of shape due to the cable's own weight.

The second method is to assume that the forces are purely horizontal at the trawl doors, meaning the only vertical force contribution is the weight of wires. This gives the angle $\theta = sin^{-1}\left(F_{G,wire} \cdot F^{-1}_{measured}\right)$. Comparing the two results, for the example trawl operation in double trawl, on the port wire, gives the following results: method 1: 29°, method 2: 19°. This means the catenary equation would not reach the seabed for the assumption of only horizontal forces at the trawl doors. For bottom trawling this is therefore not a good method of calculating the force components. For pelagic trawling, this would not give good results either, as a vertical force would be necessary to lift the trawl and trawl doors.

A third method is to assume that the weight of wire gives a force resultant at the half length of the wire. Results from this is a 34 degree angle at the ship, and 16 degree angle at the trawl. This method was done to estimate the error from not including a catenary equation. Catenary equations describe the shape of flexible cables subjected to loads, for example the weight of the cable itself. This error of 5 degrees results in a 5.2% error in horizontal forces, so the weight of the cables should not be neglected.

To more accurately find the horizontal angle between the trawl wires and the horizontal plane, catenary equations are used. Inextensible wires are assumed. The known parameters for the catenary equations are y-coordinates, i.e depth and free surface/height of deck, total tension in end-points, submerged weight of wires per meter, and the arc-length (length of wire out).

Weight of wire per meter is approximate. The diameter of the wires are given, and weight of wires with similar thickness from Anderson (2007) is used. Buoyancy is included using the Specific gravity (SG) of steel by multiplying the weight with $(SG_{steel} - SG_{seawater}) \cdot SG_{steel}^{-1}$.

From Hibbeler & Fan (2010) the following equations are found:

$$x = \frac{F_H}{w_0}\left[sinh^{-1}\left(\frac{1}{F_H}(w_0 s + C_1)\right) + C_2\right] \tag{4.4.1}$$

$$\frac{dy}{dx} = \frac{1}{F_H}(w_0 s + C_1) \tag{4.4.2}$$

$$F_H = \text{Horizontal force (constant)}$$

$$w_0 = \text{Weight per meter}$$

$$C_n = \text{Integration constants}$$

By rewriting the Equations 4.4.1 and 4.4.2, and integrating, described by Equations 4.4.3-4.4.5, Equation 4.4.6 is found, applicable to this boundary value problem.

$$sinh\left(\frac{w_0}{F_H}x - C_2\right) = \left(\frac{1}{F_H}(w_0 s + C_1)\right) \tag{4.4.3}$$

$$\frac{dy}{dx} = sinh\left(\frac{w_0}{F_H}x - C_2\right) \tag{4.4.4}$$

$$y = \frac{F_H}{w_0}cosh\left[C_2 - \frac{w_0}{F_H}x\right] + C_3 \tag{4.4.5}$$

Using Equation 4.4.1:

$$\begin{aligned} y &= \frac{F_H}{w_0}cosh\left[C_2 - \frac{w_0}{F_H}\frac{F_H}{w_0}sinh^{-1}\left(\frac{1}{F_H}(w_0 s + C_1)\right) + C_2\right] + C_3 \\ &= \frac{F_H}{w_0}cosh\left[-sinh^{-1}\left(\frac{1}{F_H}(w_0 s + C_1)\right)\right] + C_3 \end{aligned} \tag{4.4.6}$$

The boundary value problem is then solved symbolically by Matlab, using *solve*.

The boundary conditions are:

$$0 = T \cdot cos\left(tan^{-1}\left(\frac{dy}{dx}\right)\right) - F_H \tag{4.4.7}$$

$$Depth = y\,(s = L) \tag{4.4.8}$$

$$0 = y\,(s = 0) \tag{4.4.9}$$

The three boundary conditions (4.4.7-4.4.9), are used to find F_H, C_1 and C_3 in Equations 4.4.2 and 4.4.6. Depth is positive here, due to the placement of the origin.

From this solution, C_2 is calculated by setting $x = 0$ at $s = 0$ in Equation 4.4.1:

$$C_2 = -sinh^{-1}\left(\frac{C_1}{F_H}\right) \tag{4.4.10}$$

The projected length is then found by inserting the constants, and setting $s = L$, in Equation 4.4.1.

Errors related to the catenary equation

The largest error here is that drag is not modelled. The angle would be reduced due to this, increasing the amount of forces in the horizontal plane. Using Morison's equation (Faltinsen 1990), the horizontal drag force on the wires at a depth of 350 meters would approximately be:

$$\begin{aligned} F_D &= \frac{1}{2}\rho \cdot D \cdot h \cdot |u|uC_D \\ &\approx \frac{1028}{2} \cdot 0.035 \cdot 350 \cdot |2|2 \cdot 1 = 25kN \end{aligned} \tag{4.4.11}$$

This is roughly 25% of the horizontal force from the catenary equations. This does not mean that the horizontal force is 25% larger, it means the horizontal forces are slightly larger, and a quarter of them have the wrong point of attack.

4.4.3 Position of trawl relative to the ship

To accurately calculate the directions of the trawl forces, the position of the trawls must be found. The first position of the trawls are chosen by setting the mid point, the projected length behind the ships middle trawl-block along the course. The following positions are calculated by updating the trawl-blocks' position, in the

NED reference system, by moving the mid-trawl wire along a straight line between the old position and the middle block's new position until the projected length is satisfied. For the single trawl, using only port-side and starboard wires, this is done using the mean value of the two. To find the position of the trawl doors, or the port-side and starboard wire ends, the law of cosines is used (Rottmann 2003):

$$\beta = cos^{-1}\left(\frac{a^2 + c^2 - b^2}{2ac}\right) \tag{4.4.12}$$

β	Angle across from b	
a	Half the spread of trawl doors	(4.4.13)
b	Projected length of wire	(4.4.14)
c	Distance between a side trawl block, and the position of the mid-wire end.	(4.4.15)

In Equation 4.4.12, c is calculated using the Pythagorean theorem on the new position of the mid-wire end and the position of the block connected to the wire that is currently calculated, in the NED-system. Spread of trawl doors common for a bottom trawler of this size is taken from (Valdemarsen 2015). For double trawling, an additional 35 meters is added. The assumed spread of the trawl doors is set as a preferred and maximum value. The trawl spread is given a lower boundary at $2L_{proj} \cdot cos(45°)$. The spread of the trawl doors is in reality dependent on different factors; length of sweeplines, length of wire, setting of trawl doors etc., so it is a coarse assumption to keep this constant.

The trawl would take an inner turn compared to the ship. As the data-set is logged once every second, this turn is slightly too sharp. One time-step moves the ship a certain length along the course. The code is given an integer value of how many sections one time-step should be separated into when updating the trawls position. The difference is small, even when comparing a 150 steps to 1, and for the calculations 10 steps are used.

4.4.4 Track of Prestfjord and the trawl during a selected haul

The track of the vessel and the trawl for an example operation is seen in Figure 4.3. The manoeuvre presented in Subsection 1.2.1 is visible in the upper right corner, as a fairly sharp turn from east to south, then constant course for a while, before turning towards south-west. The trawl track follows a shape similar to a demi-circle. This operation is used as an example for the rest of the thesis. This particular operation is chosen as an example due to the long duration, sections with a constant course at a moderate drift-angle, and manoeuvring with different turning rates.

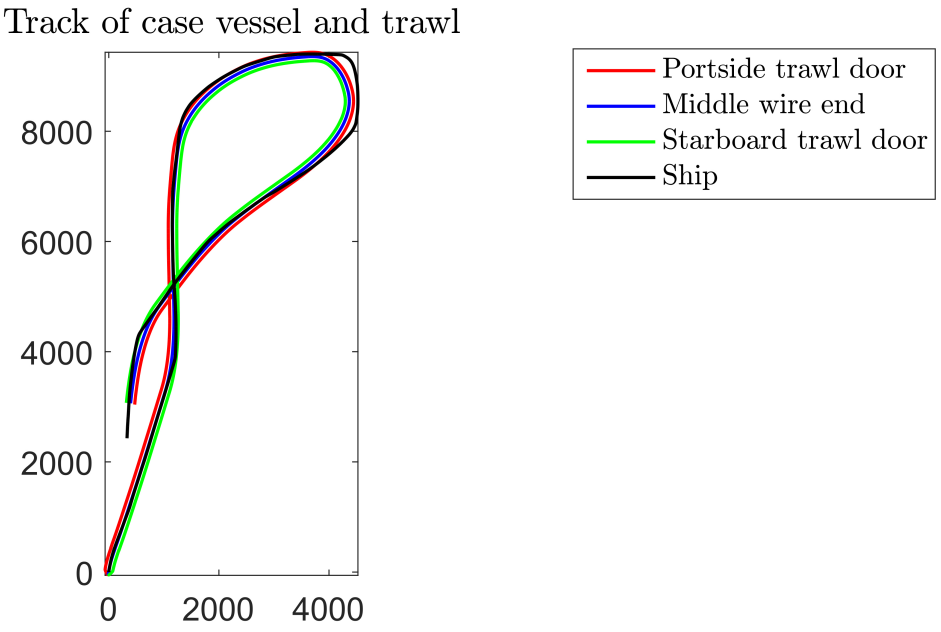

Figure 4.3. Track of the ship and trawl: Position of trawl and ship during a trawling operation with double trawl. The ships track starts at the origin.

4.4.5 Drag

When calculating the forces at the ship location, drag forces are modelled using Morison's equation (Faltinsen 1990). It is assumed that the velocity of the ship has a component orthogonal to the wire, equal to $U \cdot sin(\alpha)$ at the ship and zero at the trawl. It is further assumed that the deformation on the wires due to the drag is small enough to assume that the velocity is linearly increasing with s from the trawl position. The result is an update to the angle for decomposing the horizontal trawl forces, derived in Equations 4.4.16-4.4.18:

$$
\begin{aligned}
dF_D &= \frac{1}{2}\rho \cdot D \cdot |u| u C_D dL_0 && (4.4.16)\\
&= \frac{\rho}{2} \cdot D \cdot |U \cdot sin(\alpha)\frac{s}{L}| U \cdot sin(\alpha)\frac{s}{L} C_D dL_0 \\
&= \frac{\rho}{2} \cdot D \cdot (U \cdot sin(\alpha)\frac{s}{L})^2 C_D ds \cdot sin(\alpha) \\
F_D &= \frac{\rho}{2} \cdot D \cdot (U \cdot sin(\alpha))^2 C_D sin(\alpha) \frac{L^3}{3 \cdot L^2} && (4.4.17)
\end{aligned}
$$

The best solution would be achieved by including the drag force in the catenary equations, making a three dimensional equation of the wire profiles. Instead, the drag force is simplified. At the ship, the angle is updated using the part of the drag orthogonal to the wire:

$$\Delta\alpha = \quad - |sin(\alpha)| \cdot \frac{F_D}{T} \tag{4.4.18}$$

$$\alpha_s = \quad \alpha + \Delta\alpha \tag{4.4.19}$$

The position of the trawl is not changed due to drag. An attempt was made at changing the travel direction of the trawl by adding $tan^{-1}\left(tan(\Delta\alpha) \cdot 3^{-1}\right)$ to the angle towards the ship, assuming that all drag is placed at a quarter of the projected wire length from the ship, the centroid of the drag force. This changes the direction of travel immediately after the changed course, sending the trawl on an outer turn at the beginning of the course change. This happens because the equations used updates the shape of the wires immediately, assuming steady state. Immediately after a course change, the velocity on the wire would be a lot smaller due to the deformation, so the drag would be less. This is also an error when calculating the forces on the ship; however, the error does not propagate to the next point as it does when applying this to the trawl. A drag coefficient of $C_D = 1.2$ is found to give the best results. For a smooth infinite cylinder, this would have been roughly one at the Reynolds numbers the wires experience of $R_N \approx 8 \cdot 10^4$. When roughness is considered, the drag coefficient can be twice that of a smooth cylinder (Pettersen 2007).

4.4.6 Errors

There are large errors connected to the modelling of trawl forces. Inertial forces are unknown, and was assumed negligible due to the large friction between the bottom and the trawl. The wires are not entirely straight, and could have a different angle at the ship than at the seabed. This would lead to large errors in forces and yaw moment. The inertial effects can still be regarded as small if only considering the trawl doors; a low value for the horizontal force in one warp during single trawl is 60kN. For an acceleration of $1m \cdot s^{-1}$, a trawl door weighing ten tons would have inertia forces 16% as large as the horizontal drag force. This is a very large value for acceleration, when the velocity is roughly twice of this. Inertia forces regarding the cod-end, the trawl itself, could be a lot larger. As fish are neutrally buoyant, an estimation of the inertia forces is not done.

4.5 Equilibrium equations

In Equations 4.5.1-4.5.3, the control vector $\tau_{control}$ is written in full, including the coordinate transformations. The rest of Equation 4.1.1 is collected in the F_{man} terms. These are the three Equations to solve, when varying y_{trawl}.

$$\begin{aligned} X: \quad & D_{rud}(\alpha_{rud}, v_{rud}) \cdot cos(\beta_{rud}) - L_{rud}(\alpha_{rud}, v_{rud}) \cdot sin(\beta_{rud}) \\ & + T_{tot} - X_{man}(\dot{\boldsymbol{v}}, \boldsymbol{v_r}) \\ & + F_{N,trawl} \cdot cos(\psi) + F_{E,trawl} \cdot sin(\psi) \\ & = F_{N,residual} \cdot cos(\psi) + F_{E,residual} \cdot sin(\psi) \end{aligned} \tag{4.5.1}$$

$$\begin{aligned} Y: \quad & D_{rud}(\alpha_{rud}, v_{rud}) \cdot sin(\beta_{rud}) + L_{rud}(\alpha_{rud}, v_{rud}) \cdot cos(\beta_{rud}) \\ & - Y_{man}(\dot{\boldsymbol{v}}, \boldsymbol{v_r}) - Y_{CF}(\boldsymbol{v_r}) \\ & - F_{N,trawl} \cdot sin(\psi) + F_{E,trawl} \cdot cos(\psi) \\ & = -F_{N,residual} \cdot sin(\psi) + F_{E,residual} \cdot cos(\psi) \end{aligned} \tag{4.5.2}$$

$$\begin{aligned} N: \quad & (D_{rud}(\alpha_{rud}, v_{rud}) \cdot sin(\beta_{rud}) + L_{rud}(\alpha_{rud}, v_{rud}) \cdot cos(\beta_{rud})) \cdot x_{rud} \\ & - N_{man}(\dot{\boldsymbol{v}}, \boldsymbol{v_r}) - N_{CF}(\boldsymbol{v_r}) \\ & + (-F_{N,trawl} \cdot sin(\psi) + F_{E,trawl} \cdot cos(\psi)) \cdot x_{trawl} \\ & - (F_{N,trawl} \cdot cos(\psi) + F_{E,trawl} \cdot sin(\psi)) \cdot y_{trawl} \\ & = N_{residual} \end{aligned} \tag{4.5.3}$$

$[X_{man}, Y_{man}, N_{man}]^T$ The right hand side of Equation 4.1.1

x_{rud} Longitudinal position of rudder, relative to COG

x_{trawl} Longitudinal position of trawl blocks, relative to COG

ψ Heading

β_{rud} Zero lift angle for the rudder

y_{trawl} Transverse position of trawl blocks

Subscript: CF - crossflow, rud - rudder, N - North, E - East, r - relative to flow

Chapter 5

Upper limit of power reduction and model verification

5.1 Upper limit of power reduction

A preliminary feasibility study, assuming only rudder angle would change when moving the blocks, has been discarded. A comparison of the hull-lift force in surge, and rudder lift, showed that rudder lift was larger than hull-lift. The sway equation would be considerably changed by reducing the rudder angle. This is explained by the high thrust loading, and low ship velocity, as well as large rudder angles due to the yaw-moment from trawl. This is the result of such a study when including all three degrees of freedom. This study separates the power necessary to keep the velocity, and the extra power needed because of drift and rudder drag due to angle of attack. If the second category is too small, the concept would not be feasible. So far in the modelling work, it is no longer a preliminary feasibility study; however, it is still interesting to see the reduction in power in relation to this upper limit in addition to the total power.

5.1.1 Method

The reduction in propeller power when drift angle and rudder angle is set to zero shows the lower limit of power. Rudder drag is then at its lowest, the zero-angle drag, and the thrust is equal to the force needed to pull the vessel in the course direction at the desired velocity. Velocity reduction over the rudder is not iterated, however the velocity is found using the thrust projected onto the course direction, i.e. after removing drift angle, reducing it slightly.

5.1.2 Results

From Figures 5.1 and 5.2 it is clear that different trawl operations have different potential for reduction in propeller power. Some of the operations are done on a fairly straight course, and some contain large quantities of manoeuvring. In addition there is a difference due to drift-angle on a straight course.

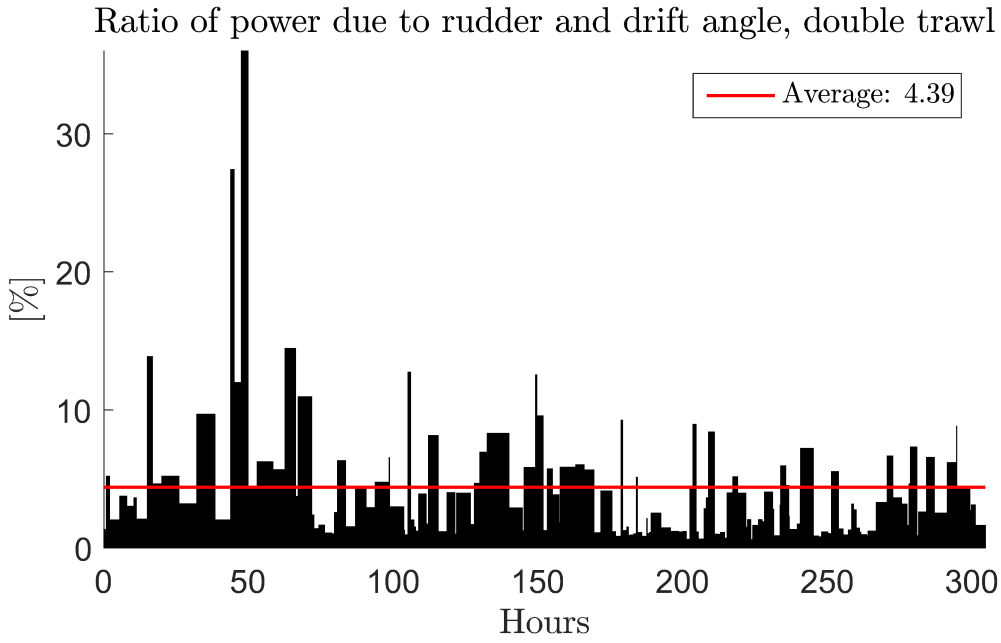

Figure 5.1. Boundary for power reduction; double trawl: Thrust is reduced to the component parallel to course, then the drag from rudder due to an angle is removed. Surge forces due to sway is then removed before finding the new power necessary. The mean value is time weighted. Each bar shows one trawl haul.

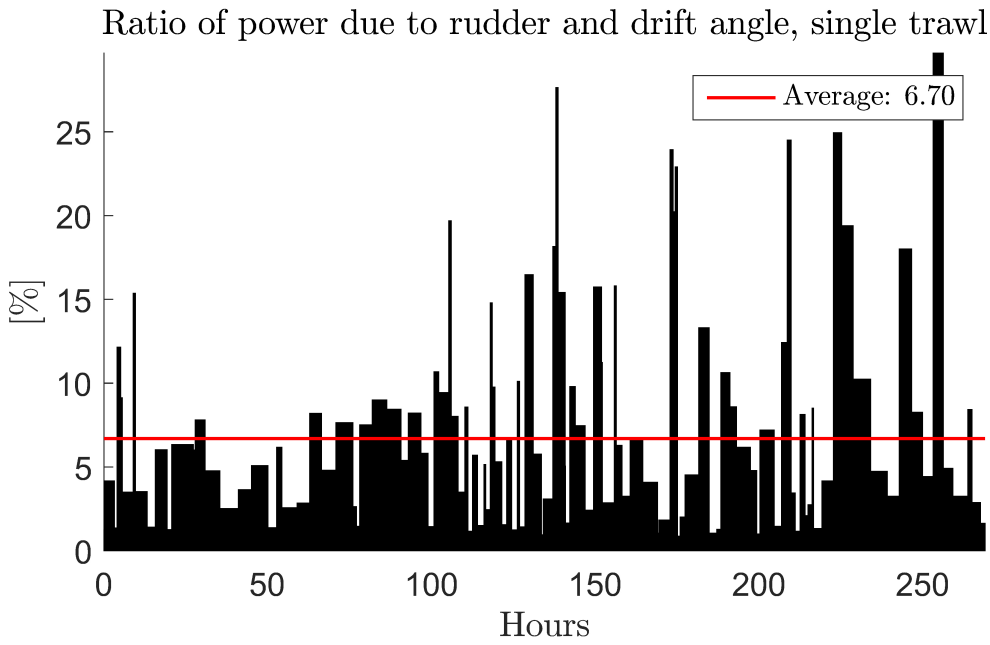

Figure 5.2. Boundary for power reduction; single trawl: Thrust is reduced to the component parallel to course, then the drag from rudder due to an angle is removed. Surge forces due to sway is then removed before finding the new power necessary. The mean value is time weighted. Each bar shows one trawl haul.

5.2 Verification and residual forces

Equations 4.5.1-4.5.3 should be in equilibrium, with residuals equal to zero. Environmental loads are not included, and as the vessel is in a seaway, some residuals are to be expected. Preferably, the wave-loads should disappear during filtering of the results, except added resistance in a seaway. Currents and wind-loads have a non-zero mean when investigating a limited time-span. As some wave loads are still present in the time series, due to frequency overlap with the actual data, wave and wind loads are still present, some residuals are to be expected. The remaining environmental forces should have a clear direction in the inertial reference frame.

An example operation with a double trawl is used to present the residuals in Figures 5.3-5.7. The track of the vessel during this example is seen in Figure 4.3. Before optimising the block position, the residual forces are found to validate the model, and to find the value of external forces not included in the model such as environmental forces.

From Figure 5.3 noise is clearly visible. There is no large deviations from equilibrium, other than the noise. Some deviations are seen during the manoeuvring between 100

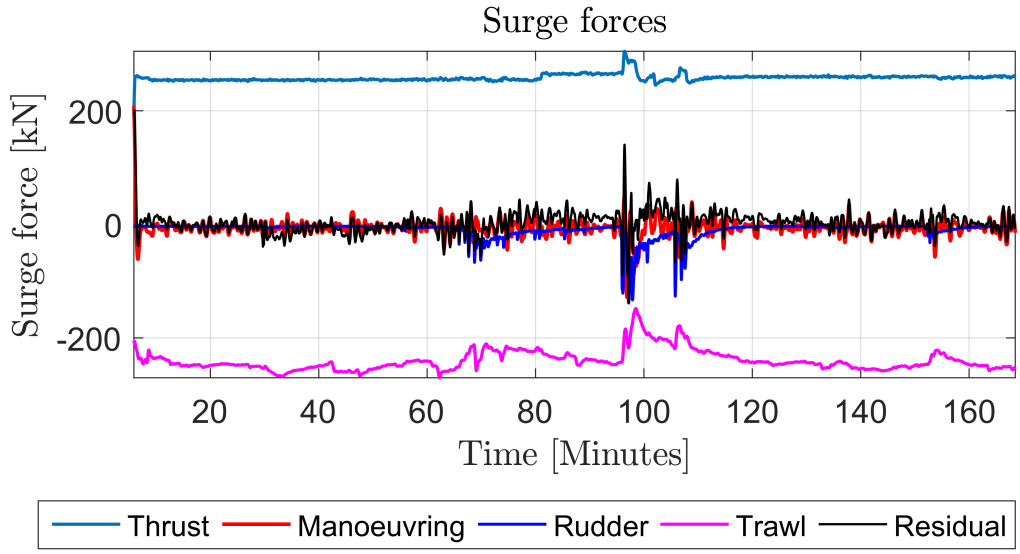

Figure 5.3. Surge; residual and force contributions: A graphical representation of the importance of different force contributions to the equilibrium equation in surge.

and 110 minutes. The manoeuvring equations are the reason for the noise, and it is clear that the frictional surge resistance is small compared to the other forces. This leads to the manoeuvring equations giving a positive surge force at the maxima of the noise. There is a clear increase in surge resistance at around 100 minutes, where the largest turning rate is found. The trawl force in surge decreases a lot during the manoeuvre, leading to a positive residual in surge. It is visible that the ship increases propeller thrust during manoeuvring.

Large residual forces are visible in Figure 5.4. The hydrodynamic forces mainly consists of hull lift. The largest force contributions in sway is the rudder and trawl forces. The forces from the trawl, and the manoeuvring model mostly acts in the same direction.

In Figure 5.5 the forces in the manoeuvring model mostly acts opposite of the trawl forces.

Figures 5.6 and 5.7 shows linear cross correlation between the sway residual and the contributions from hull-lift and trawl, respectively.

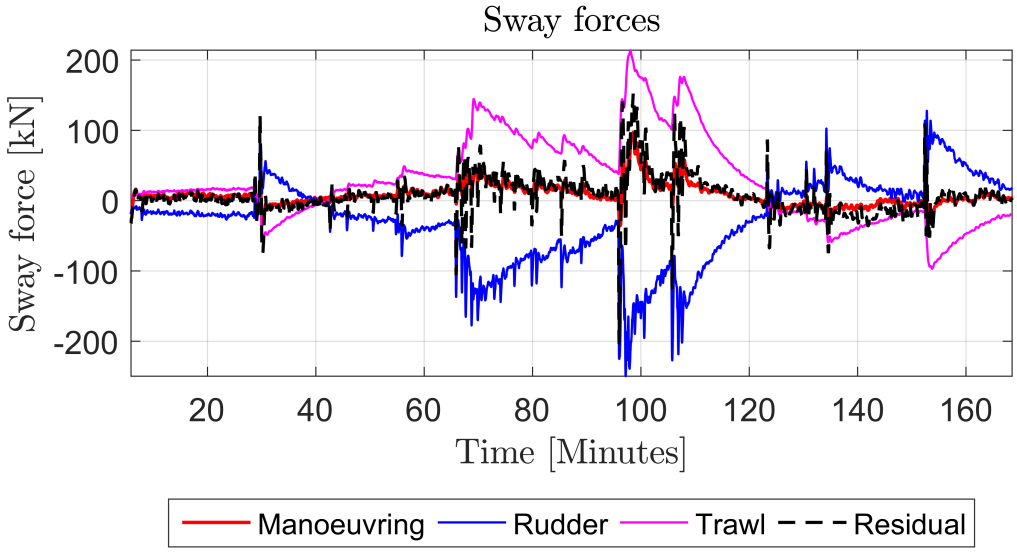

Figure 5.4. Sway; residual and force contributions: A graphical representation of the importance of different force contributions to the equilibrium equation in sway.

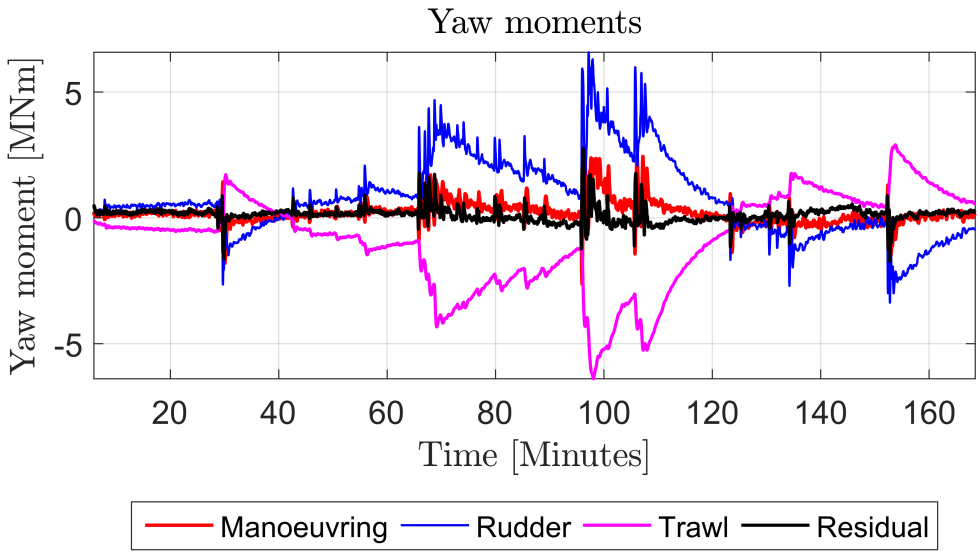

Figure 5.5. Yaw; residual and moment contributions: A graphical representation of the importance of different moment contributions to the equilibrium equation in yaw.

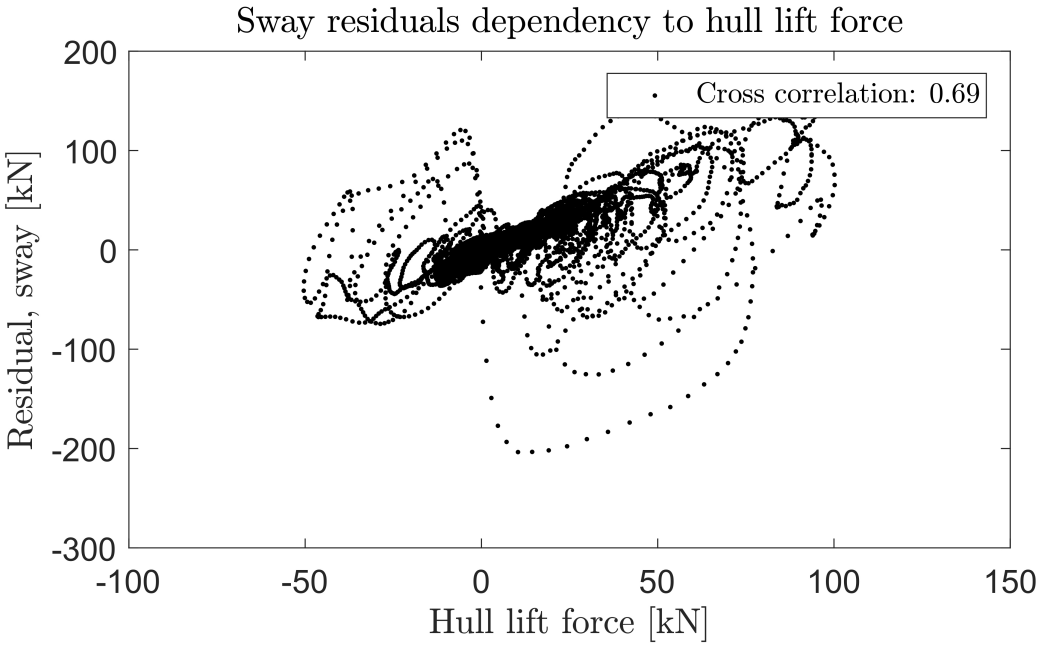

Figure 5.6. Sway residual; cross correlation to hull-lift: The cross correlation shows the proportionality between residuals, and is a measure of similarity. No phase shift(lag) is applied. Residual force in surge is plotted against the force related to Y_{uv}, hull lift.

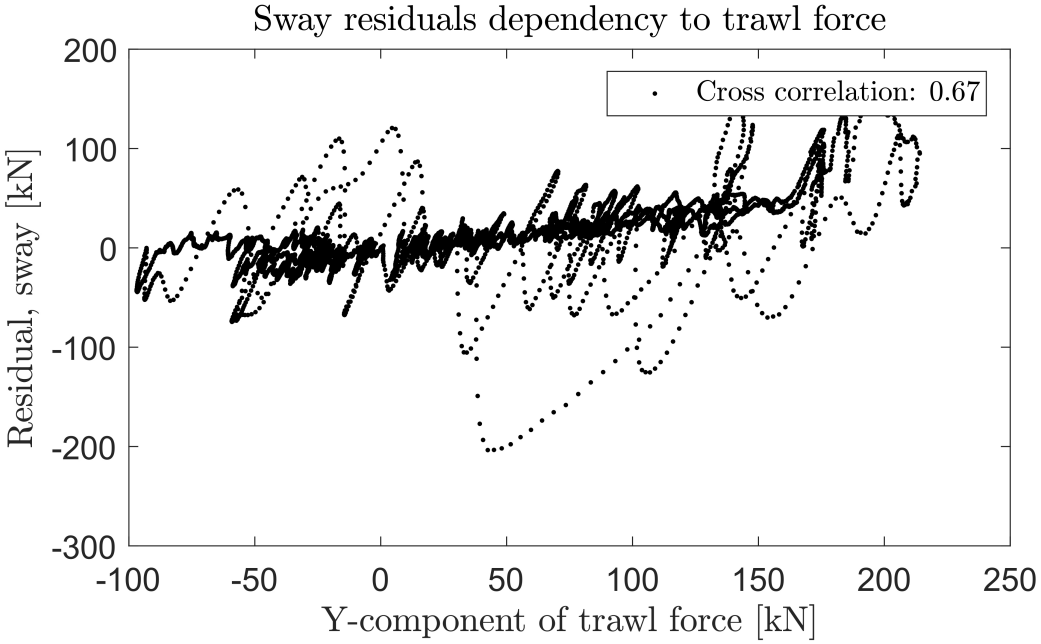

Figure 5.7. Sway residual; cross correlation to trawl forces: The cross correlation shows the proportionality between residuals, and is a measure of similarity. No phase shift(lag) is applied. Residual sway force and the trawl force in sway is plotted against each other.

5.2.1 Discussion about residual forces

In Figure 5.6, there is a clear dependency between hull-lift and residual sway force. This does not necessarily mean that this is the reason for the residual forces, as the trawl forces have a similar dependency, seen in Figure 5.7. It is assumed that the rudder force is not a source of this error, even though underestimating the rudder lift would give the same results. All of these forces would have an impact on the other equilibrium equations as well. The parameter used for hull-lift, Y_{uv} is closely related to N_{uv} and X_{uv} in the manoeuvring equations, despite only appearing in the sway-equation itself. By looking at the time 100-150 minutes in Figures 5.3-5.5, the residuals are impacted at different magnitudes for all three degrees of freedom. In Figure 5.5, the sign of the residuals response is opposite of the trawl moment, implying that the error is at least partly due to hull lift being exaggerated. It should then be noted that Y_{uv}, at the waterline originally given in ShipX (design waterline), was only two thirds of the value used, where the waterline has been changed to fit the draught values given with the data. A small error in the opposite direction is due to the simplification used for hull lift. v is rarely larger than 25% of u:

$$\begin{aligned} L &= Y_{uv} \cdot U^2 \alpha = Y_{uv} \cdot U^2 \cdot sin^{-1}\left(\frac{v}{U}\right) \qquad (5.2.1) \\ &= Y_{uv} \cdot \left(\frac{u}{cos(\beta)}\right)^2 \cdot tan^{-1}\left(\frac{v}{u}\right) \\ &\approx Y_{uv} \cdot u^2 \cdot \frac{v}{u} = Y_{uv} uv \end{aligned}$$

$$e = \frac{tan^{-1}(0.25)}{0.25(cos(0.245))^2} = 1.04 \qquad (5.2.2)$$

The Reynolds number of $R_n \approx 9.5 \cdot 10^7$ is sufficiently large to assume fully turbulent flow, and should have little influence on the troubled parameter.

The trawl forces in sway is exaggerated. A plausible reason for the yaw equation to be close to zero, when the sway equations are out of balance is that the trawl force and the hull lift force give moments in opposite directions in yaw, while acting the same way in sway. It is also seen that the trawl forces decrease in surge, giving a small positive residual. As the trawl force in surge direction is proportional to the cosine of the angle of the wires, it has a smaller effect on surge than sway.

Chapter 6

Method of optimization and processing of results

6.1 Optimisation of transverse block position

The goal of the optimisation is to reduce the necessary thrust while maintaining the same track of the vessel. The manoeuvring equations are the three equations to satisfy, and there are four variables, when setting all two or three blocks to the same position. Without a fourth equation, this is an under-determined system of equations, and therefore optimisation techniques must be used rather than equation solving. There are many possible ways to solve this; however, not all are applicable to these equations. In optimisation, it is common to use an objective function as the forth function, or as the only function, preferably having a clear global minimum at the correct solution. Many optimisation algorithms use double derivatives, due to the Hessian matrix, a matrix consisting of the second order partial derivatives. There is also Hessian free optimisation, approximating it numerically or by using the Jacobian matrix, the matrix of first order partial derivatives. Completely derivative free methods also exist, by using algorithms and function evaluations to find the minimum.

The manoeuvring equations are non-linear with infinitely many solutions, when considering angles. When bounding drift angle and rudder angle, there is still more than one solution. To find the correct solution, for minimum thrust while still being realistic, the initial point in the solver must be sufficiently close. Because of this, optimising using all four variables at the same time has a large potential for finding either the wrong point, or diverge from the solution completely. For the true solution to the problem regarding drift angle, rudder angle and thrust, leaving only the position as a variable, and the other three variables dependent on that, there is only one minimum within the boundaries as seen in Figure 6.1. The optimisation is therefore done using a pattern search method to solve for the position as an outer loop:

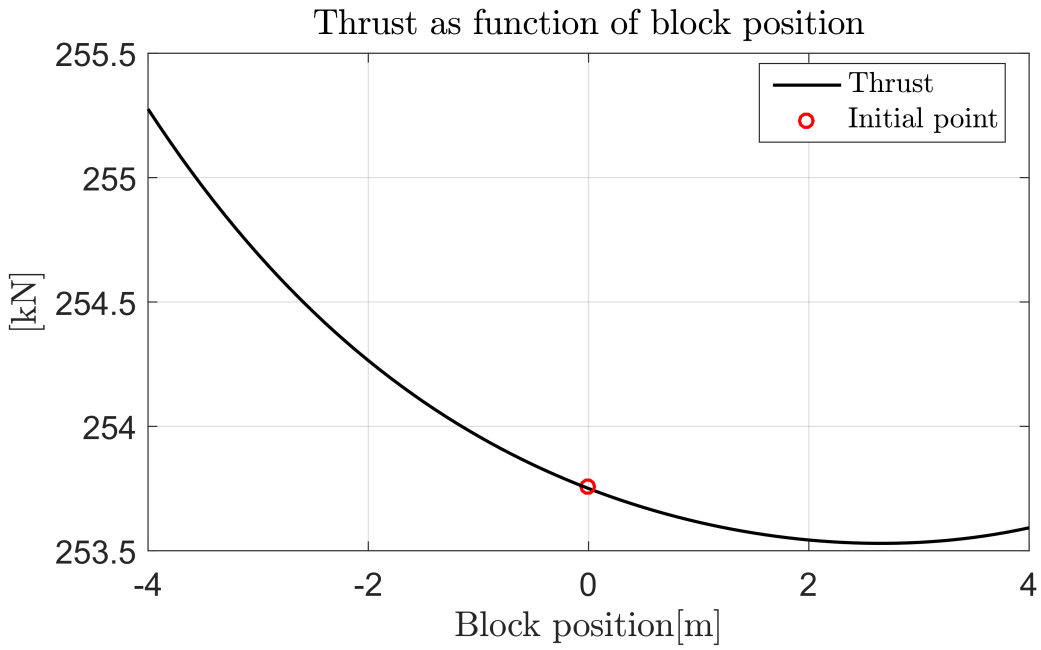

Figure 6.1. Necessary thrust for different trawl connection points: Thrust as a function of block position for a point with a small drift angle on a straight course. There is only one minima, at roughly 2.8m, in this function as long as the manoeuvring equations are solved correctly. The initial position is -1.5 cm (portside), giving the same moment as the stationary blocks.

$$y_n = y_{n-1} + b \cdot \Delta y \tag{6.1.1}$$

$$\Delta y = \begin{cases} \Delta y, & T_n < T_{n-1} \\ -\frac{\Delta y}{2}, & T_n > T_{n-1} \\ -\frac{\Delta y}{10}, & y_n = \pm y_{max} \end{cases} \tag{6.1.2}$$

$$b \qquad \text{Sign, found in a preliminary iteration} \tag{6.1.3}$$

$$y_n = sign(y_n) \cdot min(|y_n|, y_{max}) \tag{6.1.4}$$

$$e > |y_n - y_{n-1}| \qquad \text{Convergence condition} \tag{6.1.5}$$

For the iteration in Equations 6.1.1-6.1.5, the points that have converged are removed from the index vector, and the iterations stop when the index vector is

empty. The search pattern is chosen because it only needs to enter the inner loop once for each iteration, while a pattern comparing a midpoint to $\pm\Delta y$, needs to enter four times; once for every point where the upper value is best, once for points where the lower value is best, and twice for the points where the middle value is best. MATLAB's speciality is rapid calculation on vectors, while it is slow when iterating. Calculation time is therefore larger for four iterations on a quarter of the points, than for one iteration on all. Calculation time is therefore shorter for this search pattern unless the input vectors are modified.
Figure 6.2 shows a flowchart describing how the optimization is done.

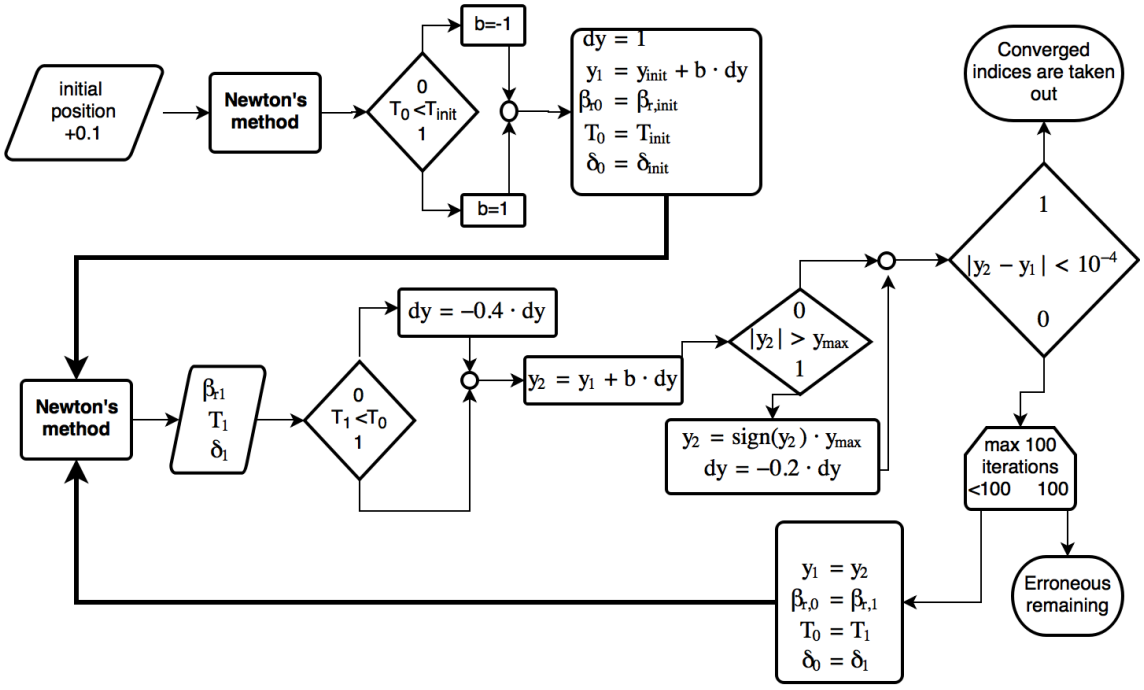

Figure 6.2. Optimization flowchart: y - block position, T - thrust, δ - rudder angle, β_r - relative drift angle (also used to update drift angle, β, and rudder inflow angle during optimization). Subscript 1 is current value, and 0 is the previous value. y has the subscript 2, as it is updated for the next iteration.

6.1.1 Newton's method for three variables

In the inner loop, translatable to the function evaluation in the pattern search, drift angle, rudder angle and thrust is found using the multivariate Newton's method (Monahan 2011):

$$\mathbf{J} = \begin{bmatrix} \frac{\partial F_X}{\partial T} & \frac{\partial F_X}{\partial \beta} & \frac{\partial F_X}{\partial \delta} \\ \frac{\partial F_Y}{\partial T} & \frac{\partial F_Y}{\partial \beta} & \frac{\partial F_Y}{\partial \delta} \\ \frac{\partial F_N}{\partial T} & \frac{\partial F_N}{\partial \beta} & \frac{\partial F_N}{\partial \delta} \end{bmatrix} \tag{6.1.6}$$

$$\approx \begin{bmatrix} \frac{F_X(T+dT)-F_X(T-dT)}{2dT} & \frac{F_X(\beta+d\beta)-F_X(\beta-d\beta)}{2d\beta} & \frac{F_X(\delta+d\delta)-F_X(\delta-d\delta)}{2d\delta} \\ \frac{F_Y(T+dT)-F_Y(T-dT)}{2dT} & \frac{F_Y(\beta+d\beta)-F_Y(\beta-d\beta)}{2d\beta} & \frac{F_Y(\delta+d\delta)-F_Y(\delta-d\delta)}{2d\delta} \\ \frac{M_N(T+dT)-M_N(T-dT)}{2dT} & \frac{M_N(\beta+d\beta)-M_N(\beta-d\beta)}{2d\beta} & \frac{M_N(\delta+d\delta)-M_N(\delta-d\delta)}{2d\delta} \end{bmatrix}$$

$$\mathbf{x}_{n+1} = \mathbf{x}_n + \mathbf{J}_n^{-1}\mathbf{f}(\mathbf{x}_n) \tag{6.1.7}$$

6.1.2 Stability of solver, erroneous points, and error sources

The solver is not entirely stable, and some points diverge from the solution. This happens even when including a factor $0 < \gamma < 1$ to reduce the step size. The gradients at the diverging points are too large for the factor to dampen it enough for a stable solution. Residuals forces and moments are generally large at these points, meaning that the solution diverges when the initial solution has low credibility. It is seen that the stability is connected to the manoeuvring equations, despite the relatively low forces connected to it. Introducing velocity over the rudder as a function of thrust also makes the solution less stable. Due to this, neither the yaw acceleration, yaw rate or velocity over the rudder is updated in the optimisation. Drift angle can both increase and decrease at the optimal point. When drift angle and rudder angle creates forces with the same sign in the body fixed y-axis, the drift angle will increase to compensate the reduced lift from the rudder. For most cases, the opposite is true, both rudder angle and drift angle is reduced because of opposite sign in their forces. This will have a small influence on yaw rate and yaw acceleration as they are related to change in heading, where heading is course minus the drift angle. Changes in drift angle are generally much smaller than the relation to a change in course, meaning it does not result in large errors.

The velocity over the rudder is not updated during the optimization. This effect is found afterwards; however, it still makes a small error in optimal placement. The reduced velocity over the rudder gives lower lift and drag from the rudder. The rudder angle must then be found again, to compensate for the lift, resulting in an increase in drag. The drag on the rudder is therefore different to the value found in the optimisation, and the optimal point would be different due to a trade-off effect between rudder drag, and effects drift angle has on course-parallel thrust and hull drag. In general, this means that the reduction in power is slightly underestimated.

6.2 Calculation of new propulsion points

The optimization finds the reduction in thrust, while the variable to minimize is power. Power decreases with thrust, and using thrust as the variable to minimize does not lead to a poor optimization. The two variables are connected through the propeller series, as power $P = Q \cdot \omega = Q \cdot 2\pi \cdot RPM/60$. RPM, as part of J, is used as the variable to find the new propulsion point in this thesis. Another option is to use pitch as the variable, leading to a reduction in power through torque. It would be best to find the optimum point for the propeller at the given thrust; however, it is expected that the difference in power from changing propeller speed instead of pitch is small compared to the reduction in thrust.

The conventional way of finding new propulsion points is to calculate $K_T \cdot J^{-2}$, and find J from a $K_T \cdot J^{-2} - J$ diagram. As the pitch is an additional variable, the gradients in the surface to represent this are steep, both with respect to $K_T \cdot J^{-2}$ and pitch. Matlab's fit-objects were unable to represent this in a precise enough manner, even if the span was reduced to the most important operational values. When pitch was left out as a variable, the curves for the given values of pitch were properly modelled. By entering all seven curves, and then interpolating for the correct pitch, fairly accurate values were found, where the corresponding thrust values were only marginally different from the desired thrust that was calculated. However, this method was very slow, as it needed a for-loop because every point needed to be individually entered due to the two-step interpolation.

Another method is to iterate a solution. Iteration is not required when using the conventional approach, as the propeller speed disappear from the x-axis K_T when divided by J^2. The main disadvantage of iteration is that it is often time-consuming and imprecise. Here it was not time-consuming, as it did not need to be looped

over every value, only until convergence of all points. An iterative approach is therefore used in this thesis, as the number of points to calculate far exceed the number of iterations needed to reach a converged value. The False-Position method was used, following Equation 6.2.1 (Weisstein 2017). Convergence is set to $(RPM_n - RPM_{n-1})/RPM_n < 10^{-6}$:

$$RPM_n = RPM_{init} - \frac{(RPM_{n-1} - RMP_{init}) \cdot K_T(RPM_{init})}{K_T(RPM_{n-1}) - K_T(RPM_{init})} \tag{6.2.1}$$

Imprecision is mainly a disadvantage when an exact solution is available. As the precise data for the Wageningen D-series available is 200 by 7 points, and the large gradients made a precise fit difficult, this is not the case here. Iteration was more precise, as it directly uses the thrust as a convergence criteria, instead of a separate interpolation of data. If a parametric model, instead of a spline, had been used for the $J-K_T$-fit in Section 4.2.2, $K_T \cdot J^{-2} - J$ could have been found from this directly.

6.3 Statistical analysis of results

During turning, the probability distribution of power reduction is skewed, and belongs somewhere in the family of Weibull distributions. Even though there is an asymmetric probability distribution, the mean value is most interesting when the goal is to estimate reduction in required power. The mean value is sensitive to outliers, a large disadvantage compared to using mode. Median and should give the same value as the mean for many points in a symmetrical probability distribution, and therefore remove the influence of outliers. Median would be better to use than mode, as it is closer to the mean. It was decided to use the mean, as the points far away from the cluster are not considered as outliers, they are a result of the impulsive rudder angles discussed in Subsection 4.3.3.

6.3.1 Precision errors

It is assumed that the mean value follows a Gaussian (normal) distribution. The standard deviations and mean values are calculated using Equations 6.3.1 and 6.3.2 (MATLAB 2015)

$$S = \sqrt{\frac{1}{N-1} \cdot \sum_{i=1}^{N} (A_i - \mu)^2} \tag{6.3.1}$$

$$\hat{\mu} = \frac{1}{N} \cdot \sum_{i=1}^{N} A_i \tag{6.3.2}$$

Following Steen (2014*a*), the precision error is found using Equations 6.3.3 and 6.3.4. The t-values are the Student's-t distributions percentile values, found using the *tinv* function, with desired probability and degrees of freedom $(N-1)$, as input parameters.

$$S_\mu = \frac{S}{\sqrt{N}} \tag{6.3.3}$$

$$P_\mu = t \cdot S_\mu \tag{6.3.4}$$

Chapter 7

Results

The results presented here where calculated with the transverse position of trawl blocks limited to $\pm 5.08m$, the original location of the port-side and starboard trawl blocks.

7.1 Removed points

For all results, some points are removed:

- The start and the end of trawl operations are removed, so the results is restricted to the region where the trawl actually is at the bottom. This is done by looking at the filtered derivative of the port side wire length, and finding the first and last point where the absolute of the derivative is less than $0.1\ ms^{-1}$.

- Complete sections where the trawl is not at the bottom: Some of the shorter identified trawl series start with decreasing wire length, and have a mean wire length less than the depth. This means that some of the trawl operations does not hoist all the way immediately, and wait for some time with the cod-end at a different depth for unknown reasons. The assumptions used is not reliable when the trawl is not at the bottom, as the hydrodynamic drag and inertia terms will be larger relative to the total wire tension. This reduces the number of points by roughly 10%.

- Points that did not converge: Newton's method diverged for some points. About half of these points managed to get a solution for other positions of the trawl wires. Points that never found a solution, or did not find enough solutions to find the optimum placement of the trawl blocks within a given number of iterations, are removed. Most of the points are in the start and end

region.

- Local minimas/false solution: A few of the points that had trouble with convergence, as mentioned above, found a solution outside reasonable bounds. This was only a problem when the initial iteration lead to a bad solution. It is assumed that an increase in power is not possible, as the initial trawl position is an option. Points with increased thrust are therefore removed.

7.2 Optimization results for the example operation

The results from optimization on the example operation is shown in Figures 7.1-7.5. The track of the vessel during this example is seen in Figure 4.3.

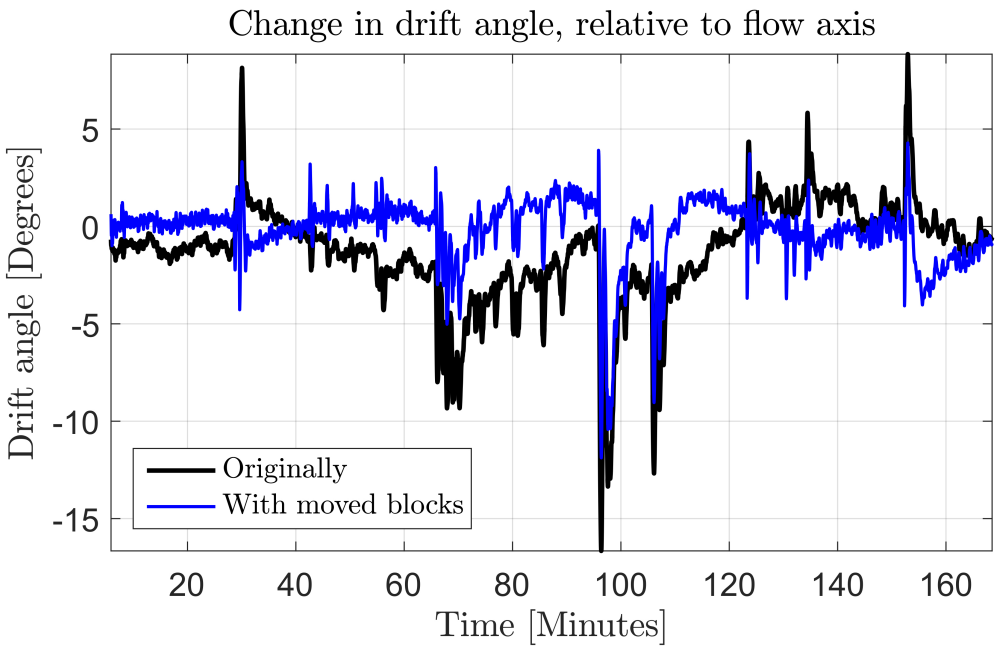

Figure 7.1. Example showing the change in flow-drift angle: The change in drift angle due to transverse movement of connection points for trawl wires.

The drift angle is visibly reduced for most points in Figure 7.1. For some points there is a change in sign, and in the proximity of 155 minutes, the magnitude of drift angle has increased.

The reduction in rudder use is seen in Figure 7.2. Unlike the drift, the sign does not change. For the first thirty minutes, the rudder angle is reduced to noise with

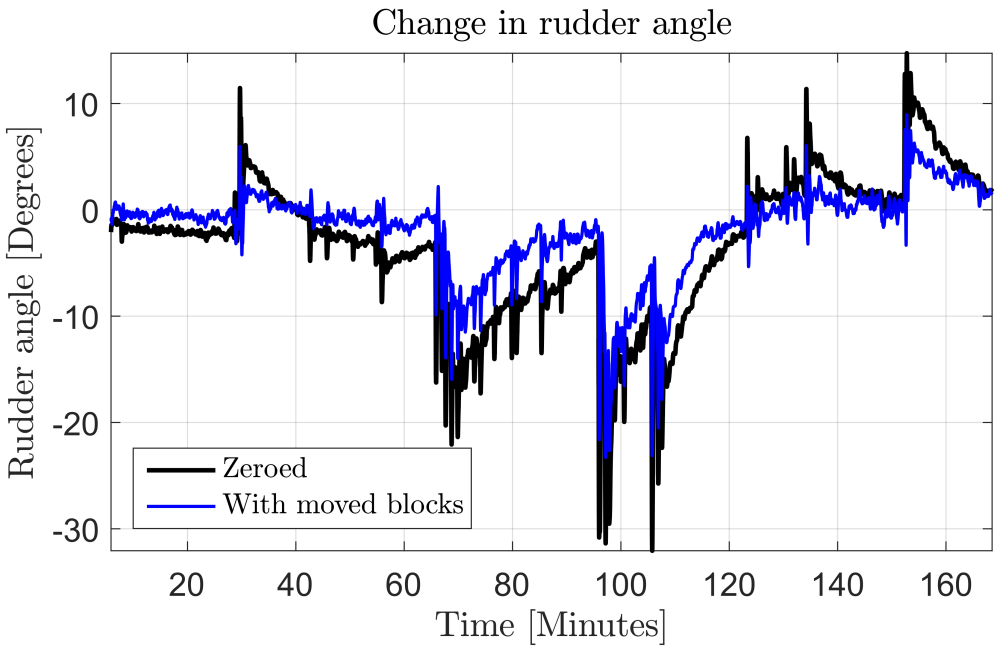

Figure 7.2. Example showing reduction of the rudder angle: The rudder angle with and without transverse movement of connection points for trawl. Both are relative to the rudder flow axis. Rudder flow axis is updated with regard to the change in flow-drift angle. The rudder angle is corrected for the change in velocity.

a zero mean. For the large rudder angles, such as the two turns between 70 and 120 minutes, the reduction is close to constant for each turn. The second turn has a smaller reduction in rudder angle.

From Figure 7.3 it is visible that the original arrangement of the trawl blocks give little moment from the x-component for this specific trawl operation, due to the force resultants small distance from zero. At the sharp manoeuvres from 70 to 120 minutes, the blocks are moved as far as allowed, giving the largest turning moment possible within the given limitations. Some spikes are visible, corresponding to oscillations in rudder angle seen in Figure 7.2.

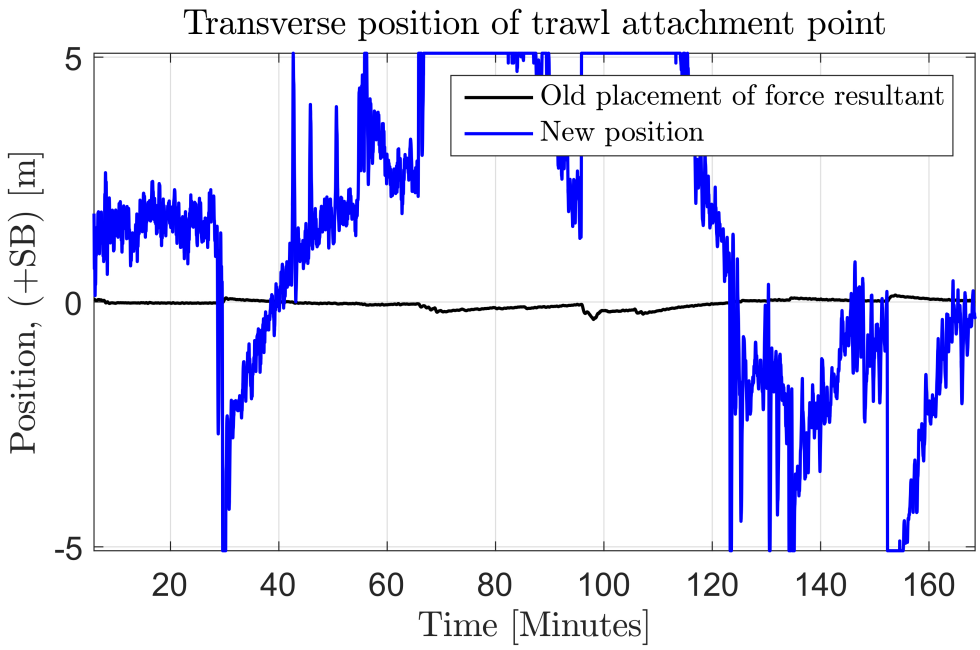

Figure 7.3. Example showing the optimised position of trawl blocks: The transverse placement of the trawl force resultant along x in the body reference frame is shown before and after the optimization. The original placement of the port-side and starboard trawl blocks are set as the limit.

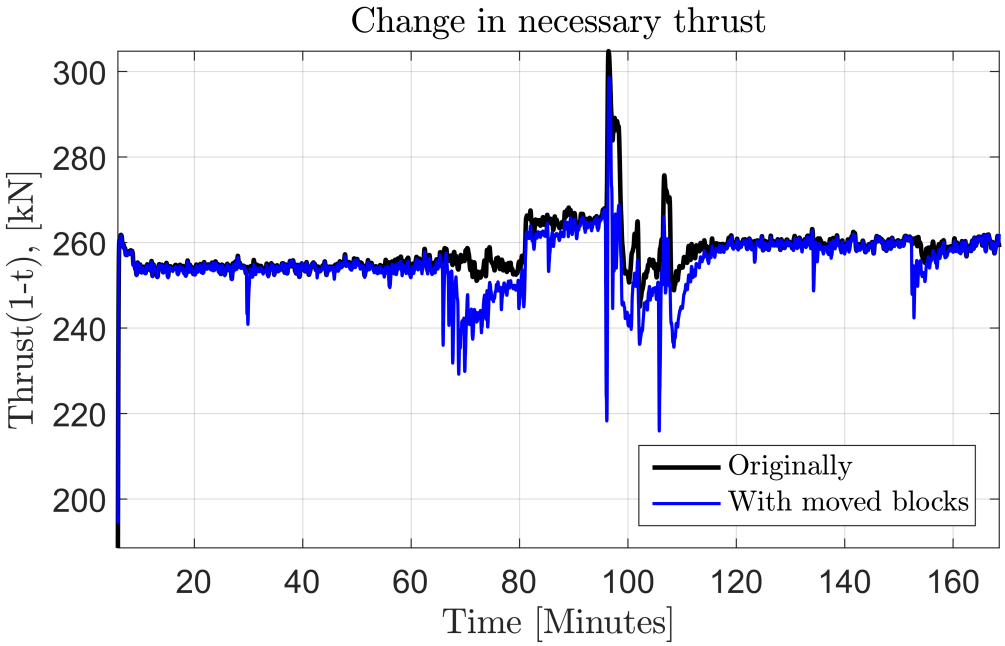

Figure 7.4. Example showing the change in required thrust: The change in thrust due to transverse movement of connection points for trawl. The thrust is corrected for the change in velocity over the rudder.

In Figure 7.4, the reduction in thrust is visible during the turns. For the reduction due to drift angle, there is a small reduction in thrust, not clearly visible from the

figure other than a thin line of black above the blue. There is a clear noise term that comes after the optimization, not present in the original thrust, at the same points large oscillations in rudder angle are seen in Figure 7.2.

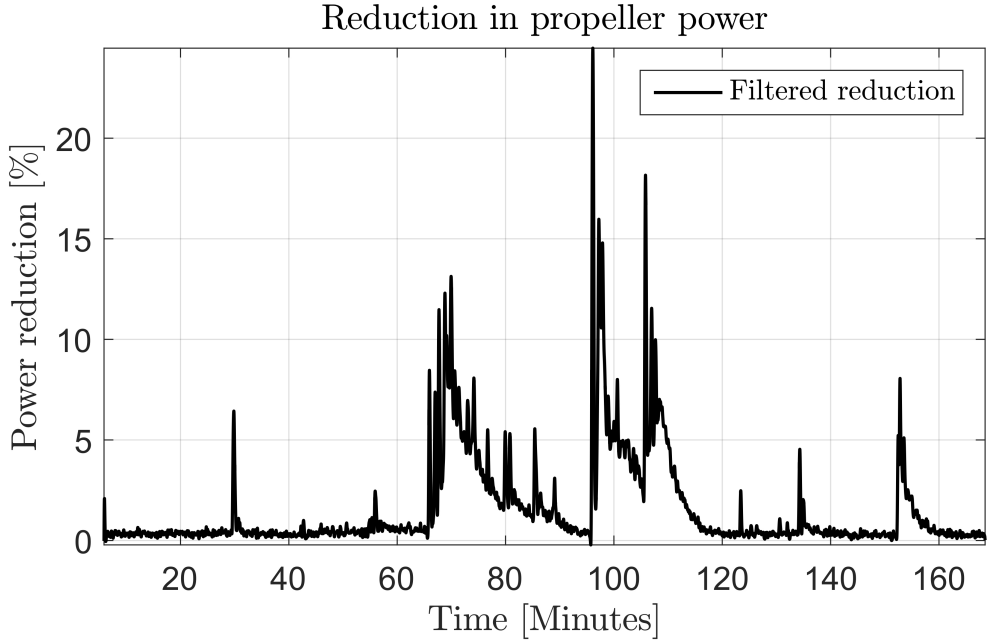

Figure 7.5. Propeller power reduction for the example operation: The filtered relative change in propeller power due to transverse movement of connection points for trawl. The reduction in power is found using the total thrust with updated velocity on rudder, including the deducted part.

The expected reduction in required power for the example is presented in Figure 7.5. The power reduction during a drift angle is more clearly visible the first thirty minutes in Figure 7.5 than 7.4. The potential for reduction in power is largest during turning.

7.3 Potential for power reduction during change of course

It is visible from Figures 7.6 and 7.7 that the some of the reduction in power is lost when the velocity across the rudder is updated. There is a fairly linear relation between the rate of turning and the potential for reduction in power up to 15° per minute. At sharper turns, it is more flat, and starts to drop. The potential for reducing power is larger when pulling a double trawl than a single.

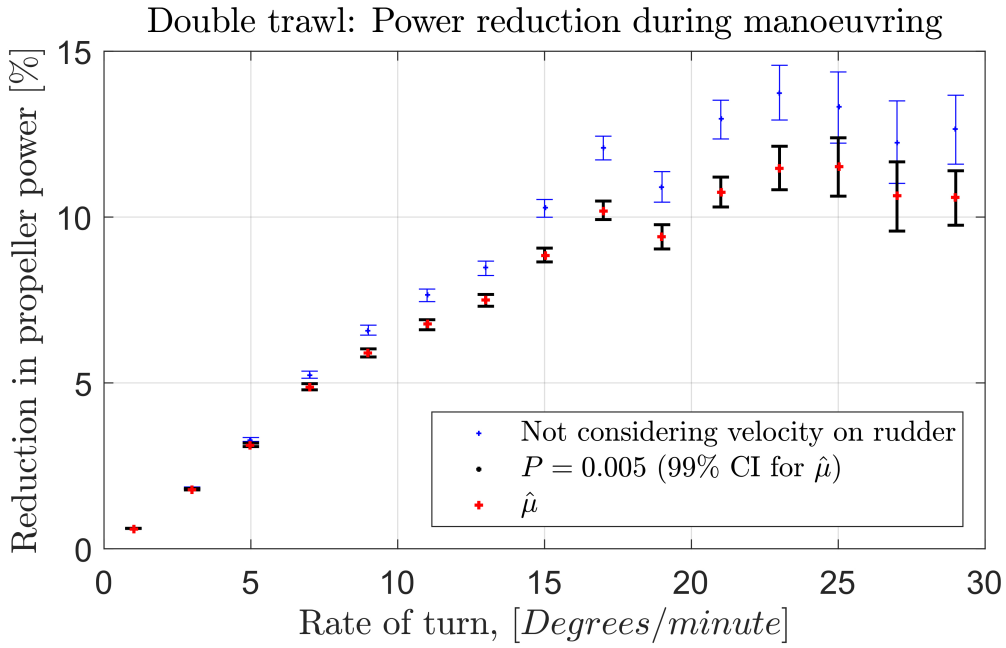

Figure 7.6. Power reduction; as a function of turning rate when pulling a double trawl: Reduction in power during manoeuvres, discretized into intervals of $2° \cdot min^{-1}$. Confidence Interval (CI) of the expected value is found using Student's-t.

Table 7.1. Tabulated power reduction; as function of turning rate when pulling a double trawl: The edges of the discretization, mean reduction in propeller power, precision error, and standard deviation is presented here.

Rate of turn $[degrees/minute]$	**Mean** [%]	**Precision error** $(99\%CI)$[%]	**Standard deviation** [%]
0-2	0.61	0.003	0.98
2-4	1.80	0.021	2.25
4-6	3.13	0.053	3.26
6-8	4.88	0.093	4.18
8-10	5.90	0.122	4.61
10-12	6.75	0.151	4.73
12-14	7.49	0.178	5.11
14-16	8.86	0.208	5.36
16-18	10.20	0.279	6.16
18-20	9.40	0.366	6.29
20-22	10.76	0.450	6.57
22-24	11.48	0.656	7.25
24-26	11.51	0.880	8.24
26-28	10.62	1.043	7.61
28-30	10.58	0.821	6.15

Tables 7.1 and 7.2 presents the same as Figures 7.6 and 7.7, with the additional standard deviation. Results for turning rates up to $30°/min$ were valid for double

trawl, while turning rates up to $40°/min$ were found for single trawl. Standard deviations increase gradually, as turning rate increases, with some exceptions.

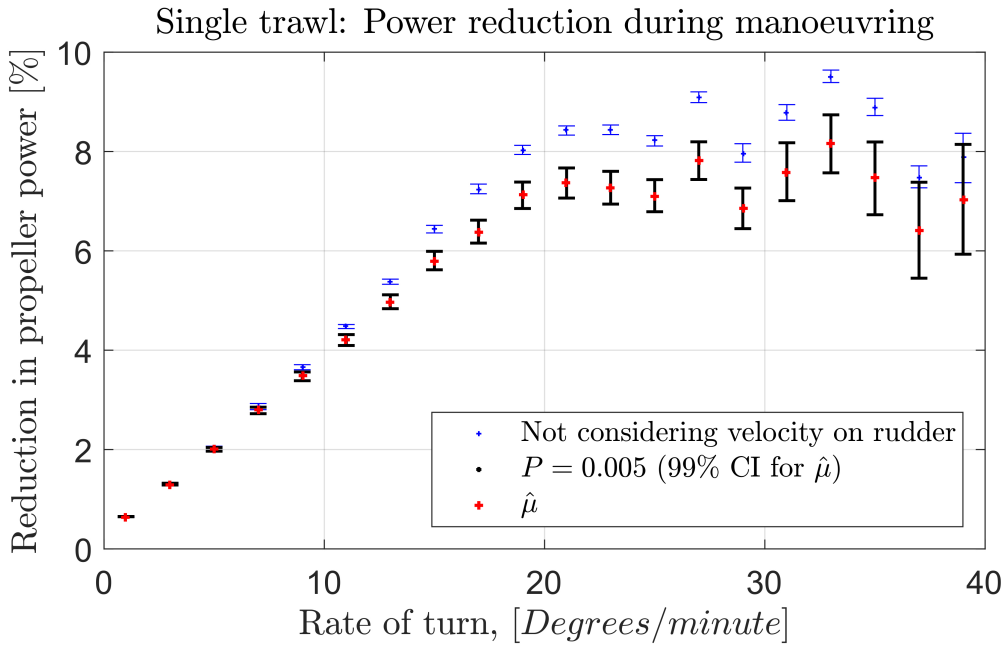

Figure 7.7. Power reduction; as a function of turning rate when pulling a single trawl: Reduction in power during manoeuvres, discretized into intervals of $2° \cdot min^{-1}$. Confidence intervals of the expected value is found using Student's-t.

Table 7.2. Tabulated power reduction; as function of turning rate when pulling a single trawl: The edges of the discretization, mean reduction in propeller power, precision error, and standard deviation is presented here.

Rate of turn $[degrees/minute]$	**Mean** [%]	**Precision error** $(99\%CI)$[%]	**Standard deviation** [%]
0-2	0.65	0.003	0.81
2-4	1.30	0.018	1.53
4-6	2.00	0.037	2.17
6-8	2.79	0.066	3.05
8-10	3.47	0.089	3.59
10-12	4.20	0.110	3.97
12-14	4.98	0.140	4.45
14-16	5.80	0.186	5.27
16-18	6.39	0.230	5.97
18-20	7.12	0.266	6.46
20-22	7.37	0.303	6.44
22-24	7.27	0.330	6.65
24-26	7.11	0.323	6.01
26-28	7.82	0.379	6.12
28-30	6.86	0.409	5.80
30-32	7.59	0.583	6.44
32-34	8.15	0.584	6.49
34-36	7.46	0.733	6.27
36-38	6.42	0.966	6.53
38-40	7.08	1.105	5.92

7.4 Potential for power reduction on a constant course with a drift angle

Figures 7.8 and 7.9 shows the power reduction for different drift angles, β, along with the precision error. Tables 7.3 and 7.4 presents the same, in addition to standard deviation. The standard deviation is more constant here than for the relation to turning rate. A clear correlation between reduction in power and the drift angle is seen in Figures 7.8 and 7.9. The effect is clearly non-linear and convex, and strongest when pulling a double trawl.

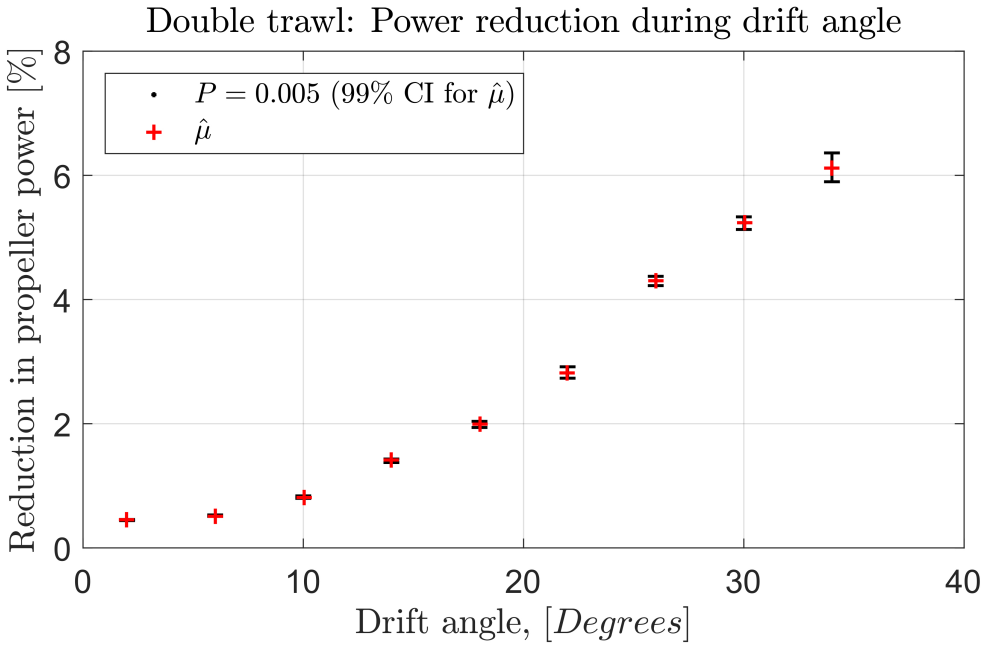

Figure 7.8. Power reduction; as a function of drift angle when pulling a double trawl: Reduction in power as a function of drift angle, when turning rate is less than $2° \cdot min^{-1}$, discretized into intervals of 4°. Confidence intervals of the expected value is found using Student's-t. Drift angles used is relative to course, not flow.

Table 7.3. Tabulated power reduction; as function of drift angle when pulling a double trawl: The edges of the discretization, mean saving, precision error, and standard deviation is presented here. Only drift angles when the turning rate is less than $2° \cdot min^{-1}$ are used.

Drift angle [*degrees*]	**Mean** [%]	**Precision error** (99%CI)[%]	**Standard deviation** [%]
0-4	0.45	0.009	2.17
4-8	0.52	0.012	2.30
8-12	0.82	0.020	2.48
12-16	1.40	0.028	1.99
16-20	1.99	0.050	2.23
20-24	2.83	0.092	2.83
24-28	4.30	0.075	1.11
28-32	5.23	0.102	1.16
32-36	6.13	0.232	1.02

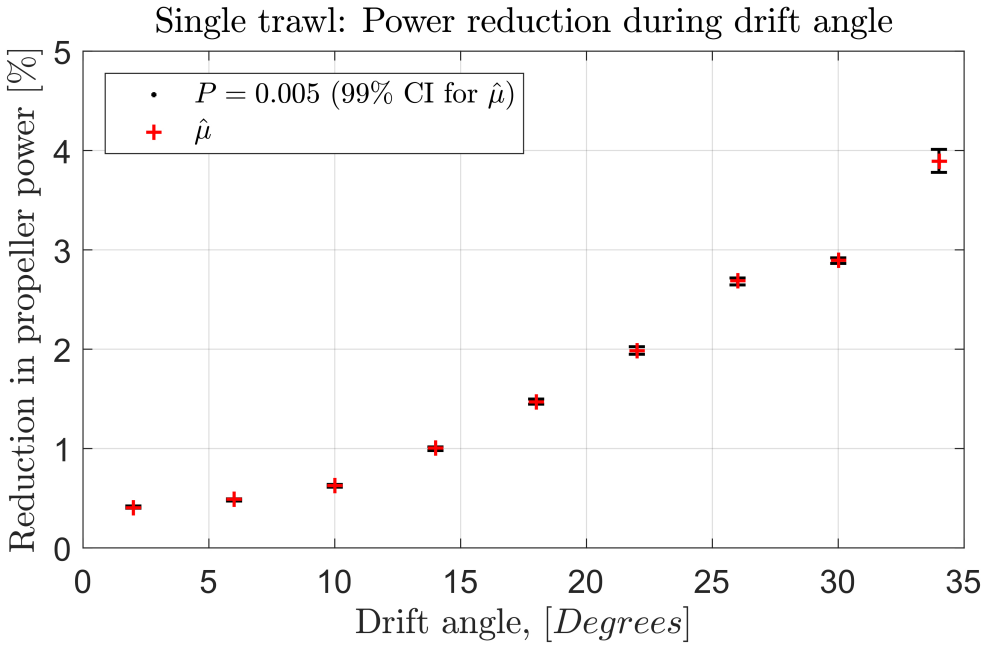

Figure 7.9. Power reduction; as a function of drift angle when pulling a single trawl: Reduction in power as a function of drift angle, when turning rate is less than $2° \cdot min^{-1}$, discretized into intervals of 4°. Confidence intervals of the expected value is found using Student's-t. Drift angles used is relative to course, not flow.

Table 7.4. Tabulated power reduction; as function of drift angle when pulling a single trawl: The edges of the discretization, mean saving, precision error, and standard deviation is presented here. Only drift angles when the turning rate is less than $2° \cdot min^{-1}$ are used.

Drift angle [*degrees*]	**Mean** [%]	**Precision error** (99%CI)[%]	**Standard deviation** [%]
0-4	0.41	0.012	2.06
4-8	0.48	0.011	1.96
8-12	0.62	0.014	2.08
12-16	1.00	0.019	2.00
16-20	1.47	0.026	1.89
20-24	1.99	0.038	1.72
24-28	2.68	0.040	0.96
28-32	2.89	0.030	0.40
32-36	3.90	0.116	0.41

7.5 Overall expected power reduction

Table 7.5. Overall power reduction: The mean reduction in power for transversely movable trawl blocks during trawling and in total.

While pulling double trawl	1.13%
Double trawl, relative to upper limit	25.7%
While pulling single trawl	1.11%
Double trawl, relative to upper limit	16.6%
For the total series	0.64%

In Table 7.5, every point is power weighted, and is in relation to propeller power, not the engine power. This is done as the ratio between power delivered to the propeller and total power is expected to be significantly different between vessels, especially those without on-board production.

Most of the propeller power is spent on pulling the trawl, and the pure surge resistance. This is of course not possible to change by moving the trawl blocks. The values in Table 7.5 that are relative to the trawl modes' upper limit, shows the power reduction found relative to the power due to rudder angle and sway velocity, presented in Section 5.1. The overall reduction in power for the entire series is power weighted, including all modes, not only trawling. The average reduction in power for the trawl modes alone is also included. Precision error is not included here, as it is small, and bias error are much larger.

Chapter 8

Discussion

8.1 The example operation

A part with increased drift angles are seen towards the end in Figure 7.1. At first glance, this makes little sense. When comparing this with the rudder angle in Figure 7.2, it is seen that the rudder angle is large, while the drift angle is small in this region, when they move in unison most other times. The reduction in rudder angle must be compensated in the sway equation with an increase in drift angle. In Figure 7.5, the reduction in power is clearly largest at the beginning of a turn, and gradually decreases. The reason for this gradual decrease is that the track of the trawl gradually aligns with the track of the ship, reducing the yaw-moment from the trawl. Overall, both rudder angle and drift angle are reduced, followed by a reduction in required propeller power. The reduction in power during the example is close to entirely related to manoeuvring.

8.2 Accuracy of results

The position of the trawl relative to the ship is assumed to not change during the optimization. Moving the point that pulls the trawl five meters, would slightly change the position. The error related to this is assumed to be smaller than the error related to modelling of the position, and the direction would be opposite. Including updates to the position would therefore increase the error of the results, for the model used. A small amount of power would be necessary to move the blocks. This is negligible, as the position of the blocks moves in the direction the y-component of trawl force acts when largest. Moving the blocks back to the initial position does not require a lot of work, as the trawl wires will be closer to parallel with the course.

8.2.1 Manoeuvring

The precision errors are small, even for most of the very large turning rates. It is important to note that the precision error does not account for bias errors; e.g. errors due to inaccurate modelling. As previously discussed regarding accuracy of the model during manoeuvring, the power reduction as a function of turning rate is only reliable at small turning rates. Especially the position of the trawl relative to the ship has large errors, which propagate for the duration of a manoeuvre. The inaccuracy related to these are a function of turning rate and duration of a turn. The errors related to turning rate is expected to give an underestimation of the actual potential for reduction in power.

The confidence intervals are clearly not valid at the high turning rates, even when disregarding bias errors. This is due to other variables that are not accounted for, such as depth and duration of the manoeuvre. As depth increases, the reduction of power during turning is less, due to a tighter inner turn of the trawl. Long duration of turns also results in the trawl following a tighter path. At the higher turning rates, the confidence intervals could therefore be tighter than they are supposed to. For example, there could be two manoeuvres of long duration at a certain depth, instead of twenty manoeuvres with short duration at different depths, with an equal total duration. This means the data is not necessarily representative of the entire distribution of power reduction at these turning rates.

8.2.2 Environmental drift

The error in trawl track is related to turning rate, and should not affect the results regarding drift angles as much. Errors in hull-lift forces should not be a large issue either, as the drift angle relative to flow should be small, as it is assumed that all of the drift angle during these points are to correct for the currents. This is not entirely accurate, as a drift angle would also be used to correct for the y-component of trawl forces after a turn, when the trawl still has not returned to the ship track. Some bias error is therefore present. Contrary to the manoeuvring, these errors would overestimate the potential for reduction in power, because the yaw moment from trawl on a straight course is overestimated due to the position of the trawl relative to the ship. The bias errors are presumably a lot smaller than during manoeuvring, as is also seen by the more continuous plots in Figures 7.8 and 7.9. From the standard

deviations in Tables 7.3 and 7.4, the data is also closer to constant, meaning the probability distribution is fairly symmetrical.

8.3 Explanation to manoeuvring results

For an accurate model it is expected that the power reduction would follow closer to the linear trend following Figure 7.7 up to $20°/min$, or Figure 7.6 up to $11°/min$, up to it's peak. At the peak, the trawl is moved as far as possible to one side, and any necessary increase in yaw-moment must be supplied by the rudder. Increasing the turning rate beyond the peak will result in a reduction in steering moment from the movable blocks, as the x-component of the tension force will decrease.

8.4 Explanation to drift angle results

For the first points in Figures 7.8 and 7.9, steering using the trawl forces completely replaces the rudder angle of attack, giving the plot a similar shape to a rudder drag-curve. When the trawl blocks are moved all the way to one side, the rudder must be used. The reduced rudder angle then gives a reduction in drag, increasing with rudder angle proportional to the non-linear part of the rudder's drag curve.

8.5 Relation to background

The vessel used in Bjørkum (1989) is small, and old, compared to the Prestfjord. Modern design of hull and propulsion units would reduce the potential for saving fuel considerably. The velocities are different for the two vessels. The vessel described in Bjørkum (1989) is a coastal shrimp-trawler, encountering strong currents, while trawling with a low velocity, Prestfjord on the other hand, operates at forward speeds roughly twice as large while at sea. The drift angles to correct for current, would therefore be smaller, and large drift angles would appear more seldom. This would explain some of the difference in expected average reduction in power.

When large drift angles are encountered, the reduction in power is much smaller than assumed in Bjørkum & Farstad (1991) based on the results in Bjørkum (1989). Drift angles in Bjørkum (1989) were typically between 10° and 20°. Rudder drag has a very low increase at angles of attack close to zero. This might not be the case for

every vessel, as it is to a large degree related to the leading edge radius of the rudder (Figure 6.4 in Steen (2014*c*)). Trawlers should have rudders with drag curves that stay low even at moderate rudder angles as rudder is used more frequently during trawling. This means that thin profiles are not suitable.

The rudder on the Prestfjord could be said to be sufficiently efficient for rudder angles to stay within the part where rudder drag is much lower than its lift. At larger angles of attack, the drag force relative to lift increases drastically, meaning a smaller, or less efficient rudder would generate much more drag while creating the same lift. As the vessels that has movable blocks installed usually installed it to increase manoeuvring capabilities (Enerhaug 2009), there is reason to believe that the rudders on these vessels are insufficient. This would lead to the rudders operating at angles where the ratio of drag to lift is large, even on a straight course with a drift angle.

There could be a potential for increased reduction in power by optimising a new rudder size for a ship with movable blocks. The increased manoeuvrability from movable trawl blocks would lead to a different optimal rudder area, as long as the current rudder is optimal (without movable blocks), instead of limited by space limitations. Smaller rudder area leads to reduced 0-angle drag. This would not reduce the fuel consumption a lot during trawling, as the zero-angle drag is already small relative to other forces. During transit, the rudder drag at zero-angle is much higher than during trawl, and a smaller rudder could have a larger effect. Usually, rudder drag is small relative to hull friction during transit. Despite the relatively large rudder trawlers have, and the following rudder drag, this is most likely the case here as well. Finding a different rudder is therefore not considered to give any significant improvement, especially when considering that the change in rudder area would be small.

8.6 Velocity on the rudder

The velocity on the rudder decreases when thrust is decreased. This leads to less drag, and lift, for the chosen rudder angle. By keeping the lift constant, the rudder angle must be increased to keep the lift, with a following increase in drag. The drag is increased more than the reduction due to the reduced velocity. By iterating a new rudder angle and thrust for the optimised point, the thrust needs to be increased slightly, and some of the potential saving from the system is lost. When the rudder

angle is small enough to be completely replaced with steerable trawl blocks, the drag is reduced from such a system; however, the effect this has on thrust is very small, as the 0-angle rudder drag is close to negligible compared to other surge forces during trawling.

8.7 Recommendations and field of application

Despite a statistically significant mean reduction in power seen in Table 7.5, it is not certain that such a system will be beneficial in an economical or environmental way if it had been installed on Prestfjord. A life-cycle analysis including the investment cost should be performed if installing such a system is in consideration for any ship. The investment costs are unknown at this time. Because of large variations between trawlers and their operations, a completely universal guideline is unlikely to be possible. If a detailed operational profile consisting of drift angles and turning rates, the results regarding drift angle on a straight course can be used as a guideline for vessels with sufficient manoeuvring capabilities. Turning rate is more variable, due to differences in depth and duration of manoeuvres.

Ships considering such a system to increase manoeuvring, should first consider a new rudder.

Chapter 9

Conclusion and Further work

9.1 Conclusion

The results are subject to uncertainties of unknown quantity, mostly related to the modelling of trawl forces.

There is small, yet statistically significant potential for reduction in power by installing movable trawl blocks. For the data-set used, Prestfjord could reduce the propeller power 0.67% on average, 1.13% during double trawl, and 1.11% during single trawl. The reduction in power is not large enough to give a definitive conclusion about economical savings, as the investment and maintenance cost of the system could be larger than the reduction of fuel costs over a ship life-cycle.

The mean reduction in reduced power will be significantly different for other ships, other operating conditions and the amount of manoeuvres. Results regarding constant course with a drift angle is expected to vary the least.

Reduction in power during manoeuvring and drift angle on straight course would also change between ships; however they can be used for quantification on ships with sufficient rudder efficiency. The reduction is largest during manoeuvring, while they are more consistent as a function of drift angle. The system will be most beneficial for vessels manoeuvring a lot during trawling. There is a connection between insufficient manoeuvring capabilities and the potential for power reduction, meaning vessels that consider a system of movable blocks for increased manoeuvrability will have a larger reduction in power than a vessel considering a system for the power reduction alone.

9.2 Further work

- **Investigation of the trawling fleet:** Prestfjord is a vessel designed for trawling, and is described as a "...new generation of environmentally friendly and reliable stern trawlers" Skipsrevyen (2012). How many vessels are in the different categories of trawlers? What is their age? How many vessels where once another type of vessel, modified into a trawler? How does the average trawler compare with the newest generation when it comes to manoeuvring and fuel consumption?
- **Longitudinal placement of trawl blocks:** Yaw moments from trawl and rudder are dominant in the yaw equation. At large turning rates most of the moment due to the trawl comes from the transverse forces. Placing the rudder and propeller further back, or the trawl blocks further forward will therefore reduce the necessary rudder angle. This does not require a system for moving the blocks, and will therefore be cheaper, while still reducing the use of rudder. The influence this has on the power should be investigated. This would also require a different design of the aft body of the vessel above the waterline, to make sure nothing is in the way of the warps.
- **Stability requirements:** As the warps have a vertical force component, moving them creates a moment in roll. Vessels with movable blocks have capsized as a consequence. A thorough calculation of the stability is needed. The Synchro system limits the possibility for capsizing, as it feeds wire when the tension increases to prevent damage.

Bibliography

Abkowitz, M. A. (1964), *Lectures on ship hydrodynamics : steering and manoeuvrability*, Vol. Hy-5 of *Report (Hydro- og Aerodynamisk Laboratorium. Hydrodynamisk Afdeling)*.

Anderson, L. (2007), *WEIGHTS AND BREAKING LOADS FOR STEEL WIRE ROPE*, PDQ Lifting.
URL: *http://www.pdqwire.co.uk/dynamicdata/assetmanager/images/weight-breaking-load.pdf*

Bhattacharyya, A., Norges teknisk-naturvitenskapelige universitet Institutt for marin, t. & Norges teknisk naturvitenskapelige, u. (2015), Ducted propellers : behaviour in waves and scale effects, Thesis.

Bjørkum, I. (1989), 'Styring av fartøy ved hjelp av slept objekt', *Fiskeriteknologisk Forskningsinstitutt* .

Bjørkum, I. & Farstad, A. (1991), *Styring av fartøy ved forflytning av slepefeste for trålvarp*, Vol. 402028.00.01 of *Marintek rapport (trykt utg.)*, Norsk marinteknisk forskningsinstitutt, Trondheim.

Brix, J. (1993), *Manoeuvring technical manual*, Seehafen Verlag, Hamburg.

Dang, J., Boom, H. v. d. & Ligtelijn, J. (2013), 'The wageningen c- and d-series propellers', *12th International Conference on Fast Sea Transportation (FAST)* .

Enerhaug, B. (2009), 'Fremtidens tråler - redskapshåndtering', *SINTEF Rapport* .

Faltinsen, O. M. (1990), *Sea loads on ships and offshore structures*, Cambridge ocean technology series, Cambridge University Press, Cambridge.

Faltinsen, O. M. (2005), *Hydrodynamics of high-speed marine vehicles*, Cambridge University Press, Cambridge.

Fossen, T. I. (1994), *Guidance and control of ocean vehicles*, Wiley, Chichester.

Fossen, T. I. (2011), *Handbook of Marine Craft Hydrodynamics and Motion Control*, Chichester, UK: John Wiley & Sons, Ltd, Chichester, UK.

Geonorge (2011), 'Dybdekurver'. Accessed: 29-03-2017.
URL: *https://kartkatalog.geonorge.no/metadata/kartverket/dybdekurver/871960a1-0f01-4c47-8f79-5d338b65197e#*

Hibbeler, R. C. & Fan, S. C. (2010), *Engineering mechanics : statics*, 12th ed. in si units. edn, Prentice Hall, Singapore.

ITTC, I. T. T. C. (Revised 2011), '1978 performance prediction method.', *ITTC-Recommended Procedures and Guidelines* (7.5-02-03-01.4).

Karlsen, L. (1997), 'Redskapslære og fangstteknologi'.

Kartverket (2016*a*), 'Dybdekurver i norske kyst- og havområder'. Accessed: 29-03-2017.
URL: *http://www.kartverket.no/data/kartdata/dybdedata/dybdekurver/#_ga=1.200930606.1453430745.1490792191*

Kartverket (2016*b*), 'Jordas rutenett'. Accessed: 29-03-2017.
URL: *www.kartverket.no/Kunnskap/Kart-og-kartlegging/Jordas-rutenett/*

Kartverket (2016*c*), 'Kva er eit kart?'. Accessed: 29-03-2017.
URL: *http://www.kartverket.no/Kunnskap/Kart-og-kartlegging/Hva-er-kart/*

Klokan Technologies (2012), 'Etrs89 / utm zone 33 + nn2000 height'. Accessed: 29-03-2017.
URL: *http://epsg.io/5973*

MATLAB (2015), *version 8.6.0 (R2015b)*, The MathWorks Inc., Natick, Massachusetts.

Merriam-Webster (2017), 'Whitefish.'. Accessed: 12 June 2017.
URL: *https://www.merriam-webster.com/dictionary/whitefish*

Molland, A. F. & Turnock, S. R. (2007), *Marine rudders and control surfaces : principles, data, design and applications*, Elsevier, Amsterdam.

Monahan, J. F. (2011), *Introduction to Optimization and Nonlinear Equations*, Cambridge Series in Statistical and Probabilistic Mathematics, 2 edn, Cambridge University Press, p. 186–218.

Oljedirektoratet (2010), 'Beskrivelse av relevante fiskeredskap og fiskeriaktivitet i norges økonomiske sone'. Accessed: 13-05-2017.
URL: *http://www.npd.no/no/Seismikk/Relevante-fiskeredskap-og-fiskeriaktivitet-/*

Pettersen, B. (2007), *Marin teknikk 3 : hydrodynamikk*, Marin hydrodynamikk, Marinteknisk senter, Institutt for marin teknikk, Trondheim.

Ringen, E. (2017), *User Manual ShipX Manoeuvring Plug-In*, SINTEF Ocean AS.

Ross, A. (2008), Nonlinear manoeuvring models for ships : a Lagrangian approach, Thesis.

Rottmann, K. (2003), 'Matematisk formelsamling'.

Åsbø, D. (2016), 'Steering and thrust loss while trawling.'. Project thesis.

Sintef (2012), 'Loggesystem installert i prestfjord'.
URL: *http://www.sintef.no/siste-nytt/loggesystem-installert-i-prestfjord/*

Skipsrevyen (2012), 'M/tr. "prestfjord"'. Accessed: 19-06-2017.
URL: *http://www.skipsrevyen.no/mtr-prestfjord/*

Steen, S. (2014*a*), 'Experimental methods in marine hydrodynamics : compendium'.

Steen, S. (2014*b*), 'Ship resistance : Tmr4220 naval hydrodynamics : lecture notes'.

Steen, S. (2014*c*), *TMR4220 Naval hydrodynamics foil and porpeller theory : lecture notes*, Vol. UK-2014-80/II of *Kompendium (Norges teknisk-naturvitenskapelige universitet. Institutt for marin teknikk)*, Akademika forlag Kompendieforlaget, Trondheim.

Steen, S. (2016), 'Comments to: Steering and thrust loss while trawling'.

Valdemarsen, J. W. (2015), 'Hvordan fange torskefisk effektivt og skånsomt i passende mengder med tråL i barentshavet?'.
URL: *http://www.sintef.no/contentassets/d4a5f1fd26e140c9b8dacff9165d931a/06-john-w-valdemarsen-hvordan-fange-torskefisk-effektivt-og-skansomt-i-passend.pdf*

Weisstein, E. W. (2017), 'Method of false position.'.
URL: *http://mathworld.wolfram.com/MethodofFalsePosition.html*

Glossary

bycatch Fish that is too small to be legally caught, and other species. Acceptable bycatch is governed by different quotas. . 3

cod-end The net containing the caught fish, sometimes used to also include the guiding net and sorting grid.. 3, 4

confidence interval A confidence interval describes the possible interval of the estimated parameter within the selected probability limit. When taking samples from a population, there is no warranty that it will represent the population, for example only pulling mostly red balls from a bowl of equal quantity red and blue balls. The confidence interval shows the limits of probability for this happening. . xi, 74

controllable pitch propeller Some propellers have a mechanism for changing the pitch of the blades. This allows for an extra degree of freedom when controlling thrust, allowing a more optimal propeller geometry at off-design conditions. This is therefore common for ships where no mode of operation is clearly dominant Steen (2014*c*). . xi, 33

course The direction the vessel is travelling. The angle between North and the velocity vector.. 10

degree of freedom A ship can move in six unique ways. Three translations; surge, sway, heave. Three rotations; roll, pitch, yaw . xi

double trawl Two trawl nets are placed between the trawl doors instead of one, increasing the horizontal opening of the net. . 3

duct Also called nozzle. A propeller duct is a ring around the propeller. The cross-section is usually foil-shaped, with the low pressure side towards the propeller, giving a lift forward and a mostly equalized component orthogonal to the ring. This gives an increased velocity, due to the foils circulation, through the propeller disk, and is therefore an accelerating duct. The forward thrust from the duct increases the total thrust; however, frictional resistance of the duct becomes larger at low thrust loading. Ducts are therefore used on vessels with high thrust loading such as trawlers and tugs. Neutral ducts(no-circulation) is used when the propeller needs protection, or to steer. Decelerating ducts are mostly used to reduce cavitation. (Steen 2014*c*) . 5

heading The direction the vessel is pointing. The angle between North and the x-axis in the body reference frame.. 10, 54

heave Translation along z-axis (vertical movement). . 20, 90

isobath Curves following points of equal depth. 45, 46

max continuous rating The maximum power an engine can produce for longer than short bursts, while staying within safe limits. Choice of engine is typically done to have most of the operations at 80%, where the specific fuel consumption often is lowest; this point is different for different engines.. xi, 13

pelagic The pelagic zone is the entire ocean water column, a term typically used when excluding the shore and the bottom. Pelagic trawling is trawling in the water-column instead of along the bottom, catching for example mackerel. . 3, 5, 47

pitch (DOF) Rotation around y-axis (tilting between aft and bow).
(propeller) Pitch is the angle of the blades, and can best be described by comparing with a screw. Pitch then describes the distance between threads. It is usually presented as the ratio between the screw distance travelled for one revolution at 70% radius to diameter, P/D. . 20, 33, 90

quadrant Here in relation to propellers. First ($0 < \beta_p < 90°$) - normal forward, second ($90° < \beta_p < 180°$) - crashback, third ($180° < \beta_p < 270°$) - normal backing, forth ($270° < \beta_p < 360°$) - crashahead. . 34

roll Rotation around x-axis. Side to side tilting motion. . 20, 90

spline In interpolation terms, it means that the equations used to represent the underlying data is not the same for the entire domain.. 35

Student's-t The probability distribution symbolizing the normal distribution when a limited amount of samples is drawn from the population. . 74, 75, 77, 78

surge Translation along x-axis (longitudinal movement). . 20, 90

sway Translation along y-axis (transverse movement). . 20, 90

sweepline The term used in trawling for the wires running between the trawl doors and the trawl net.. 3, 50

trawl door Foils that keep the trawl net open. Heavy to not be lifted off the bottom. Synonym with otter door.. 3, 47, 50, 53

warp The term used in trawling for the wires running between the ship and the trawl doors.. 2, 3

white-fish A diffuse umbrella term, here meaning fish with white, not oily flesh, such as cod. The third dictionary entry in Merriam-Webster (2017), the first is freshwater salmonid fishes. . 3, 5

yaw Rotation around z-axis (heading). . 20, 90

Appendices

Appendix A

Results, including data points

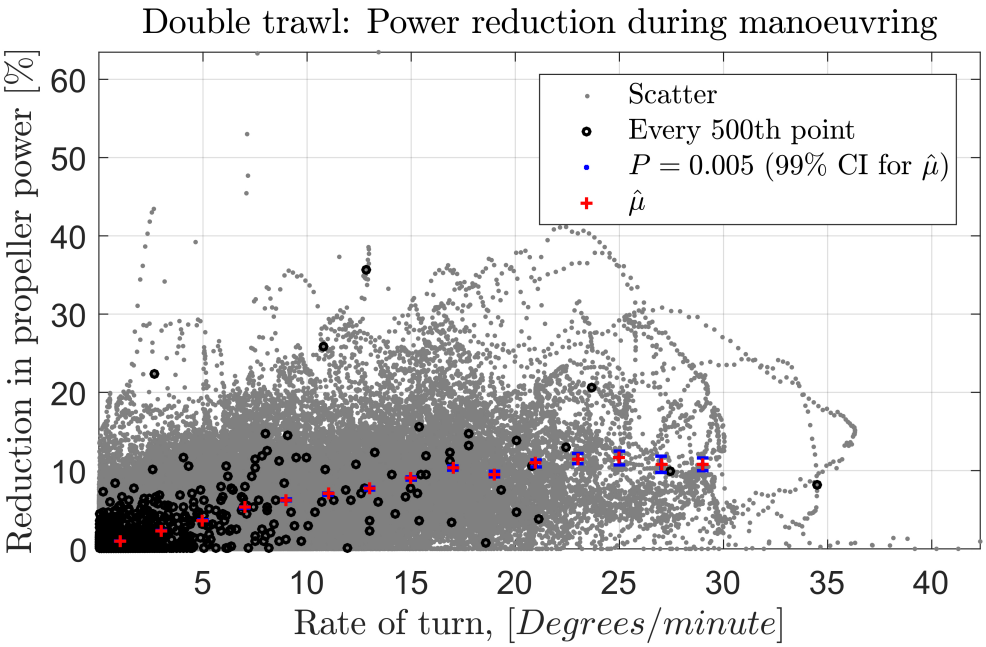

Figure A.1. Including points; power reduction as function of turning rate while pulling a double trawl: Every point is included to give a complete picture of the data the results are gathered from. Due to the large quantity of points, every 500th point is plotted as black circles to show where there are many points.

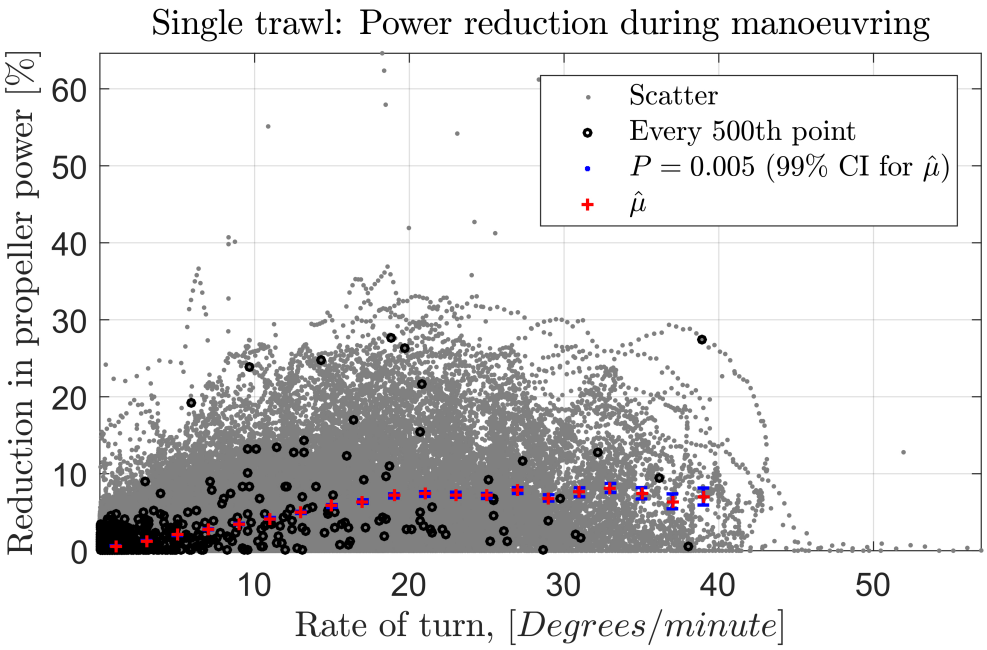

Figure A.2. OIncluding points; power reduction as function of turning rate while pulling a single trawl: Every point is included to give a complete picture of the data the results are gathered from. Due to the large quantity of points, every 500th point is plotted as black circles to show where there are many points.

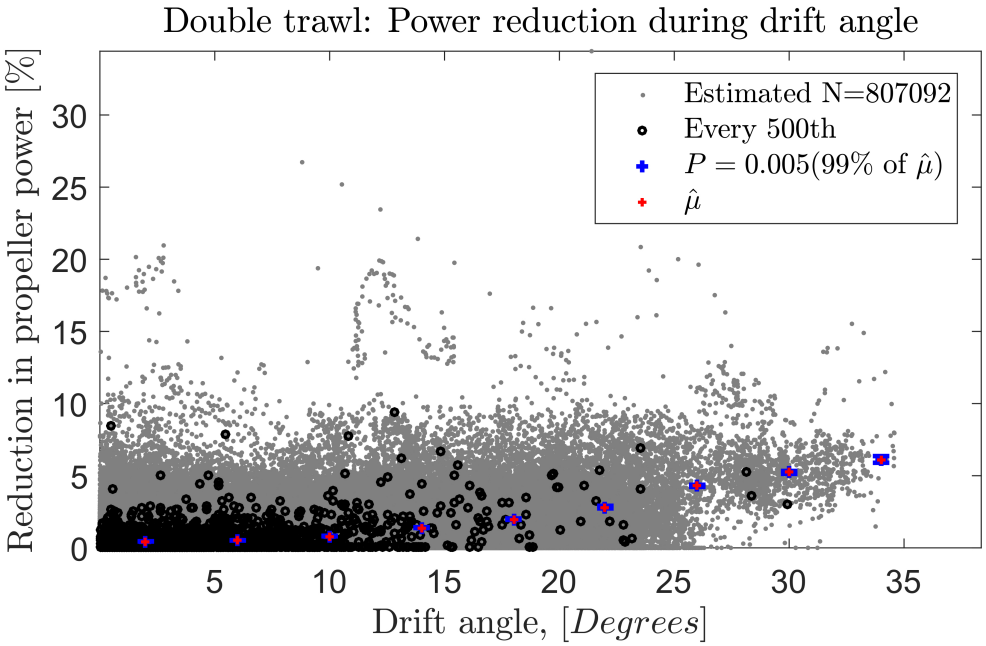

Figure A.3. Including points; power reduction as function of drift angle while pulling a double trawl: Every point is included to give a complete picture of the data the results are gathered from. Due to the large quantity of points, every 500th point is plotted as black circles to show where there are many points.

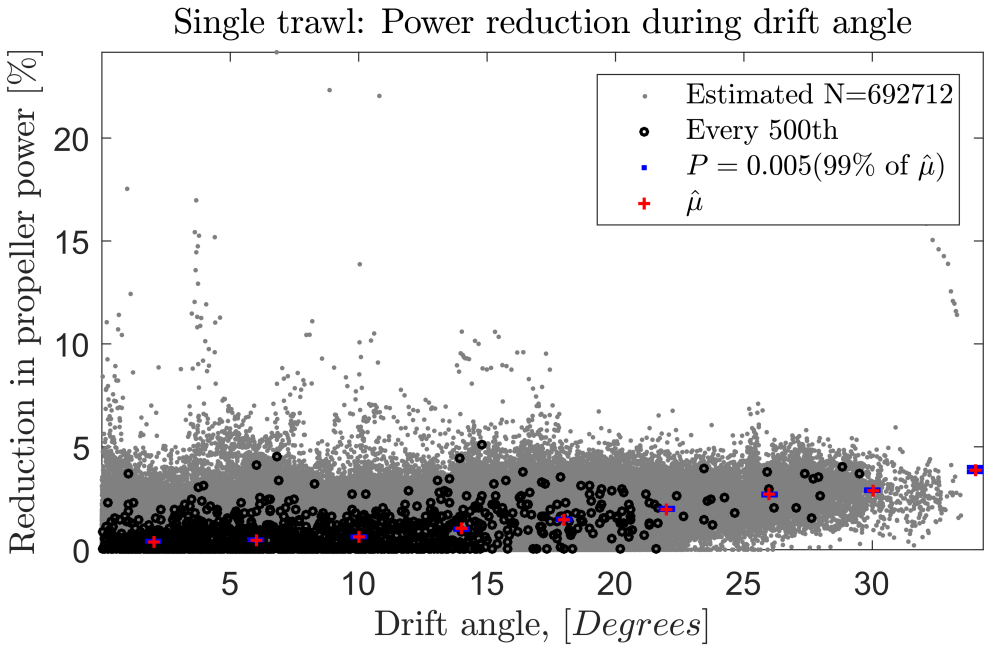

Figure A.4. Including points; power reduction as function of drift angle while pulling a single trawl: Every point is included to give a complete picture of the data the results are gathered from. Due to the large quantity of points, every 500th point is plotted as black circles to show where there are many points.

Appendix B

MATLAB codes and poster - Digital Appendix

A .zip file is attached the delivery, containing MATLAB codes and the poster presentation. The MATLAB codes used in this thesis is delivered in an additional file, and is not included in the PDF to reduce the number of pages.
The file contains a hierarchy of folders, named by the purpose of the codes inside. Most scripts are not executable as is, because the data they read or use is withheld.